Department of Energy
Office of Civilian Radioactive Waste Management
Yucca Mountain Site Characterization Office
P.O. Box 98608
Las Vegas, NV 89193-8608

WBS 1.2.5
QA: N/A

AUG 23 1995

Joseph J. Holonich, Chief
High-Level Waste and Uranium
Recovery Projects Branch
Division of Waste Management
Office of Nuclear Material Safety
and Safeguards
U.S. Nuclear Regulatory Commission
Washington, DC 20555

VOLCANISM INFORMATION REQUESTED BY THE U.S. NUCLEAR REGULATORY COMMISSION (NRC) STAFF (SCPB: N/A)

Reference: Ltr, Bell to Brocoum, dtd 7/27/95

In the referenced letter, the NRC requested copies of two data packages as follows:

1. "Effects of Magmatic Processes on the Potential Yucca Mountain Repository: Field and Computational Studies," by G. A. Valentine et al.

   This item has been published in Proceedings Site Characterization and Model Validation Focus '93 Symposium Volume, American Nuclear Society, La Grange Park, Illinois, p. 167-173, 1993. A copy of this article is enclosed. The U.S. Department of Energy obtained the copyright clearances necessary for transmittal of this item to the NRC.

   This data package is, in fact, listed twice in the Yucca Mountain Site Characterization Project Technical Data Catalog (Quarterly Supplement) dated June 30, 1995. The first listing is under Activity 8.3.1.8.1.2.1, and the second listing is under Activity 8.3.1.8.1.2.2.

2. "Geochemistry of the Lathrop Wells Volcanic Center" by F. V. Perry and K. T. Straub.

   A copy of this report is enclosed.

070012

102.8
WM-11
NH03

YMP-5

9509080318 950823
PDR WASTE
WM-11 PDR

If you have any questions, please contact me at (702) 794-7971 or April V. Gil at (702) 794-7622.

Stephan J. Brocoum
Assistant Manager for
Suitability and Licensing

AMSL:TWB-4284

Enclosures:
1. "Effects of Magmatic Processes on the Potential Yucca Mountain Repository: Field and Computational Studies"
2. "Geochemistry of the Lathrop Wells Volcanic Center"

cc w/encls:
L. H. Barrett, HQ (RW-2) FORS
Samuel Rousso, HQ (RW-40) FORS
M. S. Delligatti, NRC, Washington, DC
W. D. Barnard, NWTRB, Arlington, VA
R. R. Loux, State of Nevada, Carson City, NV
Robert Price, State of Nevada, Carson City, NV
Cyril Schank, Churchill County, Fallon, NV
D. A. Bechtel, Clark County, Las Vegas, NV
J. D. Hoffman, Esmeralda County, Goldfield, NV
Eureka County Board of Commissioners, Eureka, NV
B. R. Mettam, Inyo County, Independence, CA
Lander County Board of Commissioners, Battle Mountain, NV
Jason Pitts, Lincoln County, Pioche, NV
V. E. Poe, Mineral County, Hawthorne, NV
L. W. Bradshaw, Nye County, Tonopah, NV
Florindo Mariani, White Pine County, Ely, NV
P. A. Niedzielski-Eichner, Nye County, Chantilly, VA
William Offutt, Nye County, Tonopah, NV
P. M. Dunn, M&O, Vienna, VA
C. L. Sisco, M&O, Washington, DC
R. I. Holden, National Congress of American Indians, Washington, DC
Elwood Lowery, Nevada Indian Environmental Coalition, Reno, NV

cc w/o encls:
R. A. Milner, HQ (RW-30) FORS
A. B. Brownstein, HQ (RW-36) FORS
C. E. Einberg, HQ (RW-36) FORS
R. W. Craig, USGS, Las Vegas, NV
J. S. Stuckless, USGS, Denver, CO
J. A. Canepa, LANL, Los Alamos, NM
N. Z. Elkins, LANL, Las Vegas, NV
B. M. Crowe, LANL, Las Vegas, NV
F. V. Perry, LANL, Los Alamos, NM
G. A. Valentine, LANL, Los Alamos, NM
D. F. Fenster, M&O, Vienna, VA
P. M. Krishna, M&O, Washington, DC
T. R. Crump, M&O, Las Vegas, NV
S. E. LeRoy, M&O, Las Vegas, NV
M. A. Lugo, M&O, Las Vegas, NV
S. T. Nelson, M&O, Las Vegas, NV
S. P. Nesbit, M&O, Las Vegas, NV
S. B. Jones, YMSCO, NV
D. R. Williams, YMSCO, NV
J. C. Nesbit, YMSCO, NV
J. T. Sullivan, YMSCO, NV
S. J. Brocoum, YMSCO, NV
R. V. Barton, YMSCO, NV
A. V. Gil, YMSCO, NV
S. B. Jones, YMSCO, NV
R. G. Hawe, YMSCO, NV
C. M. Newbury, YMSCO, NV

Rec'd with letter dtd 8/23/95

Enclosure 1

Copy of

EFFECTS OF MAGMATIC PROCESSES ON THE POTENTIAL YUCCA MOUNTAIN REPOSITORY: FIELD AND COMPUTATIONAL STUDIES

102.8

EFFECTS OF MAGMATIC PROCESSES ON THE POTENTIAL YUCCA MOUNTAIN REPOSITORY: FIELD AND COMPUTATIONAL STUDIES

G.A. Valentine, K.R. Groves, & C.W. Gable
Geoanalysis Group EES-5
Mail Stop F665
Los Alamos National Laboratory
Los Alamos, NM 87545

F.V. Perry & B.M. Crowe
Nuclear Waste Management
Research & Development
Group EES-13, MS J521
Los Alamos National Laboratory
Los Alamos, NM 87545

ABSTRACT

Assessing the risk of future magmatic activity at a potential Yucca Mountain radioactive waste repository requires, in addition to event probabilities, some knowledge of the consequences of such activity. Magmatic consequences are divided into an eruptive component, which pertains to the possibility of radioactive waste being erupted onto the surface of Yucca Mountain, and a subsurface component, which occurs whether there is an accompanying eruption or not. The subsurface component pertains to a suite of processes such as hydrothermal activity, changes in country rock properties, and long-term alteration of the hydrologic flow field which change the waste isolation system. This paper is the second in a series describing progress on studies of the effects of magmatic activity. We describe initial results of field analog studies at small volume basaltic centers where detailed measurements are being conducted of the amount of wall-rock debris that can be erupted as a function of depth in the volcanic plumbing system. Constraints from field evidence of wall-rock entrainment mechanisms are also discussed. Evidence is described for a mechanism of producing subhorizontal sills versus subvertical dikes, an issue that is important for assessing subsurface effects. Finally, new modeling techniques, which are being developed in order to capture the three dimensional complexities of real geologic situations in subsurface effects, are described.

INTRODUCTION

The risk of future magmatic activity for the potential Yucca Mountain repository block is defined by the conditional probability

$$Pr_{dr} = Pr(E3 \text{ given } E2,E1)Pr(E2 \text{ given } E1)Pr(E1)$$

where Pr_{dr} is the magmatic disruption probability (i.e., the likelihood of a magmatic event causing release of radioactive waste to the accessible environment in excess of regulatory limits), $E1$ is the recurrence rate of magmatic events in the Yucca Mountain region, $E2$ is the probability that a future magmatic event intersects the repository or is close enough to have a significant effect on repository performance, and $E3$ is the probability that a given magmatic event will cause release of waste to the accessible environment in quantities that exceed regulatory limits. $E3$ is the sum of two components, $E3_e$ and $E3_s$, which denote release to the surface by eruption and release in the subsurface environment, respectively. Pr_{dr} is the primary measure for judging reduction in waste isolation as a result of magmatic processes. Research associated with E3 is divided into three parts:[1] (1) Eruptive Effects ($E3_e$), which addresses how much radioactive waste could be erupted onto the surface of Yucca Mountain if an eruptive event penetrated the potential repository; (2) Subsurface Effects ($E3_s$), which addresses processes such as local hydrothermal circulation or perturbation of the regional groundwater flow field in response to an intrusive event (with or without eruption); (3) Magma System Dynamics, which addresses, from a physical point of view, the overall processes that produce the observed patterns of volcanism in the Yucca Mountain region with the goal of supporting the conceptual basis for event probability calculations.

This paper is a sequel to the 1992 paper of Valentine et al.,[2] which was the first published report describing recent efforts to understand and estimate the effects of magmatic activity on the potential Yucca Mountain repository. This earlier paper[2] focused on strategies that had been identified for estimating eruptive and subsurface effects, and described initial studies of subsurface effects at the Paiute Ridge analog area, along with initial efforts at modeling magma system dynamics. Since that paper was written, work has proceeded on both eruptive and subsurface effects, and to a lesser extent on general concepts of magma dynamics. The current paper will emphasize initial results of eruptive effects studies.

ERUPTIVE EFFECTS ($E3_e$) STUDIES

Xenolith Abundances at Small Basaltic Centers

Valentine et al.[1,2] have described the importance of using analog basaltic centers to constrain the amount of foreign material that could be erupted onto the Earth's surface from a given depth, which in our case is the depth of the potential repository horizon. Analog studies are more desirable than theoretical studies because the physics of wall-rock entrainment into magma flowing through a dike is only poorly known. Our approach is to identify basaltic centers of similar size, composition, and eruptive styles to the Pliocene-Quaternary centers near Yucca Mountain. The additional factor is added that the subvolcanic rock types are well known and their depths beneath the volcanoes are well constrained. We then conduct detailed measurements of crustal xenolith abundances and attempt to correlate each xenolith with its depth of origin (if possible). These data then provide quantitative information on the amount of debris, including radioactive waste, which could be erupted from the potential repository horizon. There are limited studies in the literature that describe the volume fraction of shallow crustal xenoliths (*a.k.a.* lithics) in small volume Strombolian and hydrovolcanic volcanoes such as those near Yucca Mountain,[3-5] but these generally do not contain detailed data on the relative proportions and depths of derivation of the

ENCLOSURE 1

lithics. The only paper that we are familiar with that provides data on proportions of lithics as functions of depth of origin is that of Mastin,[6] which is about a rhyolite dome, not a basaltic center.

The Colorado Plateau provides an excellent setting for this study because of its well established, subhorizontal stratigraphy that is relatively unaffected by faulting; our initial work has been conducted on the eastern margin of the Colorado Plateau in the Lucero volcanic field, west-central New Mexico.[7] Basaltic volcanism in the Lucero field ranges in age from 8.3 Ma to as recent as a few thousands or tens of thousands of years. Eruptive styles ranged from broad shields with lava flows extending several tens of kilometers, to small isolated scoria cones, tuff rings, and tuff cones. Compositions are mainly tholeiite to alkali basalts.

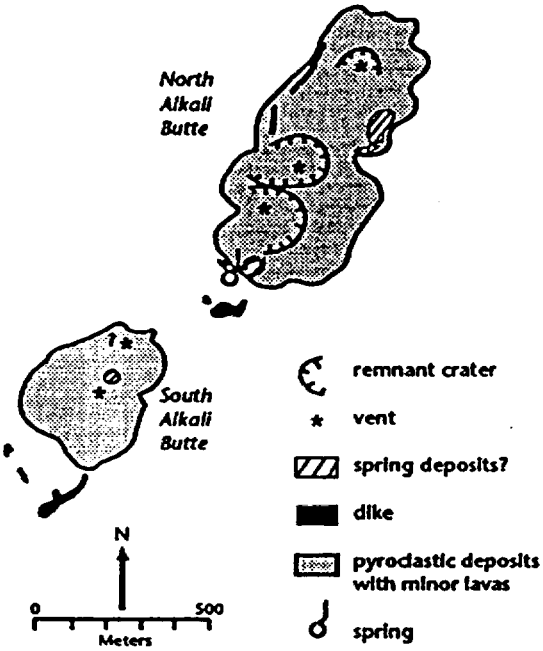

Figure 1. Simplified geologic map of Alkali Buttes, showing distribution of volcanic rocks, dikes, inferred vents, inferred crater rims, possible hot spring deposits, and an active spring. Geographic location of Alkali Buttes can be found in Ref. 7. The volcanic rocks were erupted onto a surface cut into the Upper Triassic Chinle Formation.

To date we have focused on the Alkali Buttes centers (Figure 1; see also Ref. 7), which are thought to be several hundred thousand years old. These buttes are erosional remnants of an approximately 2 km long, north-northeast trending, chain of four to five vents that is subparallel to major normal faults in the area. This chain probably formed a single continuous land form prior to erosion. South Alkali Butte is the remnant of a tuff ring or tuff cone (only the crater-filling deposits are preserved). The earliest deposits are lapilli tuffs containing abundant lapilli and block-sized lithic clasts, probably representing strongly hydrovolcanic activity. These tuffs are overlain by relatively ash-poor beds of poorly vesicular basalt lapilli with much lower lithic content than the tuffs. These lapilli beds probably represent eruptions that were influenced by a lower degree of hydrovolcanic fragmentation than the underlying tuffs. Overlying the lapilli beds are beds of coarse, vesicular scoria and small bombs, which are in turn overlain by variably agglutinated coarse spatter beds interlayered with thin lava and pillow lava flow units. Near the original crater center, the spatter beds are overlain by a mixture of mud derived from the Chinle formation (see below) and large, highly vesicular fluidal basalt clasts. The entire sequence is capped by pillow lavas which locally protrude downward into the Chinle-basalt mixture. We interpret this sequence as recording decreasing hydrovolcanic activity through the main phases of eruption (lapilli tuffs, poorly vesicular lapilli, scoria, and spatter/lava flow units). This phase was followed by an extended period of weak lava effusion and mud boiling in the lowest parts of the crater (to produce the mixed Chinle mud-basalt clast unit) and eventually production of a small volume of lava which flowed onto and into the mixed Chinle mud-basalt clast unit. The latter unit was probably a water-saturated slurry at the time (hence the formation of pillow lavas). A small area, about 50 m in diameter, on the interior of the center is littered with large (decimeter to meter) sized lithic blocks from 500-600 m depth, perhaps indicating a late-stage phreatic explosion. Possible hot spring deposits capping pillow lava in the center of the original crater indicate that hydrothermal activity persisted for some time after eruptions ceased.

North Alkali Butte consists of the remnants of three scoria/spatter cones and associated craters (Figure 1). The southern two cones filled in a previously formed tuff ring or tuff cone, of which only the inner, inward dipping deposits are preserved. As at South Alkali Butte, the lowest preserved deposits of this tuff ring/cone phase are lapilli tuffs, overlain by poorly vesicular basalt lapilli beds, then vesicular scoria and spatter beds that are variably agglutinated and are associated with the three cones. Localized lava flows were also erupted from the cones but, unlike South Alkali Butte, we found no pillow lavas. This is probably because the cones filled up the tuff ring/cone's crater to produce topographic highs. This contrasts with South Alkali Butte where the crater was not filled and thus remained a closed basin which retained water and the Chinle/lava slurry described above. The northern part of North Alkali Butte is poorly exposed, but does not seem to contain the hydrovolcanic units (lapilli tuffs and poorly vesicular lapilli beds) that occur to the south. Additionally, it may not have experienced extensive hydrovolcanic processes. Possible hot spring deposits occur on the northeast flank of North Alkali Butte. An active spring is present at the southern end of North Alkali Butte; it is collinear with the possible hot spring deposits on North and South Alkali Buttes, along a north-northeasterly trend that like the trend of the vents is subparallel to regional normal faults. North Alkali Butte was more dominated by Strombolian eruption mechanisms (driven by expansion of magmatic volatiles) than South Alkali Butte, which had a larger hydrovolcanic component.

The subvolcanic stratigraphy at Alkali Buttes is well constrained due to exposure in the nearby Lucero Uplift[8,9] and two exploratory oil wells provide subsurface control. One of these wells is located about 22 km southwest of Alkali Buttes[10] and the other is located 14 km to the northwest of Alkali Buttes.[11] Strip logs for these wells were obtained at the New Mexico Bureau of Mines and Mineral Resources in Socorro, New Mexico. The stratigraphic units consist of, in descending order:

Chinle Formation (Upper Triassic) -- Approximately 510 m thick. Mainly red to reddish brown and purple silty mudstone and clay shale with thin sandstone lenses. Lower 200 m has zones of feldspathic sandstone, and chert and limestone pebble conglomerates.

San Andres Formation (Lower Permian) -- Approximately 130 m thick. Mainly gray fine to medium grained limestones, silty limestones, gypsum, and gypsiferous shale. Distinctive petroleum odor when broken.

Glorieta Sandstone (Lower Permian) -- Approximately 60 m thick. Massive, pale yellow, fine-grained, well-sorted quatzose sandstone with abundant cross bedding. Erosionally resistant formation.

Yeso Formation (Lower Permian) -- Approximately 400 m thick. Alternating beds of pale red, yellow, and buff gypsiferous shale with grayish white to pink sandstone. Highly gypsiferous.

Abo Formation (Lower Permian) -- Approximately 280 m thick. Mainly dark red, silty sandstones and shales with lenses of limestone.

Madera Formation (Pennsylvanian) -- Approximately 230 m thick. Various combinations of tan, gray, white, and red dense limestone interbedded with white, coarse-grained sandstone and light gray to red-brown shale.

Sandia Formation (Pennsylvanian) -- Approximately 75 m thick. Tan-white and tan-brown, dense, crystalline limestone interbedded with white coarse-grained sandstone and conglomerate.

Granite Wash Formation (Precambrian) -- Coarsely crystalline granite.

The approximate thicknesses given above are estimated to be accurate to within 10% of the thickness of each formation. Most observed lithic fragments were from the Chinle, San Andres, or Glorieta formations (depths less than about 700 m).

Preliminary lithic abundance data for the Alkali Buttes centers are shown in Figures 2, 3. We have grouped the data according to the eruption facies to which they correspond, instead of specific stratigraphic or geographic locations, because our main interest here is the influence of different eruptive mechanisms on lithic abundances. Note that many more basaltic centers will be studied in order to minimize the effects of local geologic conditions on our results, which will ultimately be applied to the Yucca Mountain setting. Lithic abundance data were collected by marking off 1 m^2 with nails and a string, then measuring the long and short dimension of each lithic fragment within the area and identifying the formational origin. In some cases, especially for smaller clasts or clasts that had been baked (for example, a lithic clast within a lava bomb), the identifications were ambiguous. For the plots shown we lumped these clasts, which are a minor part of the data, with their most likely formations. Only clasts with a long dimension of 1 cm or greater were measured in the field; the abundance of smaller lithic clasts will be determined from microscopic examination of samples collected within the measured areas. Thus the data shown here are only the macroscopic component of lithics. When microscope data are included the total abundances will increase somewhat, particularly in the lapilli tuffs where it is likely that much of the ash matrix is xenolithic. Using the long and short dimension of each measured clast, we compute the area of the clast in the outcrop by approximating it as a rectangle. These areas are converted to area fractions by tallying the areas of all lithics of a given formation. The area fraction is proportional to volume fraction, although some correction will eventually be made for the fact that not all lithics are exposed at their maximum cross sectional area. This correction will probably result in a 30-40% increase in converting area fractions to volume fractions. Overall, we feel that that the error in the area fraction estimates is about 10%. A more rigorous assessment of this error will be made in the future.

Figure 2 shows lithic abundances (area fractions) as functions of depth for lapilli tuffs, poorly vesicular lapilli units, and vesicular scoria/spatter units. Also shown are total lithic abundances for each measured area. Note that we have plotted depths for each lithic type at mid level for each particular formation; each point should be considered as having a possible depth range over the entire thickness of that formation. Most of the plots show a general decrease in lithic abundance with increasing depth of origin. This simple trend is complicated by the fact that Glorieta Sandstone fragments are typically more common than fragments from the overlying San Andres Formation. There are at least two possible reasons for this. First, although the Glorieta Sandstone is very dense and has a low matrix porosity, it is highly fractured. It may therefore have acted as a fracture-dominated aquifer and therefore as a source of water for explosive magma-water interaction. The difference in abundance of fragments then reflects the relative importance of hydrovolcanic explosions at corresponding depths. This interpretation perhaps best applies for the lapilli tuffs and poorly vesicular lapilli units, which show independent evidence for an important role of hydrovolcanism (e.g., abundance of ash in the tuffs, low vesicularity of juvenile clasts). However, the vesicular scoria/spatter units, which seem to have been formed by eruptions driven mainly by magmatic volatiles, show the same trend in lithic abundances. A second and favored interpretation at this point is that the mechanical properties of the Glorieta Sandstone played the major role in controlling its abundance in eruptive deposits. In outcrop, Glorieta Sandstone is fractured into coherent blocks of various sizes that depend partly on the scale of bedding within the sandstones. This contrasts with the overlying San Andres and Chinle formations, which tend to be

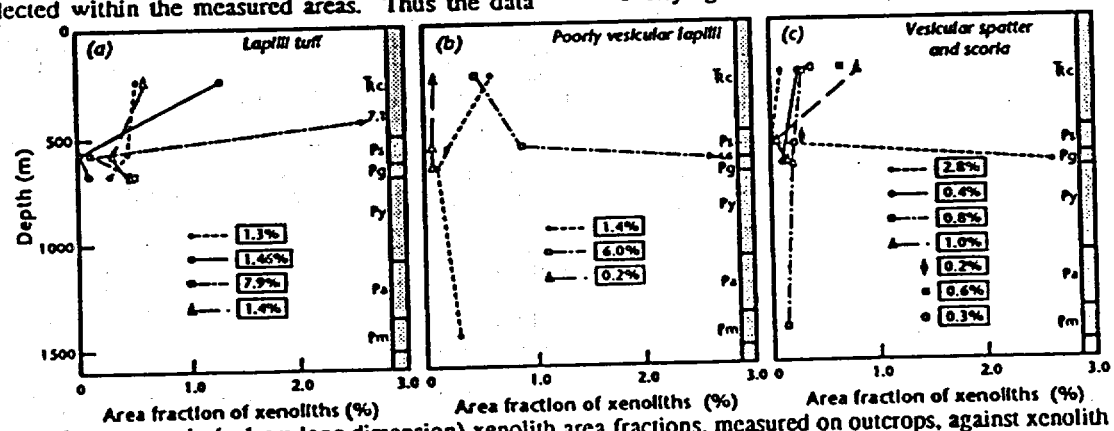

Figure 2. Plots of macroscopic (> 1 cm long dimension) xenolith area fractions, measured on outcrops, against xenolith depth of origin. Subvolcanic stratigraphy is shown on the right hand side of each graph, corresponding to appropriate depths. (a) Lapilli tuff units, (b) poorly vesicular lapilli units, and (c) vesicular spatter and scoria units. Value shown in a box by each curve is the total xenolith area fraction for that measured outcrop. Error bars are not shown, but a conservative estimate of error in area fraction values is +/-10% due to inaccuracies in measuring the outcrop area studied and because the area for each clast is computed as if the clast were a rectangle. Errors in the depth values are less constrained, and range over the entire thickness of each formation. Data have been plotted at mid level for each formation. For example, depth values for data plotted in the Chinle Formation have an error of +/-255 m. Data plotted at Glorieta Sandstone depths have errors of +/-30 m. Symbols: Trc - Chinle Formation; Ps - San Andres Formation; Pg - Glorieta Sandstone; Py - Yeso Formation; Pa - Abo Formation; Pm - Madera Formation.

less competent and have a larger proportion of nonindurated shales and mudstones, with only thin layers of more competent limestones or sandstones. These formations may not sustain fractures as well as the Glorieta Sandstone so that large coherent fragments do not break off as easily. Mechanisms for this entrainment will be discussed in the next section.

Figure 3 shows total area fraction of lithics and maximum lithic sizes for the main eruptive facies. Vertical bars within each facies type represent average values, which of course are based on only a few data at this point and are preliminary. The data show that in general the total lithic contents decrease upward in the stratigraphic sections (Figure 3a), paralleling the inferred decrease in importance of hydrovolcanic processes, which is expected. Maximum xenolith size, which is the average of the three largest lithic clasts measured at each station, also decreases between the lapilli tuffs and the vesicular spatter/scoria units. The largest lithic clasts measured in the lapilli tuffs to date are 2.2 m and 1.5 m in long dimension, and are from the San Andres and Glorieta Sandstone formations, respectively. Other lithic clasts of comparable size were, surprisingly, found in the vesicular spatter/scoria units at South Alkali Butte. These clasts are 2.7 and 3.0 m in long dimension, and are both from gypsum beds that are characteristic of the topmost Yeso Formation. Thus large meter-size blocks were erupted from depths of 500-700 m during both hydrovolcanic and magmatic eruptions at South Alkali Butte.

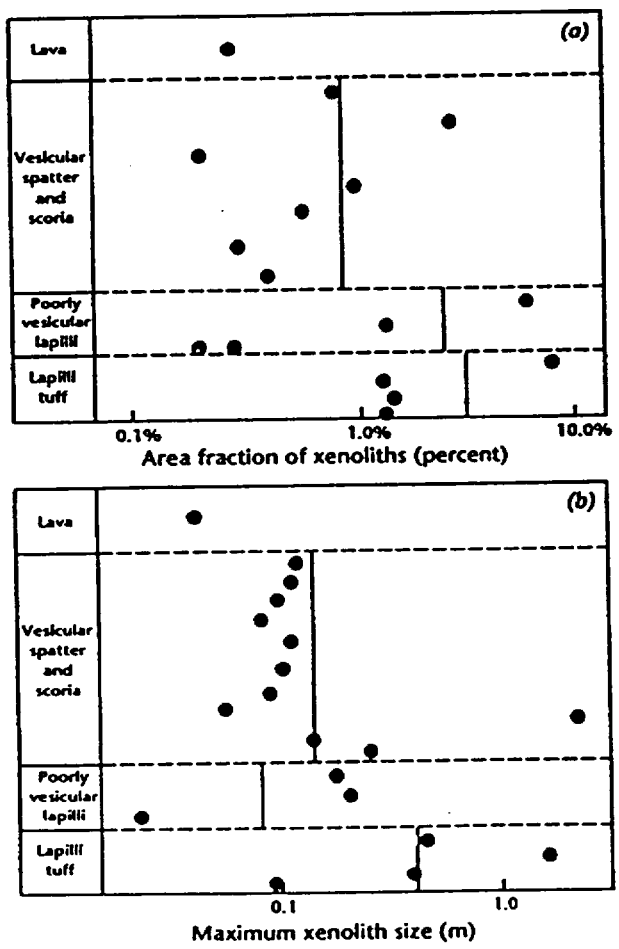

Figure 3. Plots of total area fraction of xenoliths (a) and maximum xenolith size (b) for each of the four main volcanic facies at Alkali Buttes. Note that horizontal scales are logarithmic. Vertical bars represent average values for each facies type.

These are only preliminary data, but it is useful to describe briefly how they will be used to assess eruptive effects at the potential Yucca Mountain repository. Our approach is to collect such data at several sites in a variety of settings. For each eruptive mechanism (related to the deposit facies), we will compile a range of lithic abundances for depths corresponding to the depth of the potential repository horizon. The range of volume fractions from each eruptive mechanism will then be coupled with probabilities and likely eruptive volumes for the different mechanisms to estimate total volumes of repository horizon debris that could be erupted during a volcanic event. Assuming that radioactive waste behaves similarly to the surrounding rocks, we will directly estimate the amount of actual waste erupted (we view this assumption as conservative for reasons detailed in Refs. 1, 2). Maximum xenolith size data provide constraints on the largest fragments that could be erupted in a repository disruption scenario.

Entrainment Mechanisms

It is important to understand the mechanisms by which foreign debris is entrained into a flowing dike or magma conduit in order to constrain the processes of waste disruption. As mentioned above, a theoretical treatment of this process has been elusive, so we have focused on evidence from analog sites. We have focused our initial studies on the Paiute Ridge[2,12,13] and Nye Canyon[14,15] analog sites, both of which are on the eastern border of the Nevada Test Site. Basalt intruded and erupted through silicic tuff from the Timber Mountain-Oasis Valley caldera complex at both sites, thus they are analogous to a potential basaltic event at Yucca Mountain where basalts would intrude similar tuffs. The Paiute Ridge and Nye Canyon sites have been eroded to depths of 100-300 m below their surfaces at the time of basaltic activity, so the processes recorded may be similar to those which would occur at potential repository depths in Yucca Mountain.

We have identified three main entrainment mechanisms at these analog sites (Figure 4): spalling of rock into the tip of a propagating dike, dike wall erosion due to shear from flowing magma, and inclusion of wall-rock material between a main dike and small subparallel offshoot dikes. An additional mechanism, which we do not discuss in detail here, is explosive fracturing of wall-rocks due to magma-water interaction. The first of these mechanisms, spalling into a dike tip, results from the very low pressures inside a crack that is just being pushed open[16] compared to the near lithostatic pressure in adjacent country rocks. Evidence for this process at Paiute Ridge consists of patches of brecciated wall-rock along the margins of a dike (the dike is about 2 m thick) within 20 m of its upper termination. This dike spays into two to three subparallel dikes near its termination, which probably aids in the entrainment process.

Dike wall erosion due to shear is physically similar to erosion of a stream bed. Asperities on a dike wall experience shear (and pressure variations) due to the flowing magma and if this shear is sufficiently strong the asperities will break off the walls. In competent rock such as well-cemented limestones and welded tuffs, this entrainment process is probably of minor importance. Less competent rocks, such as nonindurated shales and nonwelded tuffs, may be more strongly affected by this shear erosion process.

Inclusion of wall-rocks between a main dike and subparallel offshoots is shown at a wide range of scales both at Paiute Ridge and at Nye Canyon. In one example at Paiute Ridge, a ~1 m thick main dike is separated by about 3 m from a thin (10-20 cm) offshoot dike. Between these two dikes the tuff wall-rocks have been compressed and welded by the heat and pressure of the dikes in some places. In others the rocks have been extensively brecciated and form a complex mixture of wall-

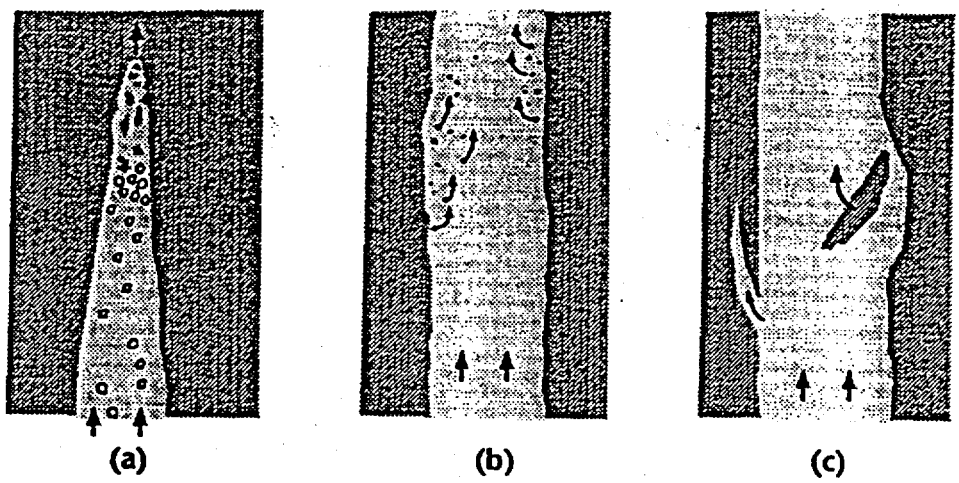

Figure 4. Mechanisms of wall rock entrainment into flowing dikes or conduits. (a) Wall rock spalls off into a propagating dike tip due to the low pressures there. (b) Entrainment by shear erosion of small fragments of wall rock. (c) Entrainment by inclusion, where small offshoot dikes separate fragments of wall rock which are then caught up in the flow of magma in the main dike.

rock breccia and injected basalt (some of the breccia may have been in existence prior to intrusion of the basalts due to a nearby normal fault). Patches of breccia extend into the main dike where they become mixed with progressively more basalt, indicating that the entrainment process was preserved in action when flow in the dike ceased. Numerous smaller scale examples of the inclusion mechanism are preserved at these two analog sites. Typically, small centimeter thick offshoot dikes will extend outward for several centimeters to a few tens of centimeters, then curve back inward to join the main dike. The small "islands" of wall-rock are then caught up in the main flow of magma. We think that the abundance of xenoliths from the Glorieta Sandstone, mentioned in the preceding section, may be a result of this inclusion process. The fractured nature of the sandstone would enhance formation of numerous offshoot dikes, which would result in incorporation of coherent blocks of sandstone more easily than in the overlying formations.

Of these mechanisms, the two that are most likely to effectively entrain intact or partially intact waste packages are the spalling of rock into a propagating dike tip and the inclusion of wall-rocks between main dikes and offshoots. It is clear from the data at Alkali Buttes that blocks with dimensions that are similar to waste packages (1-2 m) can be erupted from depth in small basaltic eruptions, although these are relatively rare. If a volcanic event were to penetrate the potential repository late in the isolation period, after waste packages have corroded, it is likely that waste could be easily incorporated into a dike.

Conduit Geometries

A third aspect of our studies of eruptive effects, which also relates to subsurface effects, is conduit geometries for small basaltic volcanoes. Such volcanoes are fed at depth by dikes, but in the near surface environment these dikes flare and flow becomes concentrated into one or a few near cylindrical conduits. Such geometrical changes could influence the amount of waste that could be intersected by magma if a volcanic event occurred at the potential Yucca Mountain site. We are in the beginning stages of surveying deeply eroded centers where these features have been exposed. Many such plugs or necks are exposed in west central New Mexico where there are good constraints on the elevation of the ground surface at the time of eruptions. We are also studying such features in the southern Great Basin of Nevada, although it is often difficult to constrain original depths because of post volcanic faulting.

SUBSURFACE EFFECTS ($E3_S$) STUDIES

Dikes vs. Sills

The subsurface effects of a dike or dike set, which would be expected to be subvertical, are probably much different from the effects of a subhorizontal sill. These effects would be strongly influenced by the planform of hydrothermal circulation resulting from an intrusion and, in the long-term, by intrusion-induced changes in hydrologic properties of the country rock. We must understand the mechanisms that cause sills to form at shallow depths (within 1 km of the surface) in order to place constraints on the probability of sill emplacement at Yucca Mountain. It is commonly assumed that sills form at a level of neutral buoyancy, where the magma and country rock densities are equal. Evidence from the Paiute Ridge analog site[2,13] suggests that other processes may be important in determining whether a sill is formed from a dike filled with rising magma. Here there are subvertical dikes several kilometers long, and typically only 1-3 m thick, from which sills extend horizontally only locally from the dikes. For example, a sill might extend horizontally from a 100 m long segment of the feeder dike that is several kilometers long. A single long dike can feed two or three separate sills along its length, all at roughly the same level (or depth below the original surface). In addition, at least two of the main feeder dikes extend 100 m or higher above the level of their daughter sills. These observations indicate that sills at Paiute Ridge result from a process other than a level of neutral buoyancy, which would cause a rising dike to divert into a sill along its entire length, and magma in the dike would not be able to flow above the level of neutral buoyancy. Most of the dikes at Paiute Ridge are coplanar with normal faults. We suggest that sills formed where asperities caused local locking along fault planes and hence local reorientation of principle stresses. We are currently exploring ways to test this hypothesis - unfortunately fault planes at Paiute Ridge are often obscured by coplanar intrusions and poor exposure. If this hypothesis is true, then we will be able to utilize subsurface data on faults at Yucca Mountain to assess the probability of sill formation there, given an intrusive event.

Modeling

In addition to field analog studies of subsurface effects, we are using numerical simulation techniques to guide our understanding of the roles of various parameters (e.g., intrusion

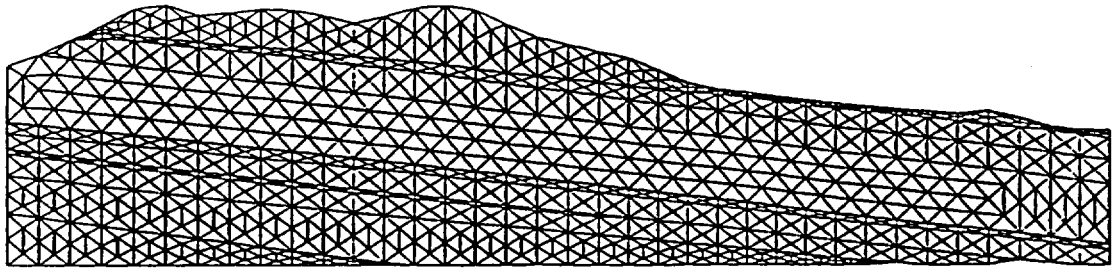

Figure 5. Two dimensional triangular mesh used for finite element modeling of flow of transport at Yucca Mountain.

volume, country rock properties) on hydrothermal and long-term hydrologic processes. This modeling has three components: parameter sensitivity analysis under simplified conditions, simulation of processes at specific analog sites to improve our interpretations of observations, and simulations of subsurface effects at Yucca Mountain. These processes are inherently three dimensional and time dependent, and depend strongly on the distribution of country rock properties such as permeability and thermal conductivity. Therefore we have devoted most of our modeling effort in the past year to developing methods of capturing the complexities of real geologic settings.

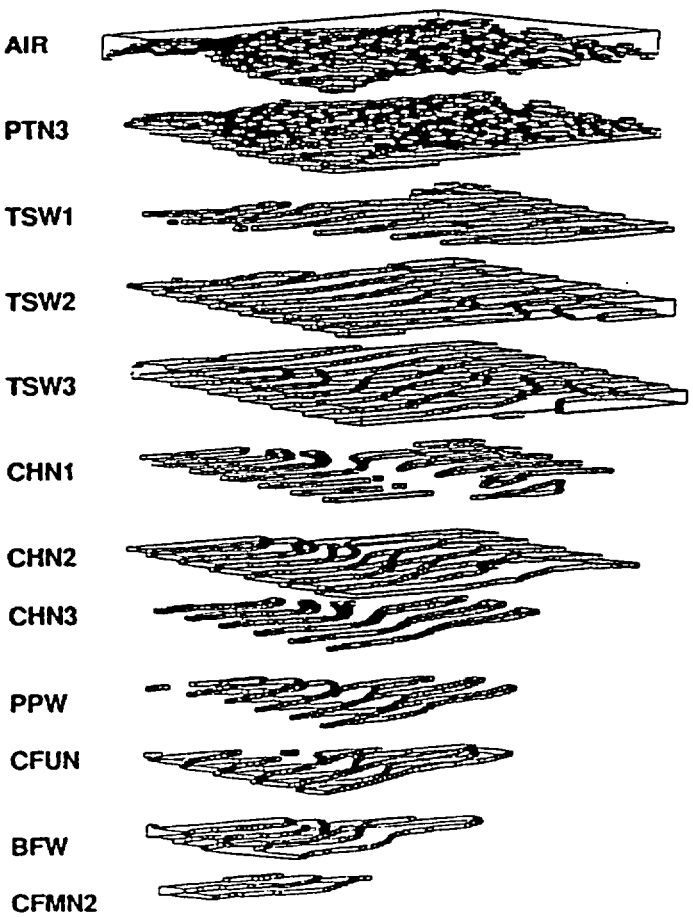

Figure 6. Representation of a three dimensional mesh used for modeling flow, transport, and hydrothermal processes at Yucca Mountain. The mesh has been expanded vertically to show how different stratigraphic units are represented. This is a finite difference mesh (each computational cell is a rectangular brick) with a resolution of 75 m horizontally and 44 m vertically and has a total of 55,981 cells.

We are developing a software package, MESHGEN, to build meshes for general problems, however, a preliminary three dimensional data base of Yucca Mountain stratigraphy produced by Sandia National Laboratory has been the main test data set (Figures 5, 6). The strategy of MESHGEN is to produce three-dimensional tetrahedral meshes (or triangles in two dimensions) which follow the geometry of geologic formations. The user is able to specify variables such as: (1) horizontal and vertical resolution; (2) subsets of data to be extracted for detailed study (e.g., two dimensional cross sections or three dimensional blocks); minimum thickness of stratigraphic units to be represented in the computational mesh; and (4) unit conversion (e.g., input in feet, output in meters). The final mesh produced is a Deleany mesh, which ensures that computations with the finite element code FEHMN will be accurate and stable.

We are currently using MESHGEN to generate meshes for flow and transport calculations for an area that completely encompasses the potential repository boundary. Once these calculations have been completed to establish baseline or ambient conditions, further calculations will investigate the influence of possible magmatic heat sources on the generation of hydrothermal flow in or near Yucca Mountain.

SUMMARY

We have briefly described recent progress in studies of eruptive and subsurface effects of magmatic activity, which will form part of the information that will be used for risk calculations and performance assessment. Eruptive effects studies to date have focused on analog studies of xenolith distribution at basaltic centers of the Lucero volcanic field, New Mexico, where well-characterized basement stratigraphy allows depths of origin to be assigned to erupted lithic fragments. Related field studies are constraining mechanisms by which waste might be entrained into a feeder dike in the event of a volcanic eruption at Yucca Mountain, as well as variations in the geometry of the volcanic plumbing with depth. Subsurface effects studies are focused on a variety of issues including the processes that produce sills, hydrothermal circulation, and long-term hydrologic processes. As these studies proceed, we believe that we will be able to place realistic constraints on the consequences of magmatism at the potential Yucca Mountain repository.

ACKNOWLEDGMENTS

This work is part of the U.S. Department of Energy's Yucca Mountain Site Characterization Project. Field data discussed above can be found in GAV's field notebooks TWS-EES-5-01-93-01 and TWS-EES-5-06-93-01. Computational work described herein has been carried out in a prototyping mode and has not been subject to software quality assurance measures. Illustrations by Mary Ann Olson are greatly appreciated.

REFERENCES

1. G.A. VALENTINE, B.M. CROWE, and F.V. PERRY, "Study Plan 8.3.1.8.1.2 Physical Processes of Magmatism and Effects on the Potential Repository" (in review).

2. G.A. VALENTINE, B.M. CROWE, and F.V. PERRY, "Physical Processes and Effects of Magmatism in the Yucca Mountain Region," *Proceedings, 1992 Conference on High Level Radioactive Waste Management*, Las Vegas, pp. 2344-2355 (1992).

3. J.D.L. WHITE, "Maar-Diatreme Phreatomagmatism at Hopi Buttes, Navajo Nation (Arizona), USA," *Bulletin of Volcanology*, Vol. 53, pp. 239-258 (1991).

4. B.F. HOUGHTON and H.-U. SCHMINCKE, "Mixed Deposits of Simultaneous Strombolian and Phreatomagmatic Volcanism: Rothenberg Volcano, East Eifel Volcanic Field," *Journal of Volcanology and Geothermal Research*, Vol. 30, pp. 117-130 (1986).

5. B.F. HOUGHTON and H.-U. SCHMINCKE, "Rothenberg Scoria Cone, East Eifel: a Complex Strombolian and Phreatomagmatic Volcano," *Bulletin of Volcanology*, Vol. 52, pp. 28-48 (1989).

6. L.G. MASTIN, "The Roles of Magma and Groundwater in the Phreatic Eruptions at Inyo Craters, Long Valley Caldera, California," *Bulletin of Volcanology*, Vol. 53, pp. 579-596 (1991).

7. W.S. BALDRIDGE, F.V. PERRY, and M. SHAFIQULLAH, "Late Cenozoic Volcanism of the Southeastern Colorado Plateau: I. Volcanic Geology of the Lucero Area, New Mexico," *Geological Society of America Bulletin*, Vol. 99, pp. 463-470 (1987).

8. H.L. JICHA, Jr., "Geology and Mineral Resources of Mesa del Oro Quadrangle, Socorro and Valencia Counties, New Mexico," *Bulletin 56*, New Mexico Bureau of Mines and Mineral Resources (1958).

9. R.E. ZILINSKI, Jr., *Geology of the Central Part of the Lucero Uplift, Valencia County, New Mexico*, MS Thesis, University of New Mexico Geology Department (1976).

10. Spanel-Heinze oil well log, #1-M Santa Fe Pacific 9612, Log No. F-278, 5-5N-7W, total depth 4992 feet (1959).

11. E.R. HILL, Sun Oil Company oil well log, #1 Pueblo of Acoma, 2-7N-7W, total depth 4794 feet (1960).

12. F.M. BYERS, Jr., and H. BARNES, "Geologic Map of the Paiute Ridge Quadrangle, Nye and Lincoln Counties, Nevada," *Map GQ-577*, U.S. Geological Survey (1967).

13 B.M. CROWE, S. SELF, D. VANIMAN, R. AMOS, and F.V. PERRY, "Aspects of Potential Disruption of a High-Level Radioactive Waste Repository in Southern Nevada," *Journal of Geology*, Vol. 91, pp. 259-276 (1983).

14. E.N. HINRICHS and E.J. MCKAY, "Geologic Map of the Plutonium Valley Quadrangle, Nye and Lincoln Counties, Nevada," *Map GQ-384*, U.S. Geological Survey (1965).

15. B.M. CROWE, K.H. WOHLETZ, D.T. VANIMAN, E. GLADNEY, and N. BOWER, "Status of volcanic hazards studies for the Nevada Nuclear Waste Storage Investigations, Volume II," *LA-9325-MS*, Los Alamos National Laboratory (1986).

16. J.R. LISTER and R.C. KERR, "Fluid-Mechanical Models of Crack Propagation and Their Application to Magma Transport in Dykes," *Journal of Geophysical Research*, Vol. 96, pp. 10,049-10,077 (1991).

Enclosure 2

Copy of

GEOCHEMISTRY OF THE LATHROP WELLS VOLCANIC CENTER

Los Alamos
NATIONAL LABORATORY

Earth and Environmental Sciences Division
EES-13–Nuclear Waste Management R&D
Mail Stop J521, Los Alamos, NM 87545
Phone (505) 667-9768, Fax (505) 667-1934

THIS IS A YMP MILESTONE

NO. 3397

September 28, 1994

EES-13-09-94-293

Mr. Robert M. Nelson, Jr., Acting Project Manager
ATTN: Mr. Jerry J. Lorenz, REECO/Technical Information Section
Yucca Mountain Site Characterization Project
US Department of Energy
P.O. Box 98608
Las Vegas, NV 89193-8608

Dear Mr. Lorenz:

Approval of Milestone 3397, "Geochemistry of The Lathrop Wells Volcanic Center," by F. Perry and K. Straub

In compliance with YAP 30.12, Milestone 3397, "Geochemistry of the Lathrop Wells Volcanic Center," by F. Perry and K. Straub is enclosed for programmatic review.

This paper will be published as Los Alamos report. It documents work done under WBS 1.2.3.2.5; does not fulfill a Level II milestone requirement; and has undergone technical, policy, and patent/security review.

In compliance with YAP-SIII.3Q, the Los Alamos data tracking number for this record package segment is LA000000000099.001.

Sincerely,

for Julie A. Canepa

JAC/SHK/fer

Enclosures: 1. Paper
2. Review Sheets

Cy w/enc 1
J.R. Dyer, YMSCO, Las Vegas, NV
W.L. Clarke, LLNL, Livermore, CA
L.R. Hayes, USGS, Denver , CO
L.E. Shephard, SNL, Albuquerque, NM
W.B. Simecka, YMSCO, Las Vegas, NV
J. Nesbit, YMSCO, Las Vegas, NV
R.K. St. Clair, M&O/TRW, Las Vegas, NV
J.A. Canepa, EES-13, MS J521
J. Mercer-Smith, EES-13, MS J521

Cy w/enc 1 and 2
S.H. Klein, EES-13, MS J521
F. Perry, EES-13, MS J521
M. Clevenger, EES-13, MS J521

Cy w/o enc
V.F. Iorii, YMSCO, Las Vegas, NV
S.B. Jones, YMSCO, Las Vegas, NV
M.M. Njegomir, EES-13, MS J521
EES-13 File, MS J521

ENCLOSURE 2

Geochemistry Of The Lathrop Wells Volcanic Center

Frank V. Perry and Kelley T. Straub

Los Alamos National Laboratory
Los Alamos, New Mexico

Abstract

Over 100 samples have been gathered from the Lathrop Wells volcanic center to assess different models of basalt petrogenesis and constrain the physical mechanisms of magma ascent in the Yucca Mountain region. Samples have been analyzed for major and trace-element chemistry, Nd, Sr and Pb isotopes, and mineral chemistry. All eruptive units contain olivine phenocrysts, but only the oldest eruptive units contain plagioclase phenocrysts. Compositions of minerals vary little between eruptive units. Geochemical data show that most of the eruptive units at Lathrop Wells defined by field criteria can be distinguished by major and trace-element chemistry. Normative compositions of basalts at Lathrop Wells correlate with stratigraphic position. The oldest basalts are primarily nepheline normative and the youngest basalts are exclusively hypersthene normative, indicating increasing silica saturation with time. Trace-element and major-element variations among eruptive units are statistically significant and support the conclusion that eruptive units at Lathrop Wells represent separate and independent magma batches. This conclusion indicates that magmas in the Yucca Mountain region ascend at preferred eruption sites rather than randomly.

Introduction

The Lathrop Wells volcanic center is the youngest volcanic center in the Yucca Mountain region and has been the primary focus of volcanism studies for the past several years (Crowe et al., 1994). The possibility that the Lathrop Wells center is *polycyclic* (i.e., eruptive activity spanning >10,000 years and involving multiple, independent magma batches) has required an unprecedented level of detail of field and geochronology studies, as well as comprehensive sampling of multiple eruptive units to characterize the geochemistry and assess alternative petrogenetic models (Study Plan 8.3.1.8.5.1, Characterization of Volcanic Features). Approximately 140 geochemical samples have been gathered from the major time-stratigraphic volcanic units of the Lathrop Wells center; subsets of these samples have been analyzed for major-elements, trace-elements, Sr, Nd and Pb isotopic ratios and mineral chemistry.

Geochemical data from Lathrop Wells were obtained for three purposes: (1) to model the magmatic evolution of the volcanic center in order to constrain the nature and dynamics of magma generation and ascent in the Yucca Mountain region, (2) to aid in interpreting the eruptive history of the volcano, primarily by geochemical correlation of eruptive units, and (3) to correlate ashes found in trenched fault exposures near Yucca Mountain with dated eruptive events at Lathrop Wells, thereby constraining the age and timing of fault movement near Yucca Mountain.

The purpose of this report is to present in a single reference all geochemical data obtained from the Lathrop Wells center to date and to describe the basic characteristics of the data. Modeling of the geochemical data to determine the origin of magmas and magmatic evolution of the Lathrop Wells center will be completed in FY96. Sampling, analysis, and correlation of ashes from trenched fault exposures will be completed in FY95.

Overview and Sampling Strategy of the Lathrop Wells Volcanic Center

The Lathrop Wells volcanic center is located approximately 20 km south of the potential Yucca Mountain repository immediately north of interstate highway 95 (Fig. 1). Field, geomorphic, geochronologic and trenching studies have led to the conclusion that the Lathrop Wells center formed during four main eruptive episodes separated by significant periods of inactivity (Fig. 2). Field evidence of significant gaps in eruptive activity between major eruptive episodes includes development of soil horizons, erosional unconformities, and differences in the degree of geomorphic preservation of eruptive features (Crowe et al., 1994). Each of the four major eruptive episodes at Lathrop Wells is defined as a *chronostratigraphic unit*, and contains one or more *eruptive units* (a volcanic deposit [lava flow or scoria fall] formed during a single time-synchronous volcanic eruption).

Chronostratigraphic unit I is the oldest eruptive episode and includes four lava flows (Ql1a-d) erupted from multiple, north to northwest-trending fissure zones marked by scoria and spatter deposits (Fig. 2). Chronostratigraphic unit II consists of the largest volume lava flow erupted at Lathrop Wells (Ql2a) on the east side of the center, several minor flow lobes on the northeast side of the center, and two sets of northwest trending scoria mounds. A wide-spread and voluminous scoria-fall and pyroclastic deposit (Qs2fs) is interbedded with the lava flows of chronostratigraphic unit II and is inferred to have erupted from a vent concealed beneath the main cinder cone of chronostratigraphic unit III. The eruptive events of chronostratigraphic unit III formed the main cinder cone (Qs3) on the west side of the center and a small-volume lava flow (Ql3) erupted from a vent on the northeast side of the center. Chronostratigraphic unit IV consists of three small-volume tephra units (Qs4a-c) erupted from a group of inferred vents south of the main cinder cone which have presumably been removed by commercial quarrying activity.

The strategy for geochemical sampling at Lathrop Wells was developed to answer the question of whether separate eruptive units defined by field geologic studies have distinct geochemical compositions. If geochemical variations exist, petrologic modeling can be used to infer the magmatic processes responsible for the variations, and thus provide insight into the physical processes responsible for the formation of basaltic volcanoes in the Yucca Mountain region. Because the range of geochemical variation at Lathrop Wells was assumed to be small, an initial concern was whether internal heterogeneity within individual eruptive units was greater than potential variations among eruptive units. For this reason, several (generally 3-6) samples were taken from each

eruptive unit to establish the degree of internal geochemical variation, and to allow statistical comparison of eruptive units (Fig. 3).

Results

Geochemical data from the Lathrop Wells volcanic center was gathered as part of Study Plan 8.3.1.8.5.1, Characterization of Volcanic Features. These data include whole-rock major-element and trace-element data obtained by x-ray fluorescence (XRF), whole-rock trace-element data obtained by instrumental neutron activation analysis (INAA) and isotope dilution, whole-rock Nd, Sr and Pb isotopic analyses obtained by solid source mass spectrometry, and mineral chemistry obtained by electron microprobe. In this report, all analytical results presented in tables and graphs are grouped by chronostratigraphic unit or eruptive unit.

Major-element chemistry

One hundred nineteen whole-rock samples from Lathrop Wells were analyzed for major-element analyses at Los Alamos by XRF following the methods described in Los Alamos Detailed Procedure LANL-EES-DP-111, R3 (Table 1). The range of major-element variation among basalts from the Lathrop Wells center is not large. All are classified as alkali basalts in terms of total alkalis versus silica, using the classification of Cox et al, 1979 (Fig. 4).

A commonly used indicator of the degree of major-element evolution of a basalt due to fractional crystallization is *Mg number*, defined as $\left[\left(\frac{Mg}{Mg + Fe^{2+}}\right) \times 100\right]$, where Mg and Fe are the cation abundance. Unfractionated, primitive basalts in equilibrium with mantle olivine have Mg numbers in the range 68-72. Mg numbers of Lathrop Wells basalt cluster tightly around a value of about 54 (Fig. 5), indicating significant fractionation of either olivine or clinopyroxene prior to eruption (Crowe et al., 1994).

Normative compositions of Lathrop Wells basalt range from about 3 % normative nepheline to 15% normative hypersthene (Table 1). The variations in normative composition generally correlate with chronostratigraphic unit, with a trend of increasing silica saturation with decreasing age (Fig. 6). Basalts of chronostratigraphic unit I are primarily nepheline normative, basalts of chronostratigraphic unit II contain both normative nepheline and hypersthene, basalts of chronostratigraphic unit III are primarily hypersthene normative, and basalts of chronostratigraphic unit IV are exclusively hypersthene normative with normative hypersthene contents as high as 15%.

Trace-element chemistry

Whole rock trace-element analyses of V, Cr, Ni, Zn, Rb, Sr, Y, Zr, Nb and Ba were performed at Los Alamos by XRF using the procedures described in LANL-EES-DP-111, R3 (Table 1). Table 2 lists whole rock trace-element INAA analyses of Rb, Sc, Co, Sr, Ba, La, Ce, Nd, Sm, Eu, Tb, Yb, Lu, Hf, Ta and Th for 99 samples analyzed at Washington University, St. Louis, using procedures described in Korotev (1987). For each of three sample groups analyzed at Washington University, four blind replicate samples were analyzed to monitor analytical precision (Table 3). The replicate analyses indicate that all trace elements except Rb and Nd have analytical precision of <3%. Table 4 lists sixteen samples analyzed for Sm, Nd, Rb, Sr and Pb by isotope dilution at the University of Colorado using procedures described in Farmer et al. (1991). Analytical precision based on 6 replicate analyses is <1% for Sm, Nd, and Sr, and approximately 2% and 3% for Rb and Pb, respectively (Table 5).

Lathrop Wells basalts are notable in having high concentrations of trace elements such as the rare earth elements, Sr, Ba and Th compared to typical alkali basalts, combined with low concentrations of Rb (Vaniman et al., 1982). While part of the trace-element enrichment may be due to fractionation processes, an unusual trace-element enriched lithospheric mantle source is probably the primary cause (Vaniman et al., 1982; Farmer et al., 1989).

Isotope chemistry

Isotopic compositions of Nd, Sr and Pb for 16 Lathrop Wells basalts (Table 4) were analyzed at the University of Colorado using methods described in Farmer et al. (1991). Analytical precision based on 6 replicate analyses is 0.001% for $^{143}Nd/^{144}Nd$, 0.002% for $^{87}Sr/^{86}Sr$, 0.114% for $^{208}Pb/^{204}Pb$, 0.085% for $^{207}Pb/^{204}Pb$ and 0.058% for $^{206}Pb/^{204}Pb$ (Table 5).

The total range in Nd and Sr isotopic compositions at Lathrop Wells is fairly small with ε_{Nd} values ranging from -9.7 to -10.3 and $^{87}Sr/^{86}Sr$ ranging from about 0.7070 to 0.7071 (Fig. 7). As a group, samples of chronostratigraphic unit I have slightly higher $^{87}Sr/^{86}Sr$ (mean=0.707054, n=5) than samples of chronostratigraphic unit II (mean=0.0707016, n=7). This difference is statistically significant at the 95% confidence level using the two-tailed *t* test. The Sr and Nd isotopic compositions of Lathrop Wells basalts are highly unusual for continental alkali basalts of the western U.S. and indicate derivation from a trace-element enriched lithospheric mantle source (Farmer et al., 1989).

Petrography and Mineral Chemistry

Basalts of Lathrop Wells are sparsely porphyritic with phenocrysts of olivine and plagioclase in a fine-grained groundmass of plagioclase, olivine, titanomagnetite and clinopyroxene. The percentage of olivine phenocrysts is fairly constant at 1-4% for basalts of most eruptive units (Fig. 8). Plagioclase phenocrysts and microphenocrysts are

most abundant in eruptive units of chronostratigraphic unit I. Plagioclase phenocrysts are largely absent in basalts of chronostratigraphic unit II, III and IV (Fig. 8).

Mineral chemistry was obtained by electron microprobe using methods described in Los Alamos Detailed Procedure LANL-EES-DP-131, R0. Mineral chemistry does not vary significantly by eruptive unit. The maximum forsterite content of analyzed olivine phenocrysts from all eruptive units is 78±1% (Figs. 9-16). In every case, olivine from lava flows is more zoned (Figs. 9-11, 13) than olivine from tephra units (Figs. 12, 14-16), probably because tephra was quickly quenched upon eruption, while lava flows cooled more slowly, allowing continued crystal growth after eruption. Olivine from tephra units show very limited zoning (<2% forsterite content) and also in some cases display slight reverse zoning (e.g., Fig. 14). Compositions of olivine are listed in Tables 6-13.

Plagioclase phenocrysts occur in units Ql1b, Ql1c, and Ql1d of chronostratigraphic unit I. The phenocrysts are moderately zoned labradorite with An contents ranging from about An 69 to An 60 (Figs. 17-18). Compositions of groundmass plagioclase in lavas of chronostratigraphic unit I (Ql1d and Ql1b) extend to significantly more sodic compositions (Figs. 19-20), while compositions of groundmass plagioclase in lavas of chronostratigraphic unit II and III (Ql2a and Ql3) include compositions as calcic as phenocrysts in lavas of chronostratigraphic unit I (Figs. 21-22). Compositions of plagioclase are listed in Tables 14-17.

Clinopyroxene occurs as a groundmass phase in all of the lava units at Lathrop Wells. We analyzed groundmass clinopyroxene from eruptive units Ql1d and Ql2a. Clinopyroxenes from unit Ql1d have higher MgO and less TiO_2 than clinopyroxene from Ql2a (Figs. 23-24, Tables 18-19).

Magnetite occurs as inclusions in olivine and in the groundmass of all eruptive units. Magnetites are titaniferous (7-22% TiO_2) and magnetite inclusions in olivine generally have higher Cr concentrations that magnetite from the groundmass (Tables 20-23).

Geochemistry of Eruptive Units

To illustrate the range of compositional variations within eruptive units and differences between eruptive units, we have created normalized line plots of compositions of individual samples grouped by eruptive unit (Figs. 25-36). All of the major and trace elements so plotted are incompatible during fractionation of olivine, the major phenocryst phase in these rocks. Sample compositions were normalized to the average Lathrop Wells composition using a combination of XRF and INAA data (n=99). This approach emphasizes similarities and differences between samples at Lathrop Wells and allows direct inspection of percent differences between samples. In general, individual eruptive units are geochemically homogeneous and show a limited range of geochemical variation (e.g., Figs. 25-28, 32-33, 35-36). The voluminous lava flow and tephra fall deposit of chronostratigraphic unit II appear to have the most internal heterogeneity (Figs. 30-31).

Averaged compositions of the major eruptive units grouped by chronostratigraphic unit are illustrated in Figs. 37-40. In general, individual eruptive units within each of the four chronostratigraphic units share similar geochemical characteristics. All of the eruptive units within chronostratigraphic unit I show similar geochemical patterns that include relatively low concentrations of Th and La, and relatively high concentrations of K, Sr, P, Sm, Eu and Ti compared to the Lathrop Wells compositional mean (Fig. 37). Eruptive units within chronostratigraphic unit II are characterized by a lack of significant variation from the mean Lathrop Wells composition (Fig. 38). The two eruptive units of chronostratigraphic unit III are geochemically similar and are marked by high concentrations of Th and low concentrations of Sr, P, Sm, Eu and Ti (Fig. 39). The three eruptive units of chronostratigraphic unit IV are geochemically diverse. Eruptive unit Qs4b is distinguished from all other eruptive units at Lathrop Wells by having the highest concentrations of Th and Rb (Rb not plotted, see Tables 1 and 2), and the lowest concentrations of Sr and Ti (Fig. 40). Eruptive unit Qs4c is characterized by generally low concentrations of all incompatible elements (Fig. 40). The geochemical differences between eruptive units should permit correlation of ashes in trenched fault exposures near Yucca Mountain to individual eruptive units at Lathrop Wells.

Isotope dilution is a high-precision method of determining trace-element concentrations (Table 5) and offers an independent method of assessing geochemical differences between eruptive units. The isotope dilution data are compatible with the INAA data discussed above and show that most eruptive units are geochemically distinct, with eruptive units of chronostratigraphic unit I having the highest concentrations of Sr and the middle rare-earth elements (Nd and Sm), and unit Ql4c having the lowest concentrations of Sr, Nd and Sm (Figs. 41-42).

At what level are differences in the mean compositions of different eruptive units statistically significant? As an example, we consider eruptive units Ql1a and Ql1d, adjacent lava flows which show moderate (1-8%) differences in average elemental concentrations (Fig. 43). To test for the statistical significance of these differences, we use the two-tailed *t* test, which calculates the probability that two sample means are equal. Probabilities of < 0.05 indicate that two sample means represent different populations at the 95% confidence level. In the case of Ql1d and Ql1a, the average concentrations of Ba, Th, K, Ce, Sr and Eu can be distinguished at the 95% confidence level (Fig 43). From these results, we conclude that differences in average elemental concentrations as small as 1-2% are statistically significant for elements with the highest analytical precision (e.g., Ce, Table 3) and are almost always significant for average differences of >3-4%. Differences in average elemental concentrations between eruptive units of different chronostratigraphic units are commonly 5-10% and are >35% in the case of Th (Figs. 37-40).

The capability of geochemically discriminating eruptive units at Lathrop Wells provides a useful tool for constraining the eruptive history of the center and to tie the eruptive history to tectonic studies of the Yucca Mountain region. For example, the most

voluminous tephra and pyroclastic surge deposit at Lathrop Wells (Qs2fs) was assumed, by analogy to other basalt centers, to be part of the eruptions which formed the main cinder cone of chronostratigraphic unit III (Figure 2). Because of its volume and widespread distribution, ash of unit Qs2fs is most likely the dominant ash found in fault exposures near Yucca Mountain. Geochemical differences between eruptive units Qs2fs and Qs3 indicate that the two eruptive units are not the same (Fig. 44). This observation, combined with stratigraphic and geomorphic evidence, led to the assignment of unit Qs2fs to chronostratigraphic unit II (Crowe et al., 1994). This interpretation places the inferred correspondence of volcanic and tectonic activity recorded by ashes in fault fissures farther in the geologic past. The ability to discriminate eruptive units at Lathrop Wells will provide the primary basis for correlating basaltic ashes in trenched fault exposures near Yucca Mountain to dated eruptive units at Lathrop Wells.

The earliest evidence that the Lathrop Wells volcanic center is polycyclic was the recognition of a soil horizon between tephra unit Qs4b and underlying tephra of Qs3, the deposits of the main scoria cone (Wells et al., 1988). The soil was interpreted to represent a hiatus between eruptions at Lathrop Wells of at least several thousand years. An alternative interpretation was that tephra Qs4b is reworked tephra from the slope of the main cinder cone, an interpretation which does not require a polycyclic history of the center (Turrin et al., 1992). Geochemical differences between Qs3 and Ql4b confirm that Ql4b cannot be reworked tephra from Qs3 (Fig. 45). Its unique geochemical composition compared to all other Lathrop Wells eruptive units, combined with a thermoluminescence date of ~ 4 ka on the underlying soil, indicate that it represents a distinct eruptive episode and supports the conclusion that the Lathrop Wells center is polycyclic with eruptions that extended into the Holocene (Crowe et al., 1994).

A final example of how geochemical correlation can provide evidence of polycyclic activity is the relationship between vent conduits and overlying tephra in the southeast quarry area. The tephra overlying these conduits was assumed to be related to the conduits on the basis of field mapping. Geochemical data show that the vent conduits are geochemically similar to lavas of chronostratigraphic unit I and are in the appropriate location for vents of the southern flows of chronostratigraphic unit I (Fig. 2). The overlying tephra unit, however, is geochemically distinct from the vent conduits and most similar to tephra of Qs2fs (Fig. 46). The vent conduits were significantly stripped and eroded before emplacement of the overlying, geochemically distinct tephra, signifying a significant period of geologic time between the emplacement of the conduits and the overlying tephra.

In detail, geochemical differences between eruptive units at Lathrop Wells cannot be accounted for by simple fractional crystallization of a single magma batch (Crowe et al., 1994). For instance, variations of Th/K at the same Mg number for the major eruptive units of chronostratigraphic unit I, II, and III indicate at least 4 separate magma batches. (Fig. 47). Preliminary modeling of more complex magmatic processes including magma recharge also indicate the existence of distinct magma batches.

Implications for Volcanic Risk Assessment

Field, geomorphic and geochemical evidence indicate a complex and extended eruptive history at Lathrop Wells involving multiple magma batches and several eruptive episodes that were separated by significant periods of inactivity. The eruption of several independent magma batches at a single location in the Yucca Mountain region suggests that eruptions in the region will not occur at random locations in the near future (10^4-10^5 years), but probably near the site of previous eruptions at Lathrop Wells. If this conclusion of preferred eruption sites is correct, the calculated probability of magma ascending at the potential Yucca Mountain repository during the next 10,000 years is lower than that calculated for models which assume random sites of future eruptions.

Acknowledgments

Sample and data collection information and documentation for this report are contained in Field Notebooks TWS-EES-13-LV-12-89-03 and EES-13-LV-02-93-07, Sample Logbooks TWS-EES-13-LV-12/89-04, TWS-EES-13-LV-04-91-01 and LA-EES-13-05-94-006, and Scientific Notebooks TWS-EES-13-LV-12-89-05 and TWS-EES-13-07-93-044. The Los Alamos Data Tracking Number for this report is LA000000000099.001. This work was supported by the Yucca Mountain Site Characterization Project Office as part of the Civilian Radioactive Waste Management Program. This program is managed by the U.S. Department of Energy, Yucca Mountain Site Characterization Office.

References

Cox, K. G., J. D. Bell, and R. J. Pankhurst, "The interpretation of igneous rocks," George Allen & Unwin Ltd, London, 450 pp. (1979).

Crowe, B. C., F. V. Perry, J. Geissman, L. McFadden, S. Wells, M. Murrell, J. Poths, G. A. Valentine, L. Bowker, and K. Finnegan, "Status of Volcanism Studies for the Yucca Mountain Site Characterization Project," *Los Alamos National Laboratory Report*, in press (1994)

Farmer, G. L., F. V. Perry, S. Semken, B. Crowe, D. Curtis, and D. J. DePaolo, "Isotopic evidence on the structure and origin of subcontinental lithospheric mantle in southern Nevada," *Journal of Geophysical Research* 94, 7885-7898 (1989).

Farmer, G. L, D. E. Broxton, R. G. Warren, and W. Pickthorn, "Nd, Sr, and O isotopic variations in metaluminous ash-flow tuffs and related volcanic rocks at the Timber Mountain/Oasis Valley caldera complex, SW Nevada: implications for the origin and evolution of large-volume silicic magma bodies," *Contrib. Mineral. Petrol.* 109, 53-68 (1991).

Korotev, R. L., "National Bureau of Standards coal flyash (SRM 1663a) as a multielement standard for instrumental neutron activation analysis," *Journal of Radioanalytical and Nuclear Chemistry*, 110, 159-177 (1987).

Turrin, B. D., D. E. Champion, and R. J. Fleck, "Measuring the age of the Lathrop Wells volcanic center at Yucca Mountain-Reply," *Science* 257, 556-558 (1992).

Vaniman, D. T., B. M. Crowe, and E. S. Gladney, "Petrology and geochemistry of hawaiite lavas from Crater Flat, Nevada," *Contrib. Mineral. Petrol.* 80, 341-357 (1982).

Wells, S. G., L. D. McFadden, C. E. Renault, and B. M. Crowe, "Geomorphic assessment of late Quaternary volcanism in the Yucca Mountain area, southern Nevada: Implications for the proposed high-level waste repository," *Geology* 18, 549-553 (1990).

Figure Captions

Figure 1. Location of Lathrop Wells in relation to the potential Yucca Mountain repository. From oldest to youngest, basaltic volcanic centers are Thirsty Mesa (TM), Buckboard Mesa (BB), Amargosa Valley (AV), Crater Flat (CF), Sleeping Butte (SB) and Lathrop Wells (LW).

Figure 2. Geologic map of the Lathrop Wells volcanic center.

Figure 3. Geochemistry sample locations at the Lathrop Wells volcanic center.

Figure 4. Alkalis versus silica for basalts of Lathrop Wells. All of the basalts of Lathrop Wells are classified as alkaline basalt according to the classification scheme of Cox et al. (1979).

Figure 5. Histogram of Mg numbers for basalts of Lathrop Wells.

Figure 6. Normative compositions of Lathrop Wells basalts grouped by chronostratigraphic unit (Fig. 2) plotted within ternary fields bounded by Ne-Ol-Di-Hy.

Figure 7. ε_{Nd} versus $^{87}Sr/^{86}Sr$ for eruptive units of the Lathrop Wells volcanic center.

Figure 8. Percent olivine and plagioclase phenocrysts and microphenocrysts determined by point counting for representative samples of eruptive units from the Lathrop Wells volcanic center. Samples counted from each eruptive unit are LW20FVP from Ql1d, LW73FVP from Ql1b, LW11FVP from Ql1a, LW40FVP from Ql2a, LW97FVP from Qs2fs, LW61FVP from Ql3, LW80FVP from Qs3, LW78FVP from Qs4b and LW151 from Qs4a.

Figure 9. Forsterite content of olivine phenocrysts from LW21FVP of Ql1d determined by rim to rim microprobe traverses.

Figure 10. Forsterite content of olivine phenocrysts from LW73FVP of Ql1b determined by rim to rim microprobe traverses.

Figure 11. Forsterite content of olivine phenocrysts from LW40FVP of Ql2a determined by rim to rim microprobe traverses.

Figure 12. Forsterite content of olivine phenocrysts from LW135FVP of Qs2fs determined by rim to rim microprobe traverses.

Figure 13. Forsterite content of olivine phenocrysts from LW61FVP of Ql3 determined by rim to rim microprobe traverses.

Figure 14. Forsterite content of olivine phenocrysts from LW80FVP of Qs3 determined by rim to rim microprobe traverses.

Figure 15. Forsterite content of olivine phenocrysts from LW78FVP of Qs4b determined by rim to rim microprobe traverses.

Figure 16. Forsterite content of olivine phenocrysts from LW151FVP of Qs4a determined by rim to rim microprobe traverses.

Figure 17. Anorthite content of plagioclase phenocrysts from LW21FVP of Ql1d determined by rim to rim microprobe traverses.

Figure 18. Anorthite content of plagioclase phenocrysts from LW73FVP of Ql1b determined by rim to rim microprobe traverses.

Figure 19. Feldspar compositions from LW21FVP of Ql1d plotted within the ternary field Or-Ab-An. Open squares are compositions of phenocryst interiors, open circles are compositions of phenocryst rims and groundmass crystals.

Figure 20. Feldspar compositions from LW73FVP of Ql1b plotted within the ternary field Or-Ab-An. Open squares are compositions of phenocryst interiors, open circles are compositions of phenocryst rims and groundmass crystals.

Figure 21. Feldspar compositions from LW40FVP of Ql2a plotted within the ternary field Or-Ab-An. Open circles are compositions of groundmass crystals.

Figure 22. Feldspar compositions from LW61FVP of Ql3 plotted within the ternary field Or-Ab-An. Open circles are compositions of groundmass crystals.

Figure 23. Pyroxene compositions from LW21FVP of Ql1d plotted within the ternary field Wo-En-Fs. Filled circles are compositions of groundmass crystals.

Figure 24. Pyroxene compositions from LW40FVP of Ql2a plotted within the ternary field Wo-En-Fs. Filled circles are compositions of groundmass crystals.

Figure 25. Line plot of incompatible element concentrations for samples of eruptive unit Ql1a normalized to the average concentration of each element for all analyzed Lathrop Wells samples (n=99). Normalizing values are Ba=1361.96 parts per million (ppm), Th=6.867 ppm, K=15,249.49 ppm, Ta=1.378 ppm, La=93.353 ppm, Ce=181.668 ppm, Sr=1469.56 ppm, P=5298.62 ppm, Sm=12.239 ppm, Eu=3.149 ppm, Zr=370.652 ppm, Hf=7.219 ppm, Ti=11,522.39 ppm, Tb=1.135 ppm, Yb=2.369 ppm, Lu=.344 ppm. Ba, K, Sr, P, Zr and Ti were determined by XRF; all other elements determined by INAA.

Figure 26. Line plot of incompatible element concentrations for samples of eruptive unit Ql1b normalized to the average concentration of each element for all analyzed Lathrop Wells samples (n=99).

Figure 27. Line plot of incompatible element concentrations for samples of eruptive unit Ql1c normalized to the average concentration of each element for all analyzed Lathrop Wells samples (n=99).

Figure 28. Line plot of incompatible element concentrations for samples of eruptive unit Ql1d normalized to the average concentration of each element for all analyzed Lathrop Wells samples (n=99).

Figure 29. Line plot of incompatible element concentrations for samples of eruptive unit Qs1u normalized to the average concentration of each element for all analyzed Lathrop Wells samples (n=99). Qs1u represents all analyzed vents of chronostratigraphic unit I.

Figure 30. Line plot of incompatible element concentrations for samples of eruptive unit Ql2a normalized to the average concentration of each element for all analyzed Lathrop Wells samples (n=99).

Figure 31. Line plot of incompatible element concentrations for samples of eruptive unit Qs2fs normalized to the average concentration of each element for all analyzed Lathrop Wells samples (n=99).

Figure 32. Line plot of incompatible element concentrations for samples of eruptive unit Ql3 normalized to the average concentration of each element for all analyzed Lathrop Wells samples (n=99).

Figure 33. Line plot of incompatible element concentrations for samples of eruptive unit Qs3 normalized to the average concentration of each element for all analyzed Lathrop Wells samples (n=99).

Figure 34. Line plot of incompatible element concentrations for samples of eruptive unit Qs4a normalized to the average concentration of each element for all analyzed Lathrop Wells samples (n=99).

Figure 35. Line plot of incompatible element concentrations for samples of eruptive unit Qs4b normalized to the average concentration of each element for all analyzed Lathrop Wells samples (n=99).

Figure 36. Line plot of incompatible element concentrations for samples of eruptive unit Qs4c normalized to the average concentration of each element for all analyzed Lathrop Wells samples (n=99).

Figure 37. Line plot of average compositions of eruptive units from chronostratigraphic unit I.

Figure 38. Line plot of average compositions of eruptive units from chronostratigraphic unit II.

Figure 39. Line plot of average compositions of eruptive units from chronostratigraphic unit III.

Figure 40. Line plot of average compositions of eruptive units from chronostratigraphic unit IV.

Figure 41. Rb versus Nd (ppm) for eruptive units of the Lathrop Wells volcanic center.

Figure 42. Sr versus Sm (ppm) for eruptive units of the Lathrop Wells volcanic center.

Figure 43. Line plot comparing average compositions of eruptive units Ql1a and Ql1d. Values below each element are the probability that the sample means of each element represent the same populations using the two-tailed *t* test. Values in bold indicate elements with statistically significant (95% confidence level) differences in average composition (also indicated by data points enclosed in rectangles).

Figure 44. Line plot comparing average compositions of eruptive units Qs3 and Qs2fs. Average concentrations of Th and Ti for the two units are statistically different at the 95% confidence level using the two-tailed *t* test.

Figure 45. Line plot comparing average compositions of eruptive units Qs3 and Qs4b.

Figure 46. Line plot comparing samples from Qs1 vent conduits (dashed lines) and samples of oxidized scoria that are probably part of scoria fall sheet Qs2fs (solid lines).

Figure 47. Mg number versus Th/K for selected eruptive units of the Lathrop Wells volcanic center. Arrow represents the qualitative change in Mg number and Th/K for a magma undergoing fractional crystallization of olivine, clinopyroxene, or plagioclase. Different Th/K values of eruptive units indicate that the units are not derived from a single magma undergoing fractional crystallization.

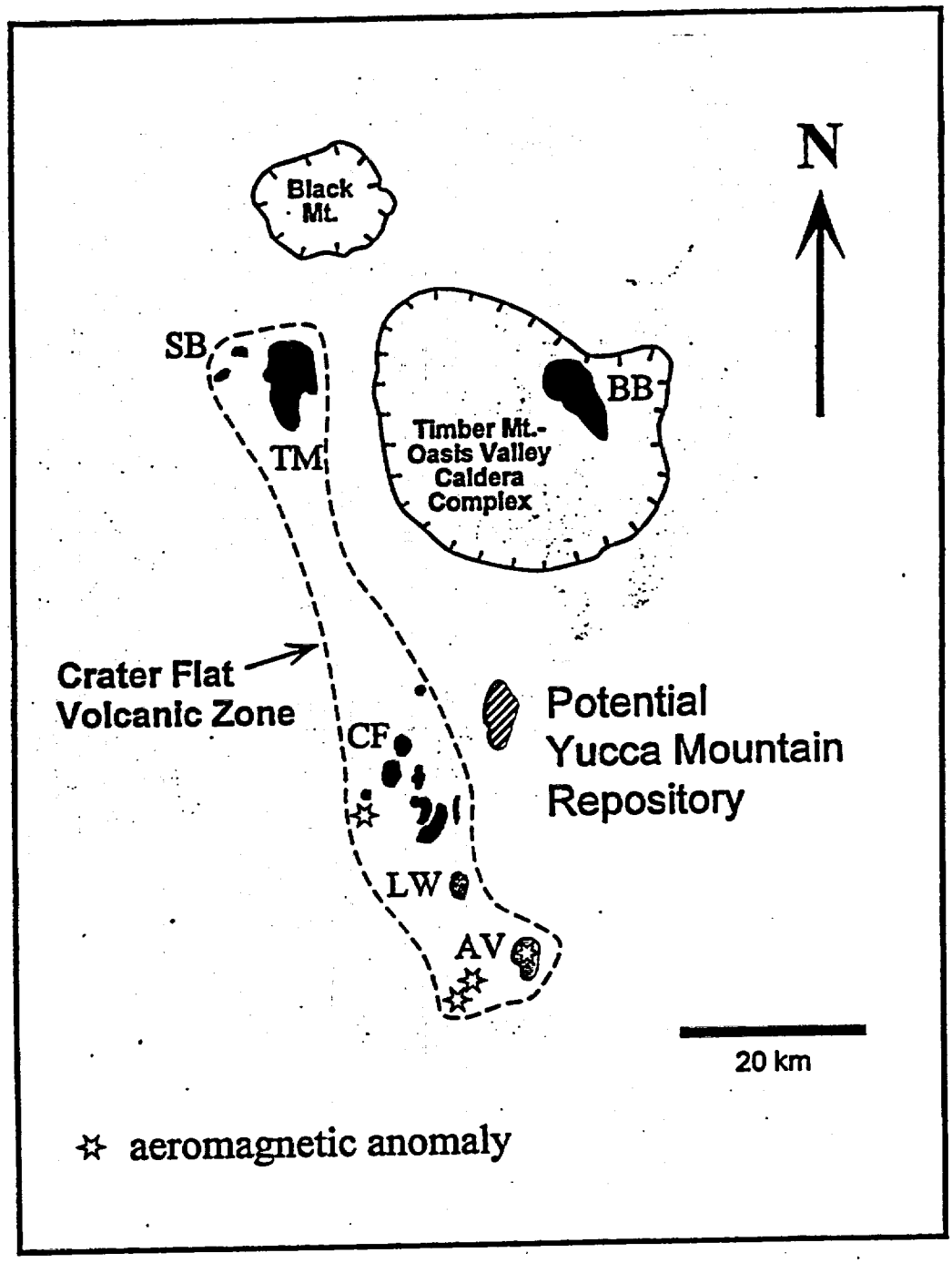
N
Black Mt.
SB
TM
BB
Timber Mt.-Oasis Valley Caldera Complex
Crater Flat Volcanic Zone
CF
LW
AV
Potential Yucca Mountain Repository
20 km
aeromagnetic anomaly

Figure 1

Lathrop Wells Volcanic Center

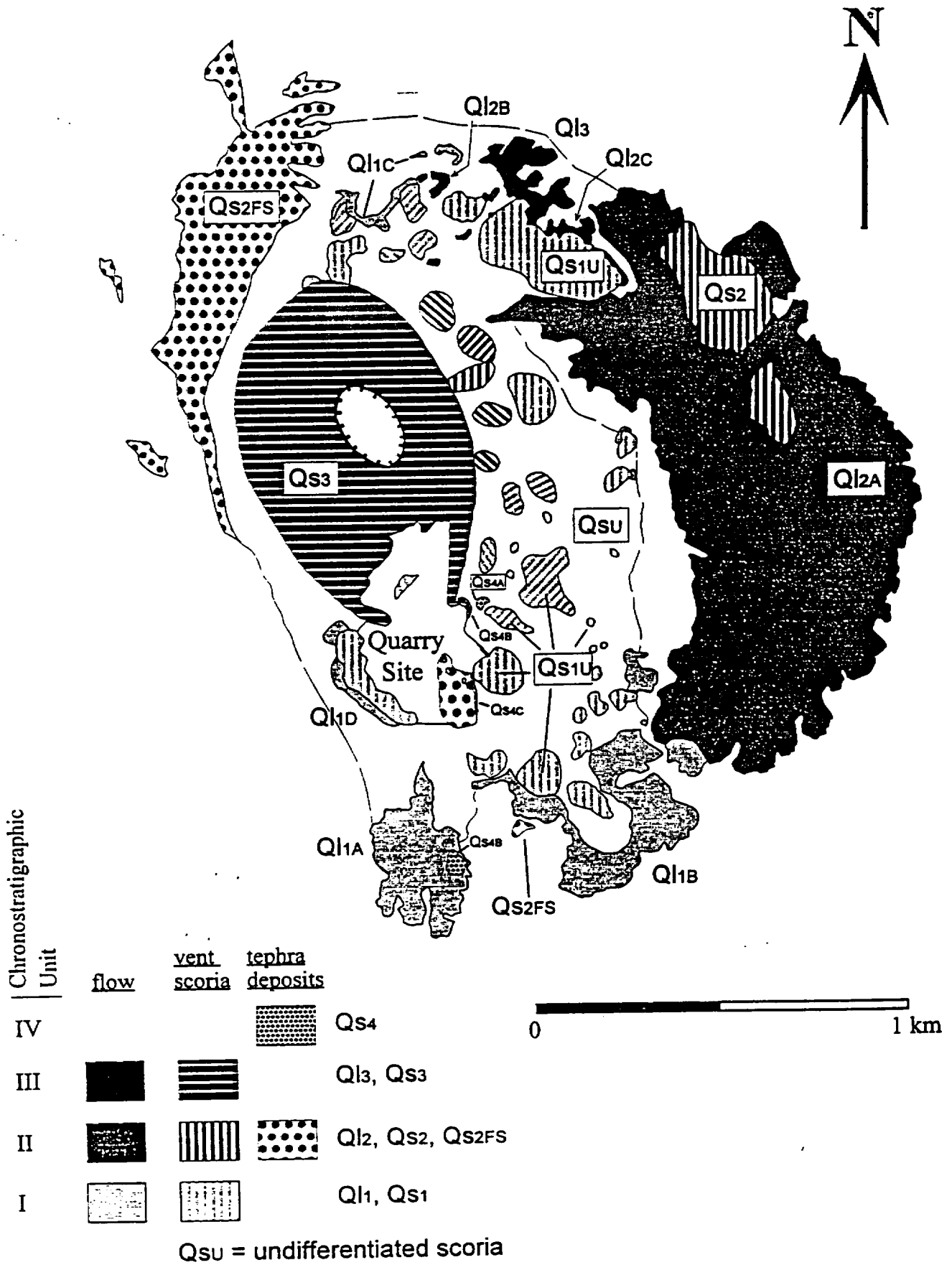

Figure 2

Geochemistry sample locations, Lathrop Wells volcanic center

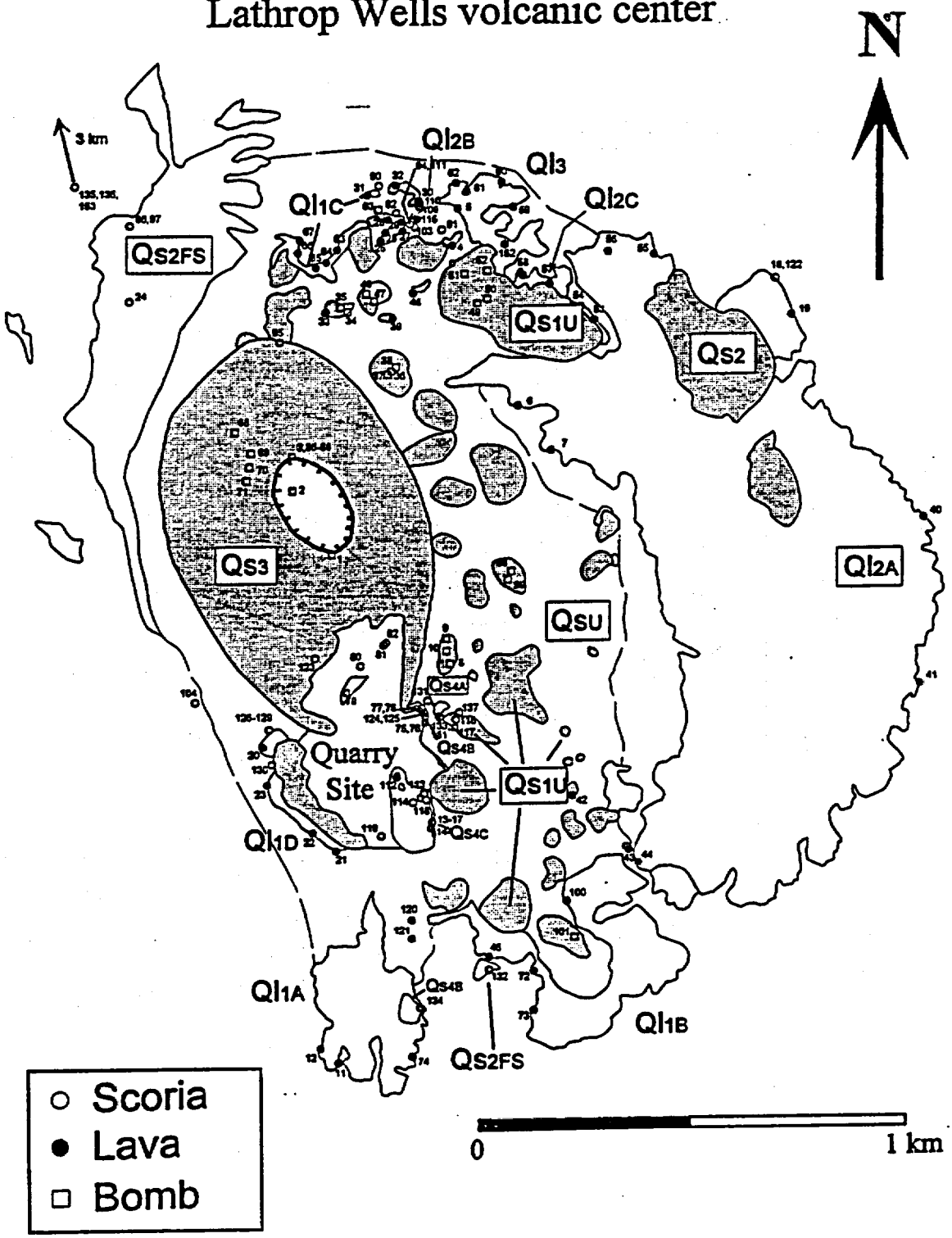

Figure 3

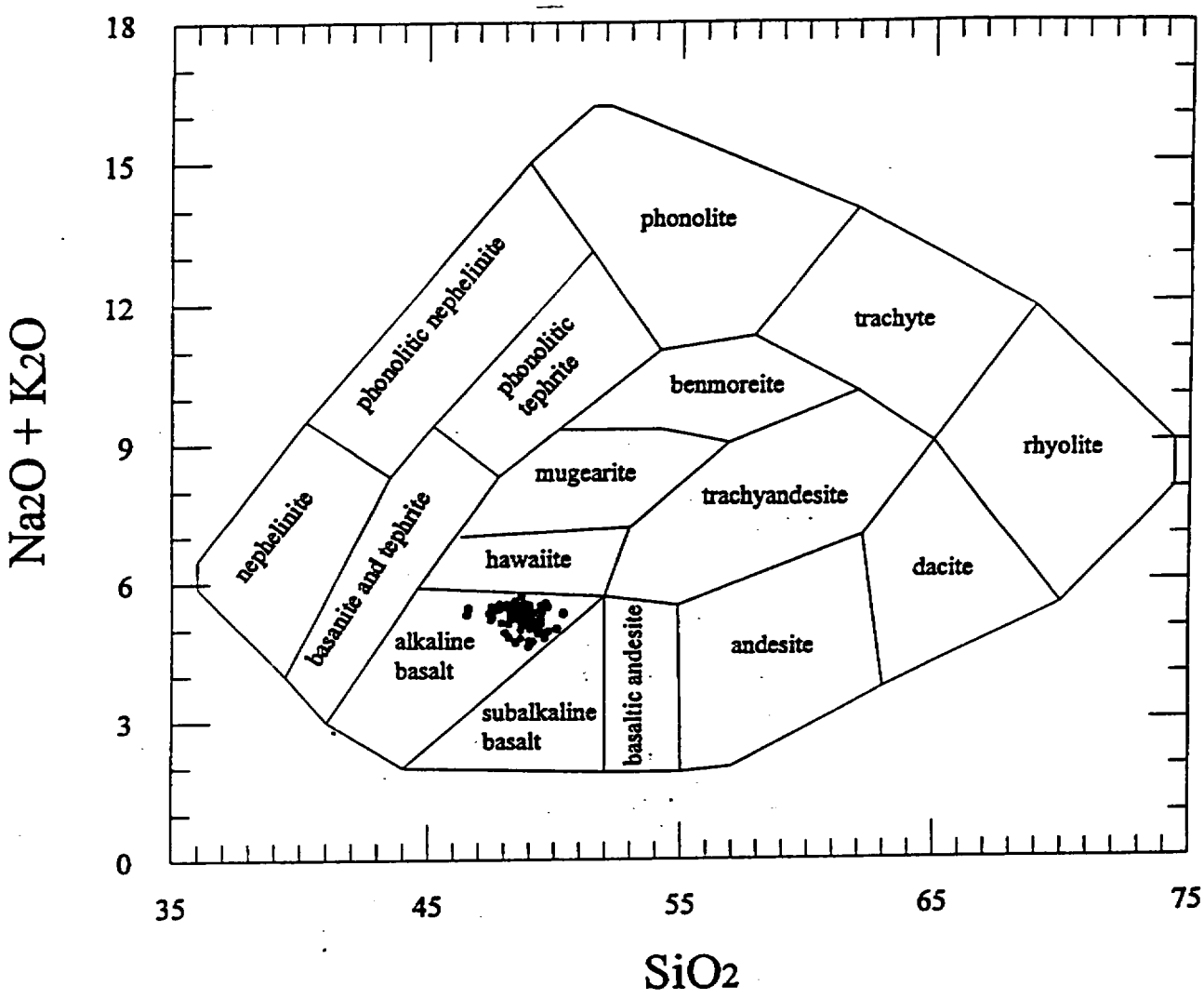
18
15
12
9
6
3
0
35
45
55
65
75
Na2O + K2O
SiO2
phonolite
trachyte
rhyolite
phonolitic nephelinite
phonolitic tephrite
benmoreite
mugearite
trachyandesite
nephelinite
basanite and tephrite
hawaiite
dacite
alkaline basalt
andesite
subalkaline basalt
basaltic andesite

Figure 4

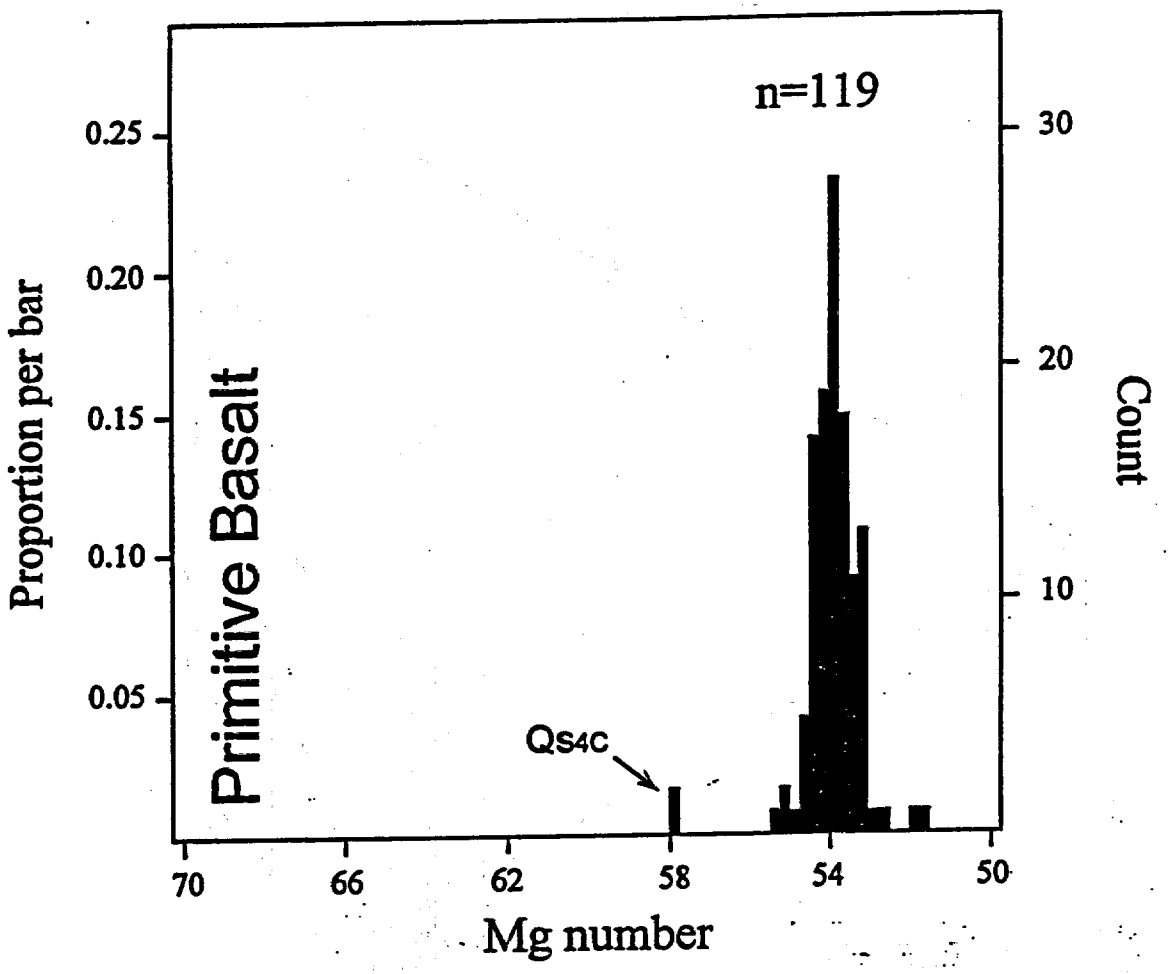
n=119
Primitive Basalt
Qs4c
Proportion per bar
0.25
0.20
0.15
0.10
0.05
Count
30
20
10
70
66
62
58
54
50
Mg number

Figure 5

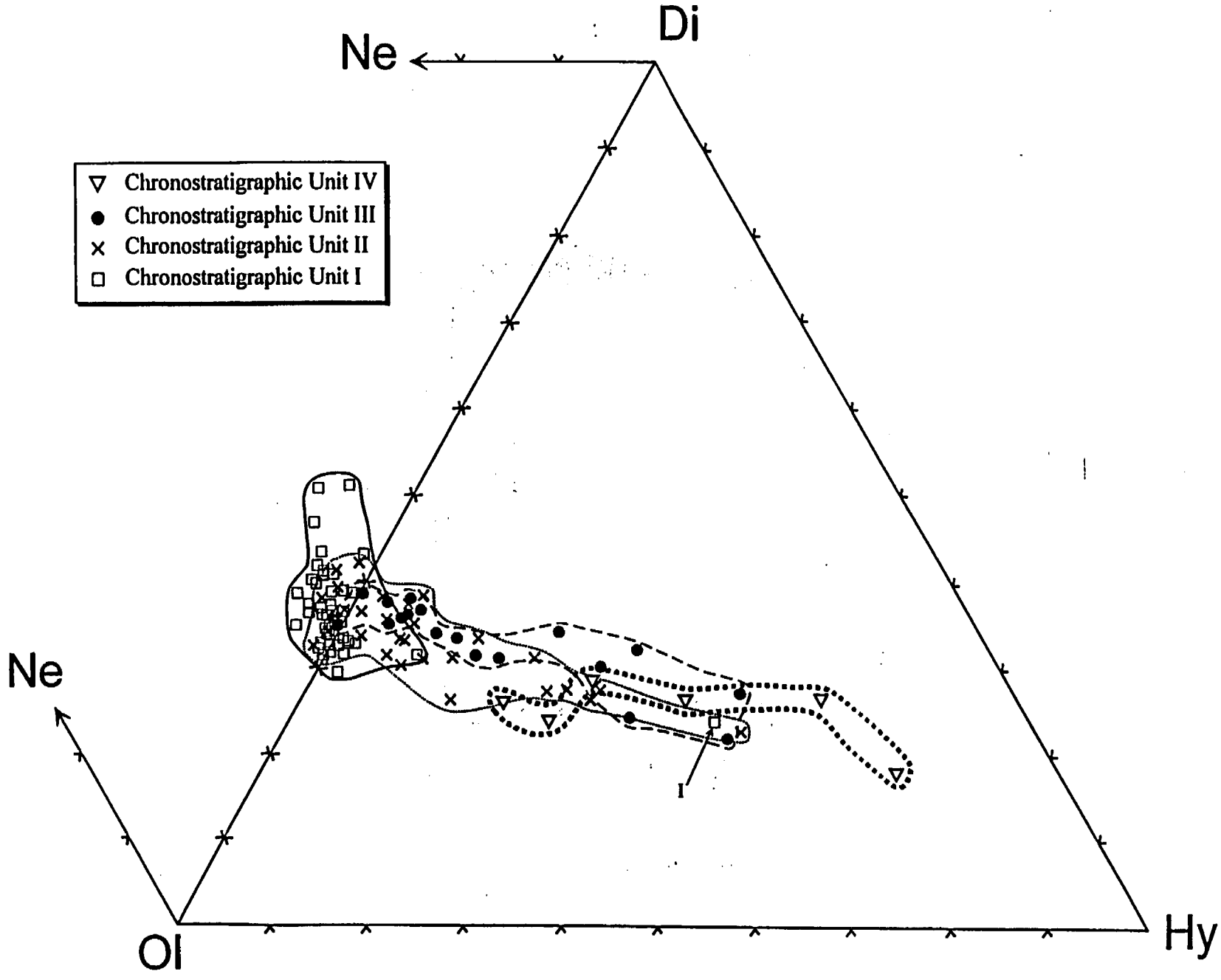
Di
Ne
Ne
Ol
Hy
Chronostratigraphic Unit IV
Chronostratigraphic Unit III
Chronostratigraphic Unit II
Chronostratigraphic Unit I
I

Figure 6

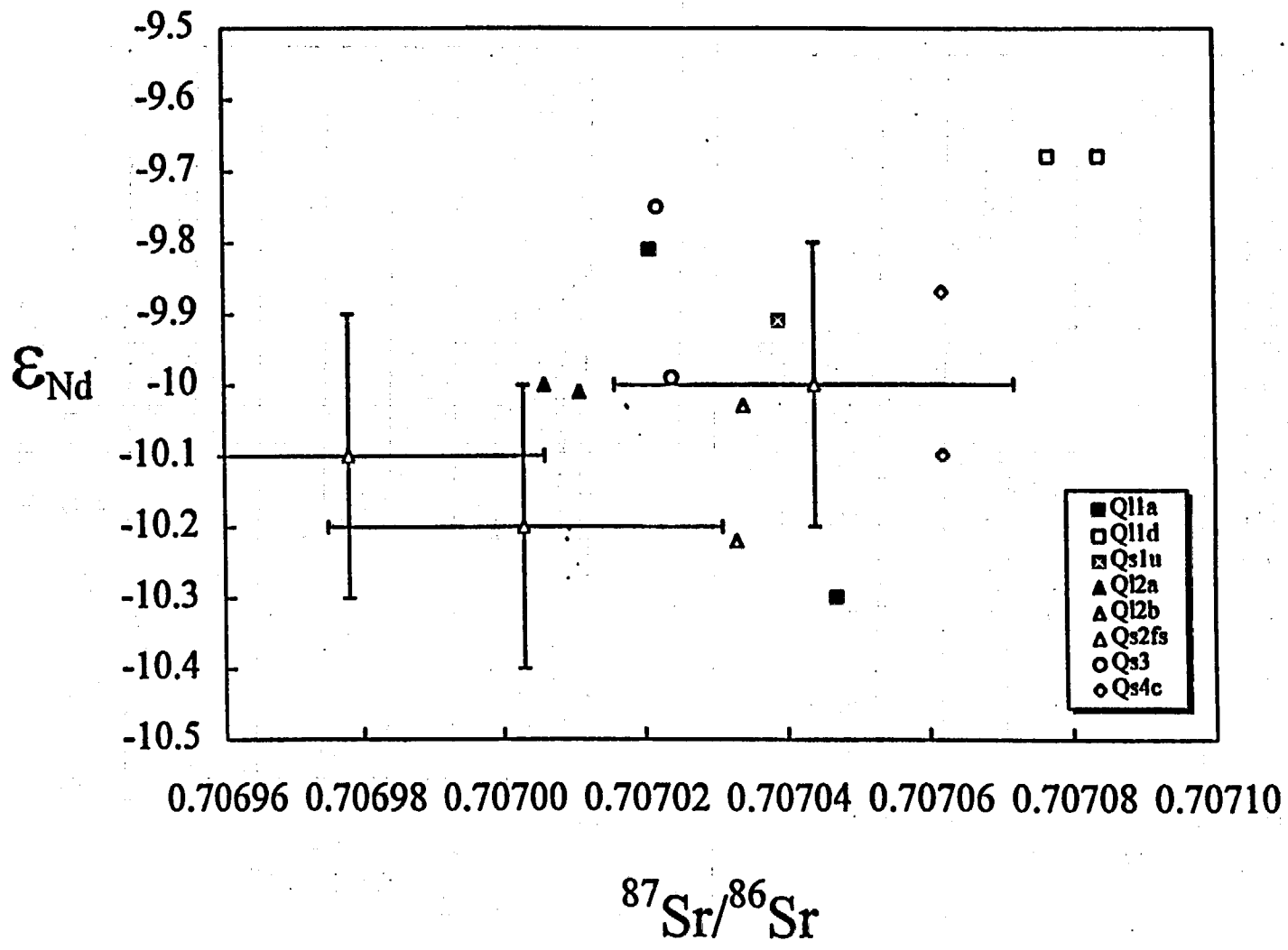
-9.5
-9.6
-9.7
-9.8
-9.9
-10
-10.1
-10.2
-10.3
-10.4
-10.5
εNd
0.70696 0.70698 0.70700 0.70702 0.70704 0.70706 0.70708 0.70710
87Sr/86Sr
Ql1a
Ql1d
Qs1u
Ql2a
Ql2b
Qs2fs
Qs3
Qs4c

Figure 7

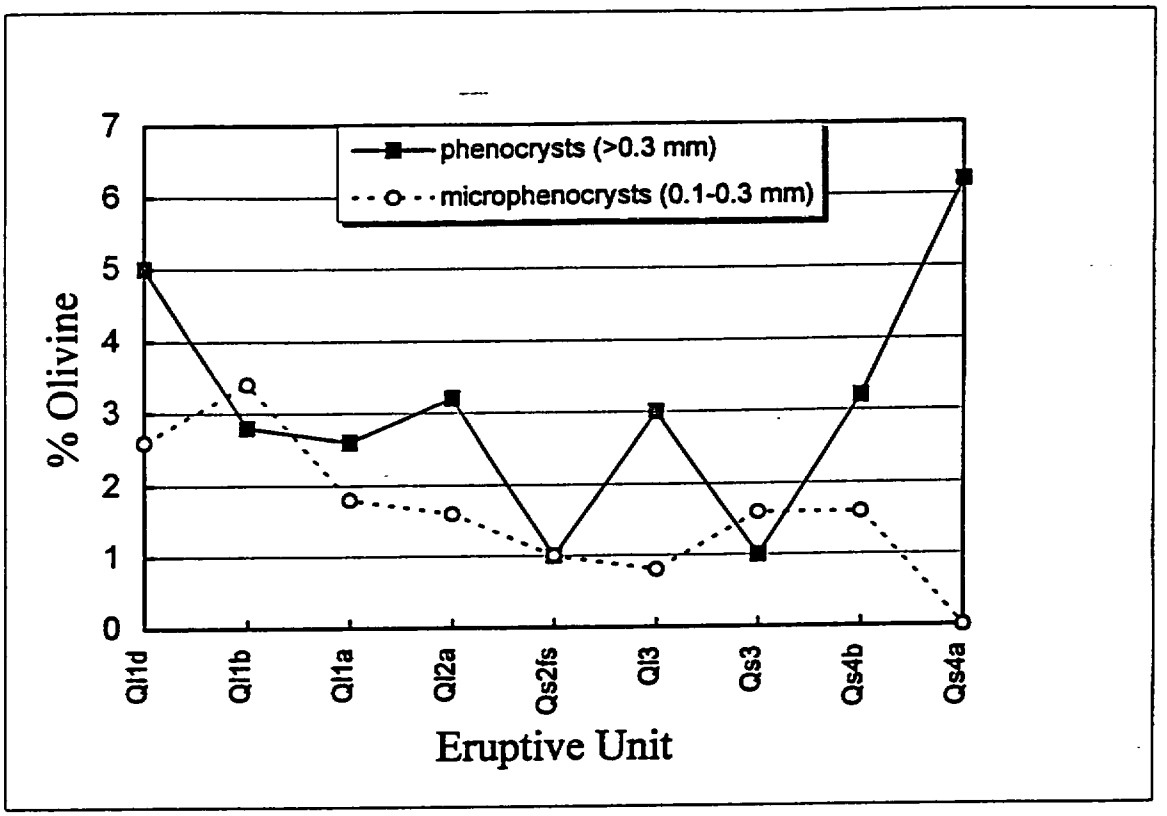
phenocrysts (>0.3 mm)
microphenocrysts (0.1-0.3 mm)
% Olivine
0
1
2
3
4
5
6
7
Ql1d
Ql1b
Ql1a
Ql2a
Qs2fs
Ql3
Qs3
Qs4b
Qs4a
Eruptive Unit

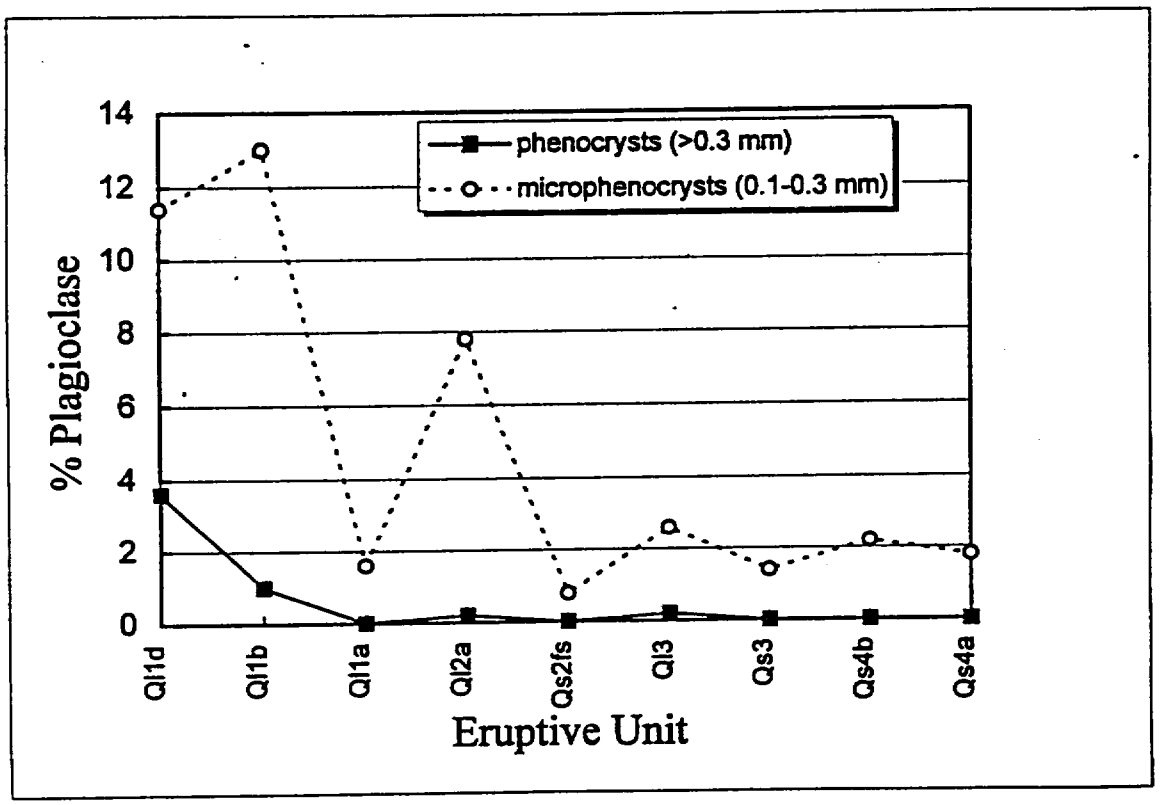
phenocrysts (>0.3 mm)
microphenocrysts (0.1-0.3 mm)
% Plagioclase
0
2
4
6
8
10
12
14
Ql1d
Ql1b
Ql1a
Ql2a
Qs2fs
Ql3
Qs3
Qs4b
Qs4a
Eruptive Unit

Figure 8

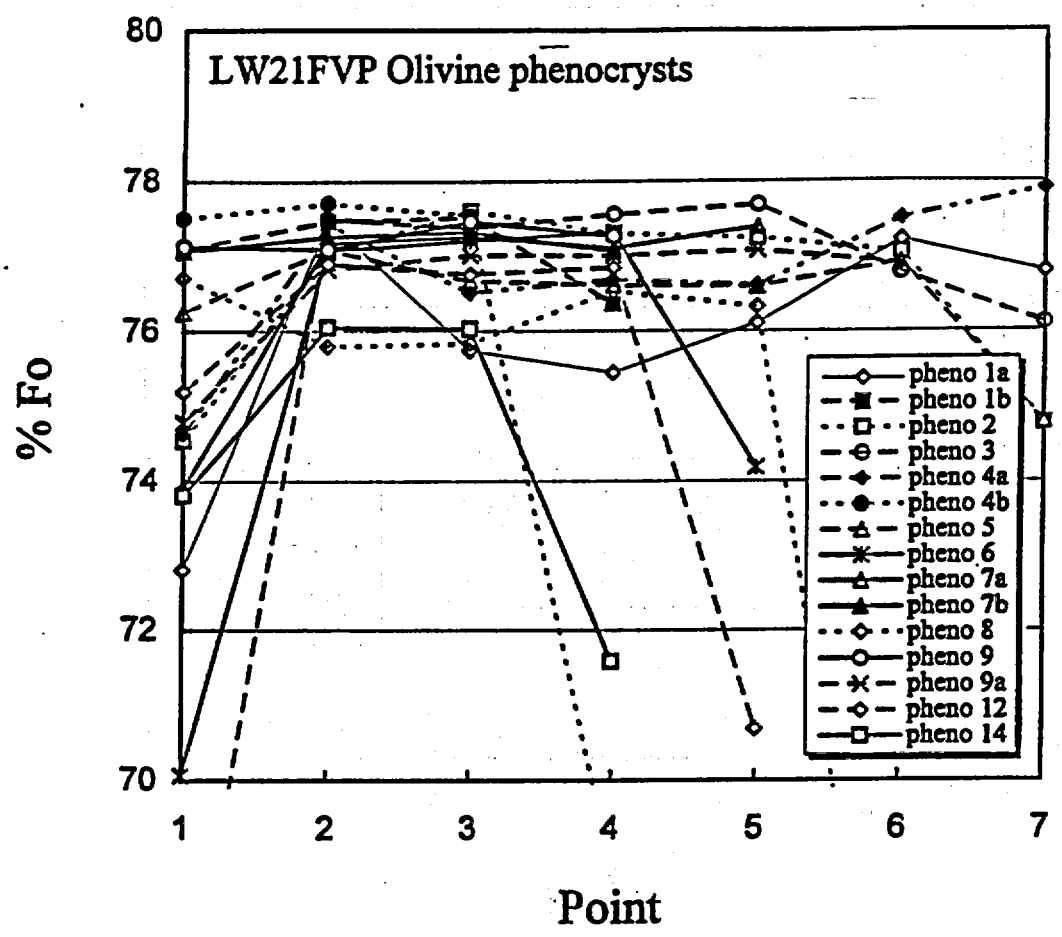
LW21FVP Olivine phenocrysts
80
78
76
74
72
70
% Fo
1
2
3
4
5
6
7
Point
pheno 1a
pheno 1b
pheno 2
pheno 3
pheno 4a
pheno 4b
pheno 5
pheno 6
pheno 7a
pheno 7b
pheno 8
pheno 9
pheno 9a
pheno 12
pheno 14

Figure 9

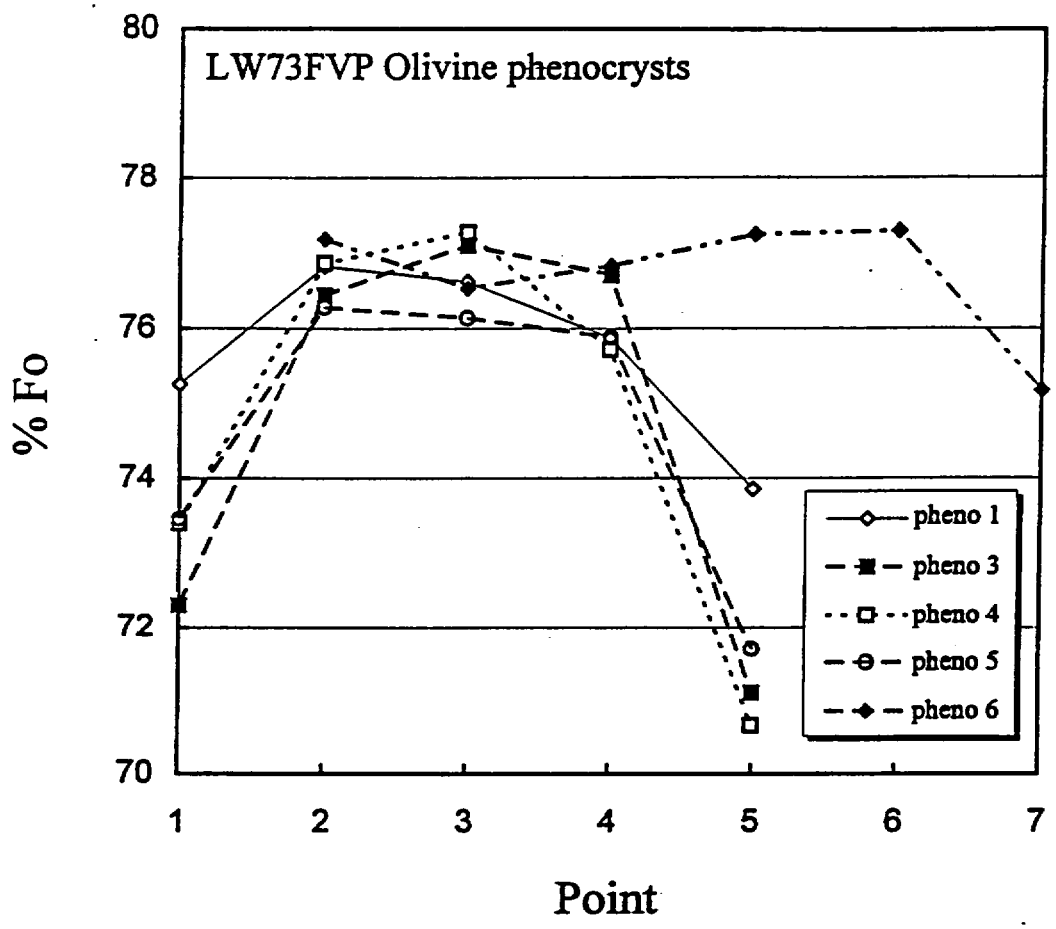
LW73FVP Olivine phenocrysts
80
78
76
74
72
70
% Fo
1
2
3
4
5
6
7
Point
pheno 1
pheno 3
pheno 4
pheno 5
pheno 6

Figure 10

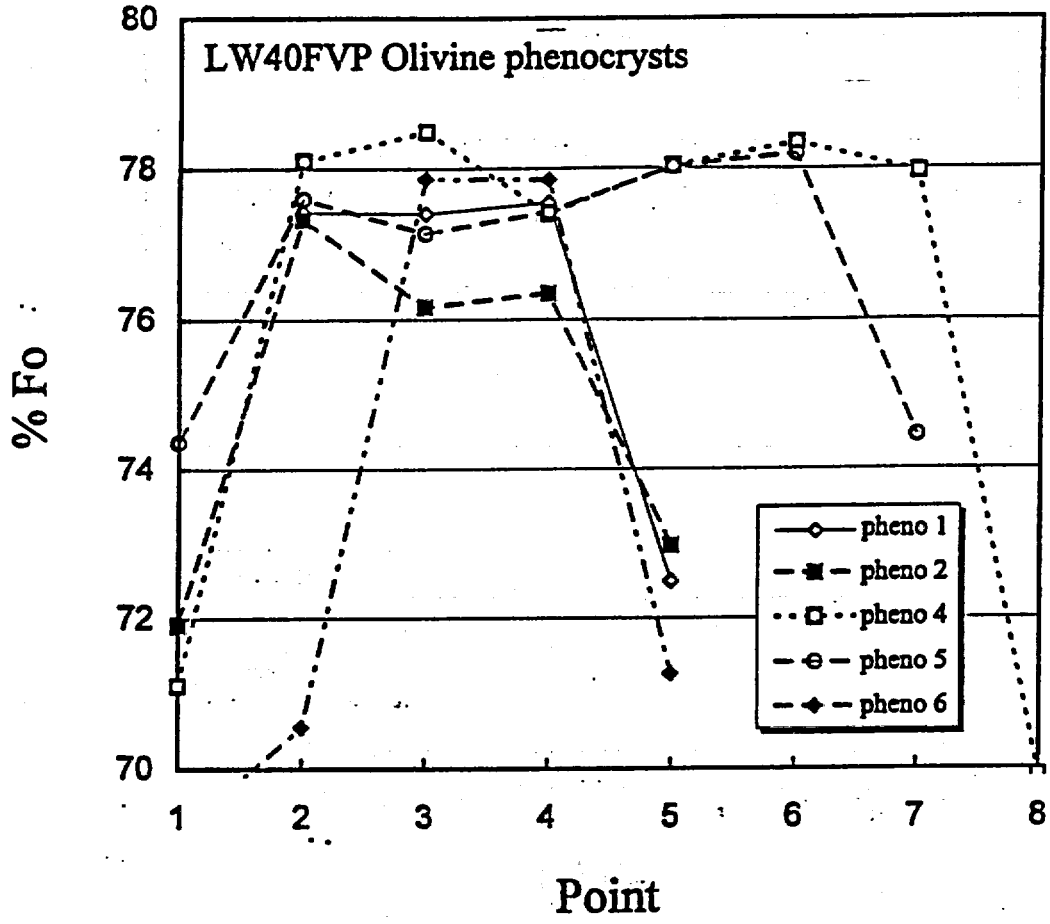
LW40FVP Olivine phenocrysts
80
78
76
74
72
70
% Fo
1
2
3
4
5
6
7
8
Point
pheno 1
pheno 2
pheno 4
pheno 5
pheno 6

Figure 11

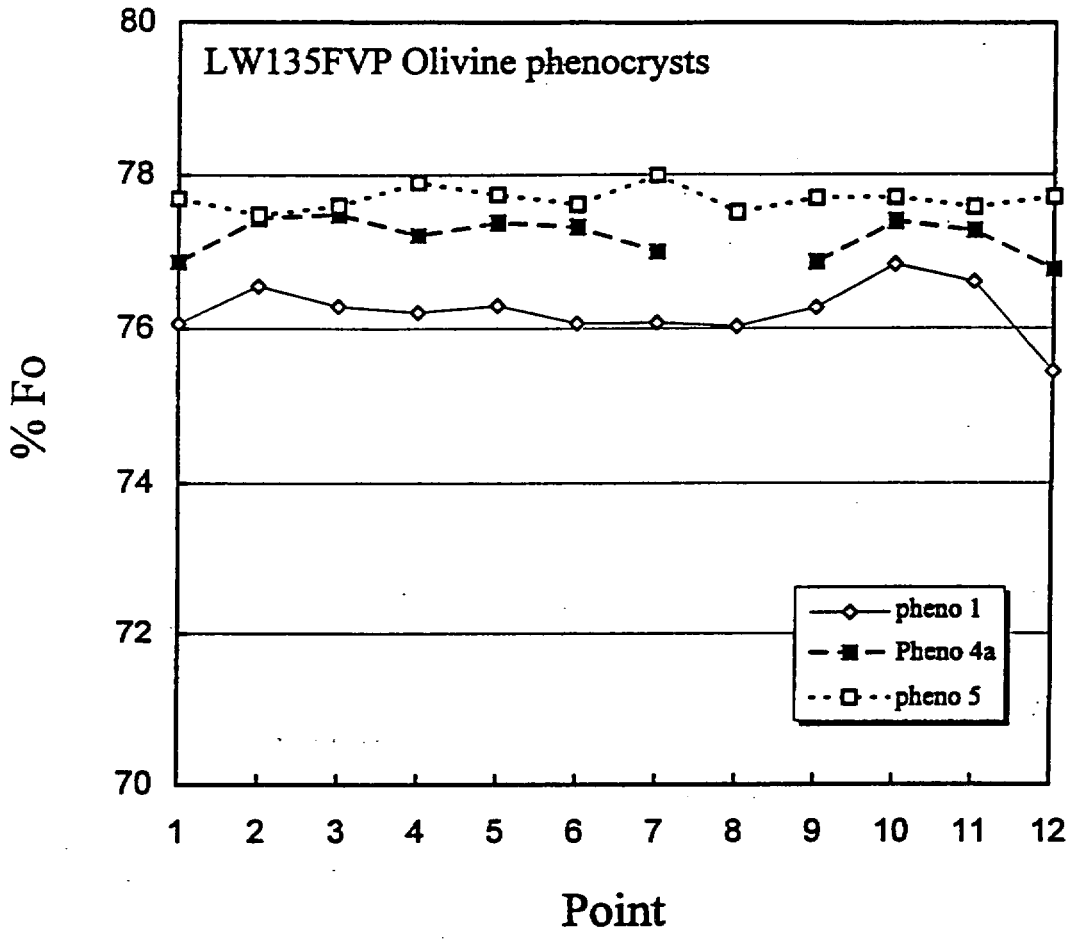
LW135FVP Olivine phenocrysts
80
78
76
74
72
70
% Fo
1
2
3
4
5
6
7
8
9
10
11
12
Point
pheno 1
Pheno 4a
pheno 5

Figure 12

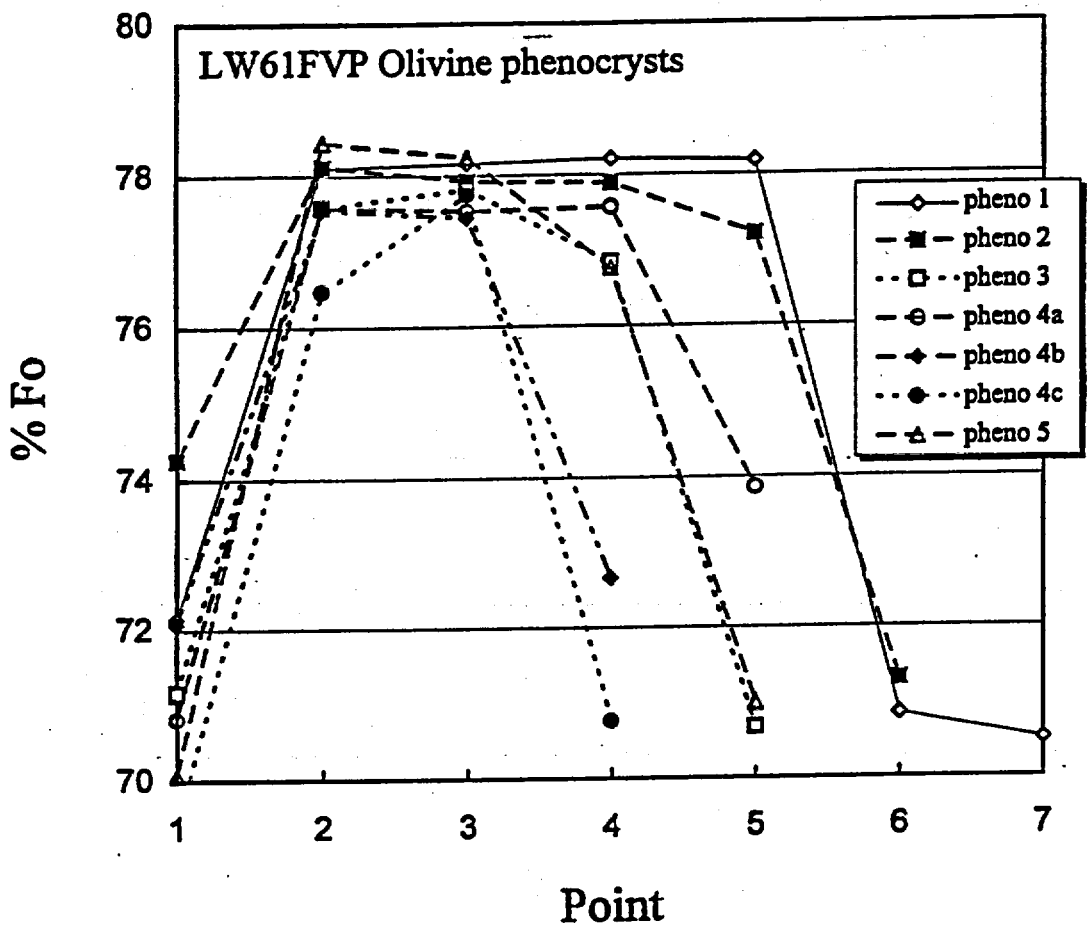
LW61FVP Olivine phenocrysts
80
78
76
74
72
70
% Fo
1
2
3
4
5
6
7
Point
pheno 1
pheno 2
pheno 3
pheno 4a
pheno 4b
pheno 4c
pheno 5

Figure 13

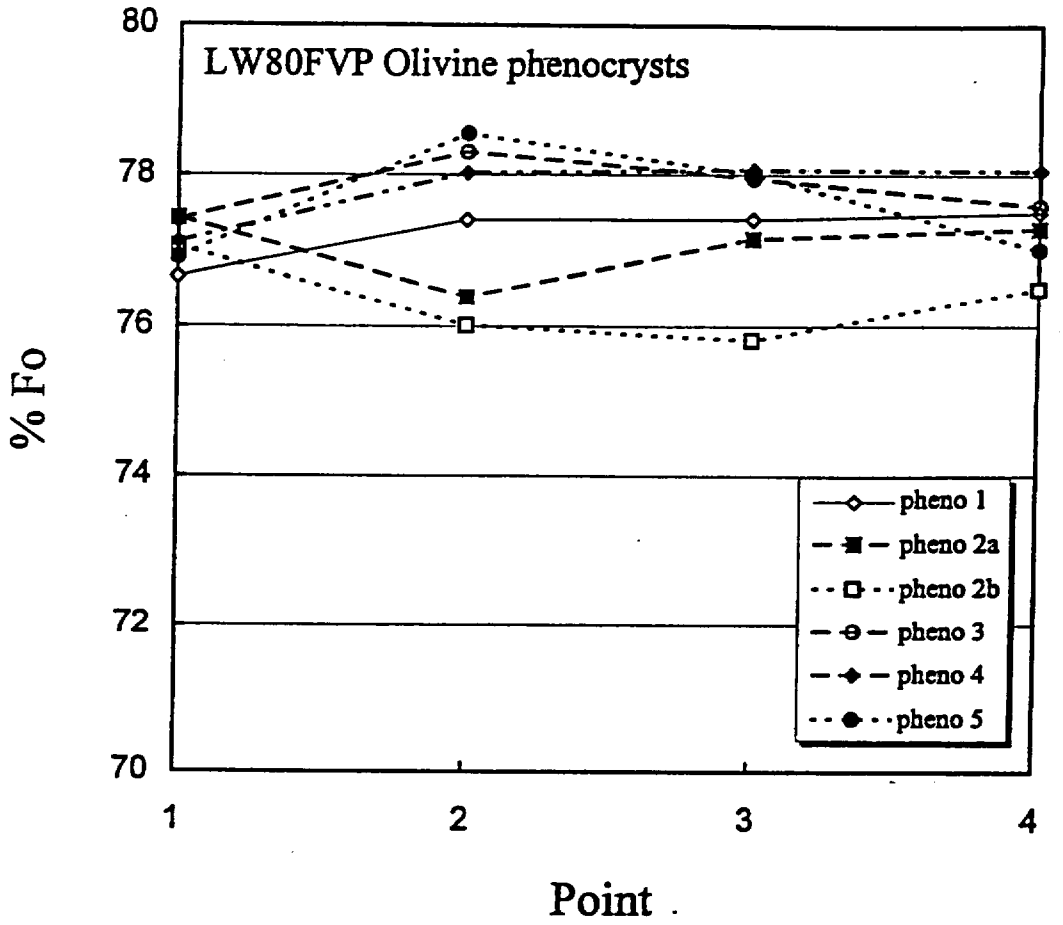
LW80FVP Olivine phenocrysts
80
78
76
74
72
70
% Fo
1
2
3
4
Point
pheno 1
pheno 2a
pheno 2b
pheno 3
pheno 4
pheno 5

Figure 14

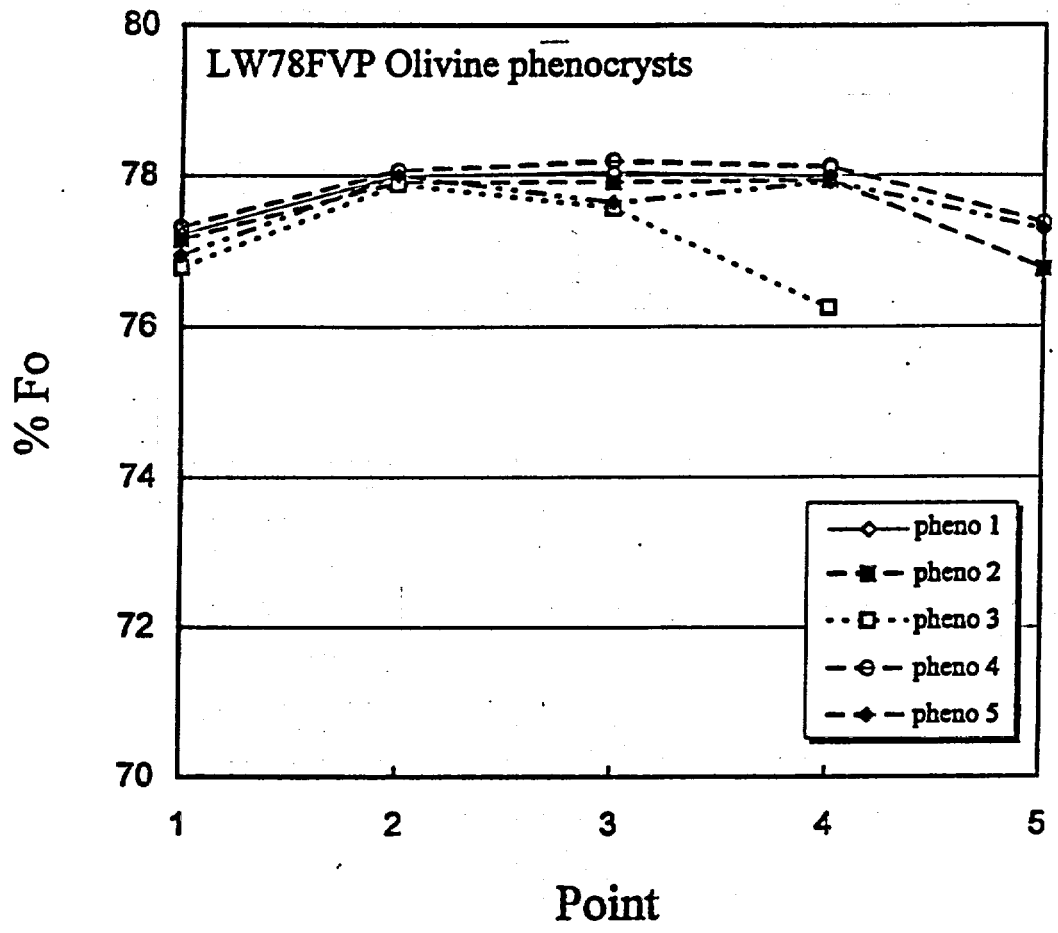
LW78FVP Olivine phenocrysts
80
78
76
74
72
70
% Fo
1
2
3
4
5
Point
pheno 1
pheno 2
pheno 3
pheno 4
pheno 5

Figure 15

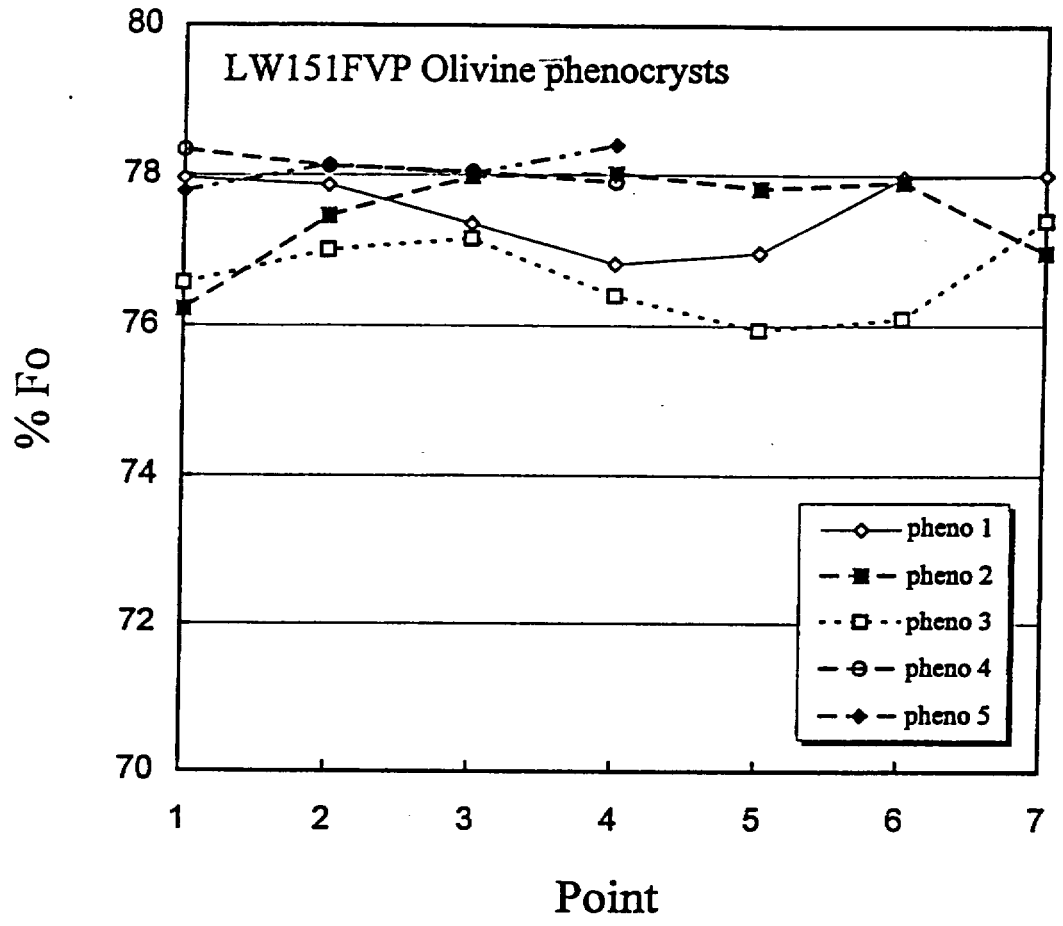
LW151FVP Olivine phenocrysts
80
78
76
74
72
70
% Fo
1
2
3
4
5
6
7
Point
pheno 1
pheno 2
pheno 3
pheno 4
pheno 5

Figure 16

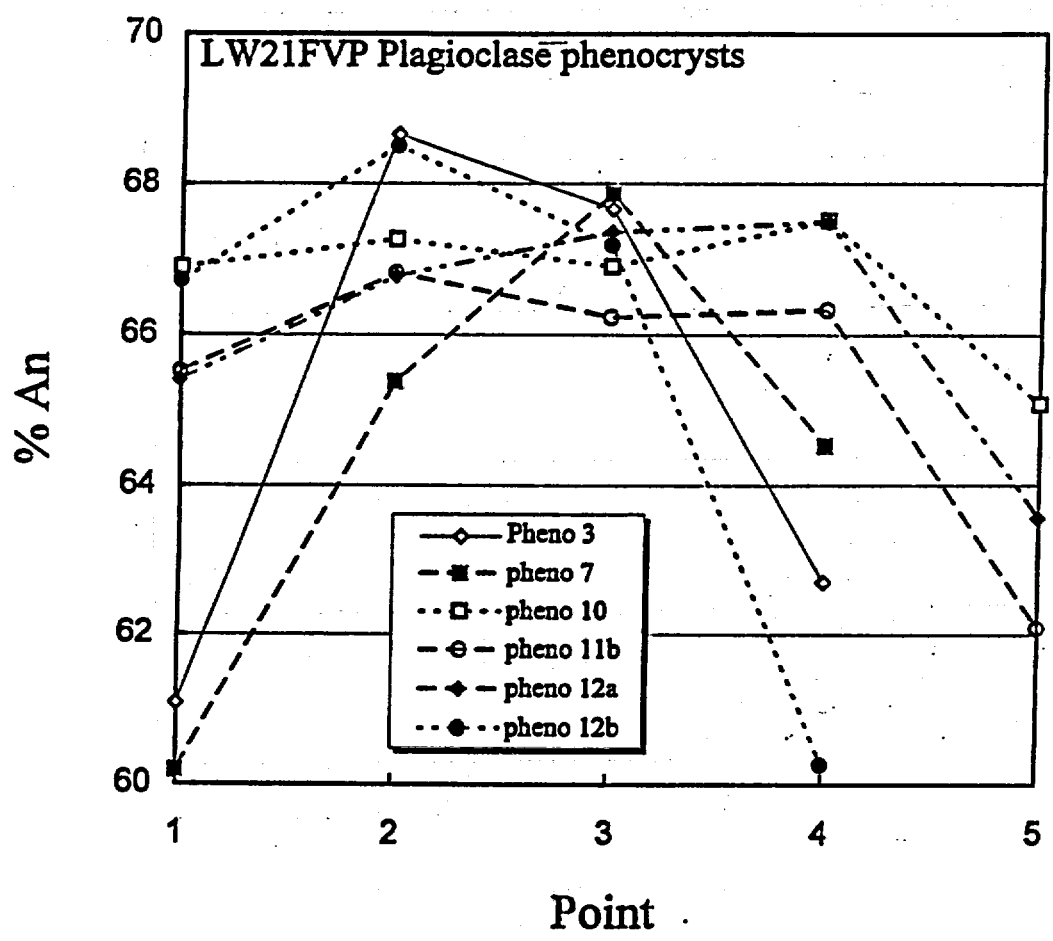
LW21FVP Plagioclase phenocrysts
70
68
66
64
62
60
% An
1
2
3
4
5
Point
Pheno 3
pheno 7
pheno 10
pheno 11b
pheno 12a
pheno 12b

Figure 17

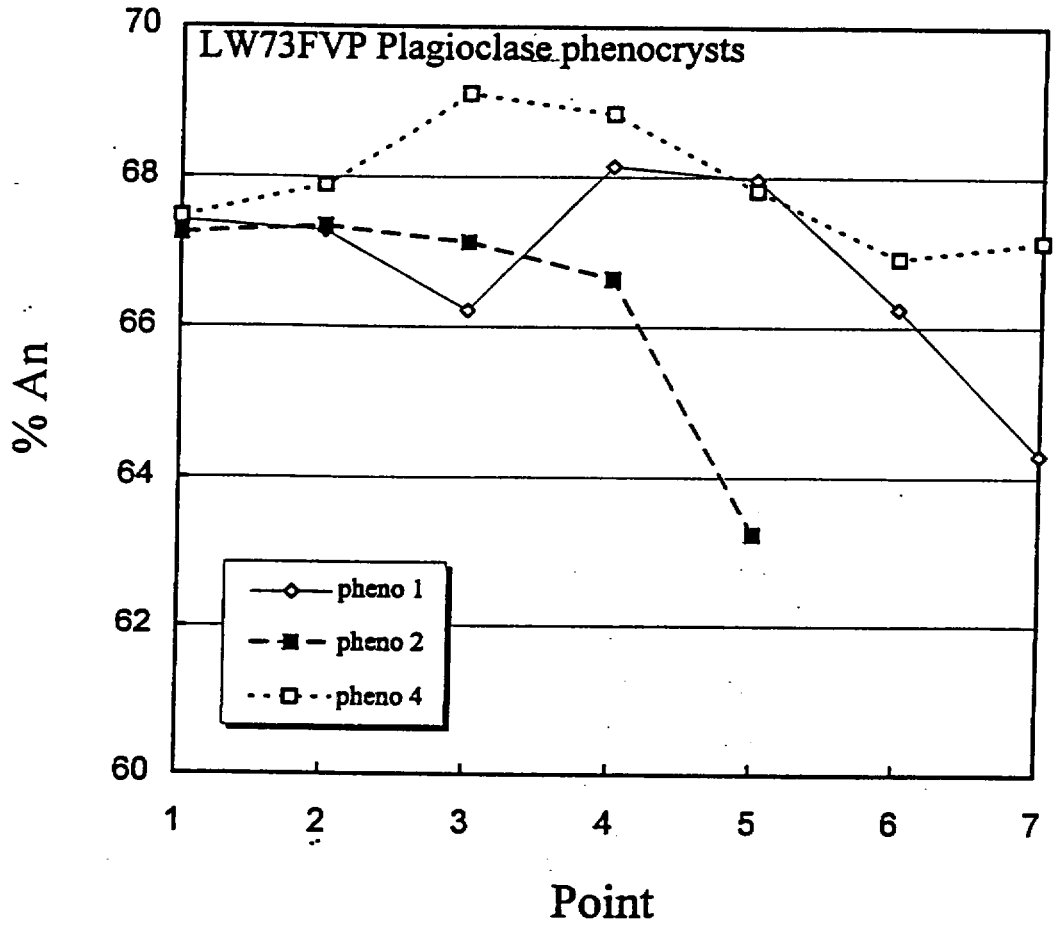
LW73FVP Plagioclase phenocrysts
70
68
66
64
62
60
% An
1
2
3
4
5
6
7
Point
pheno 1
pheno 2
pheno 4

Figure 18

LW21FVP plagioclase compositions

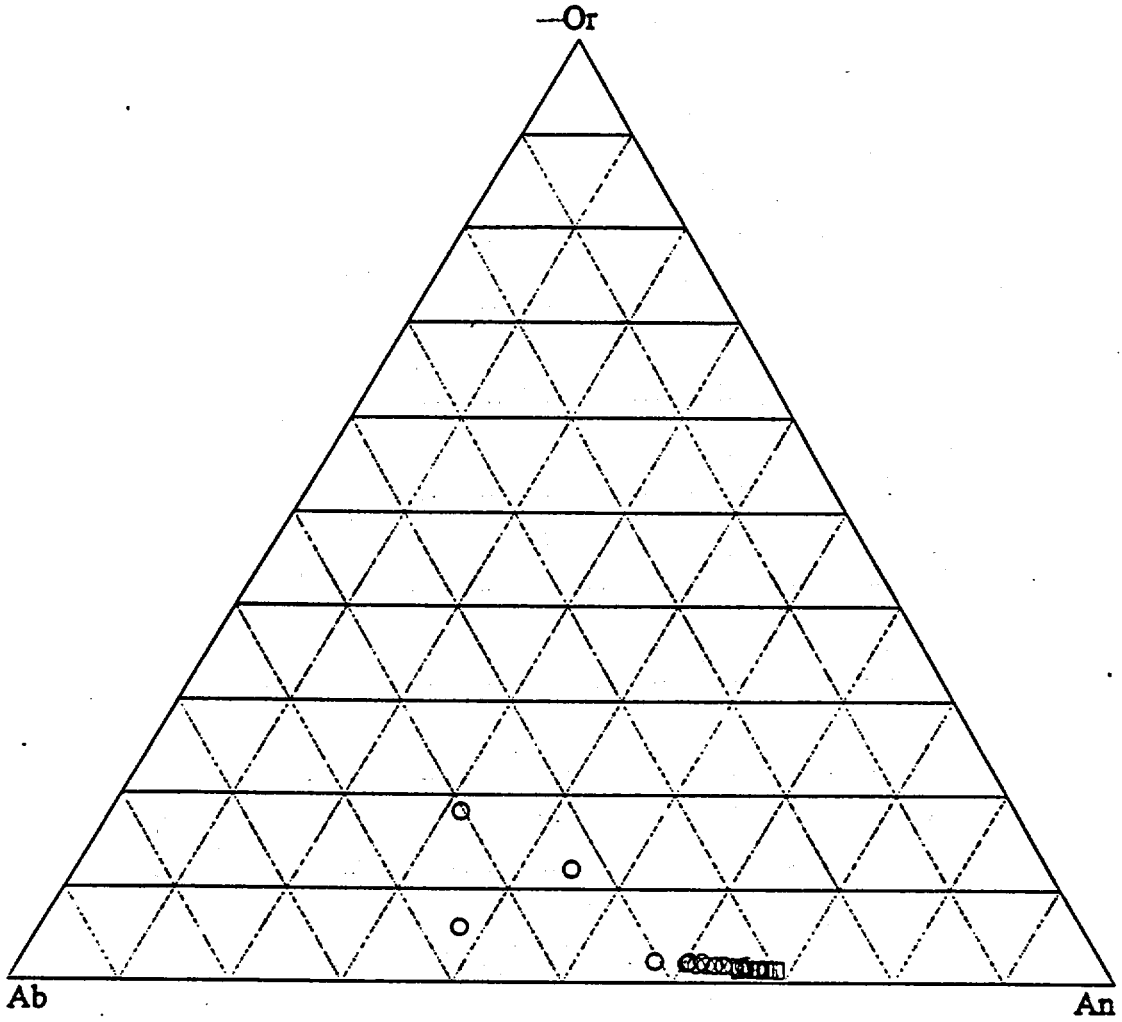

Figure 19

LW73FVP plagioclase compositions

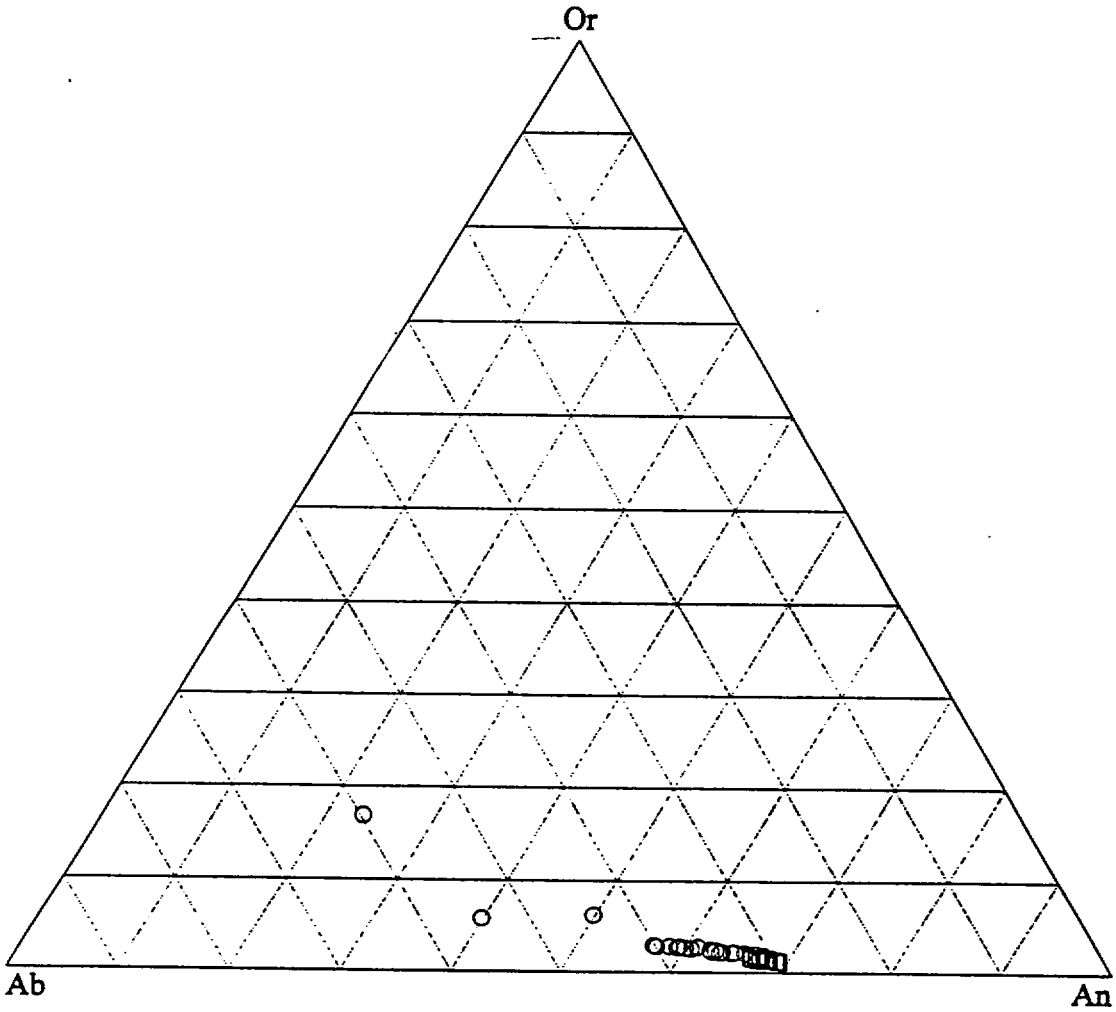

Figure 20

LW40FVP plagioclase compositions

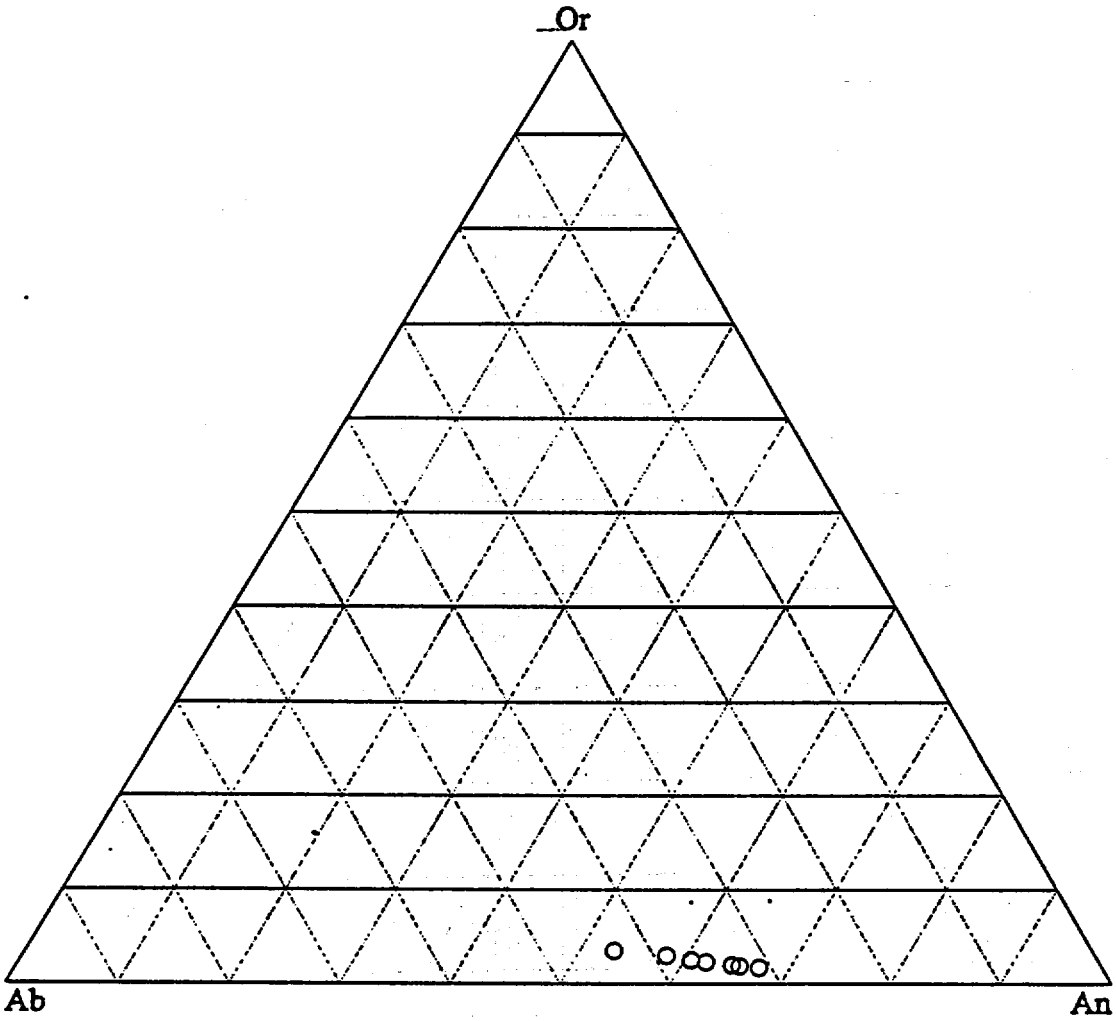

Figure 21

LW61FVP plagioclase compositions

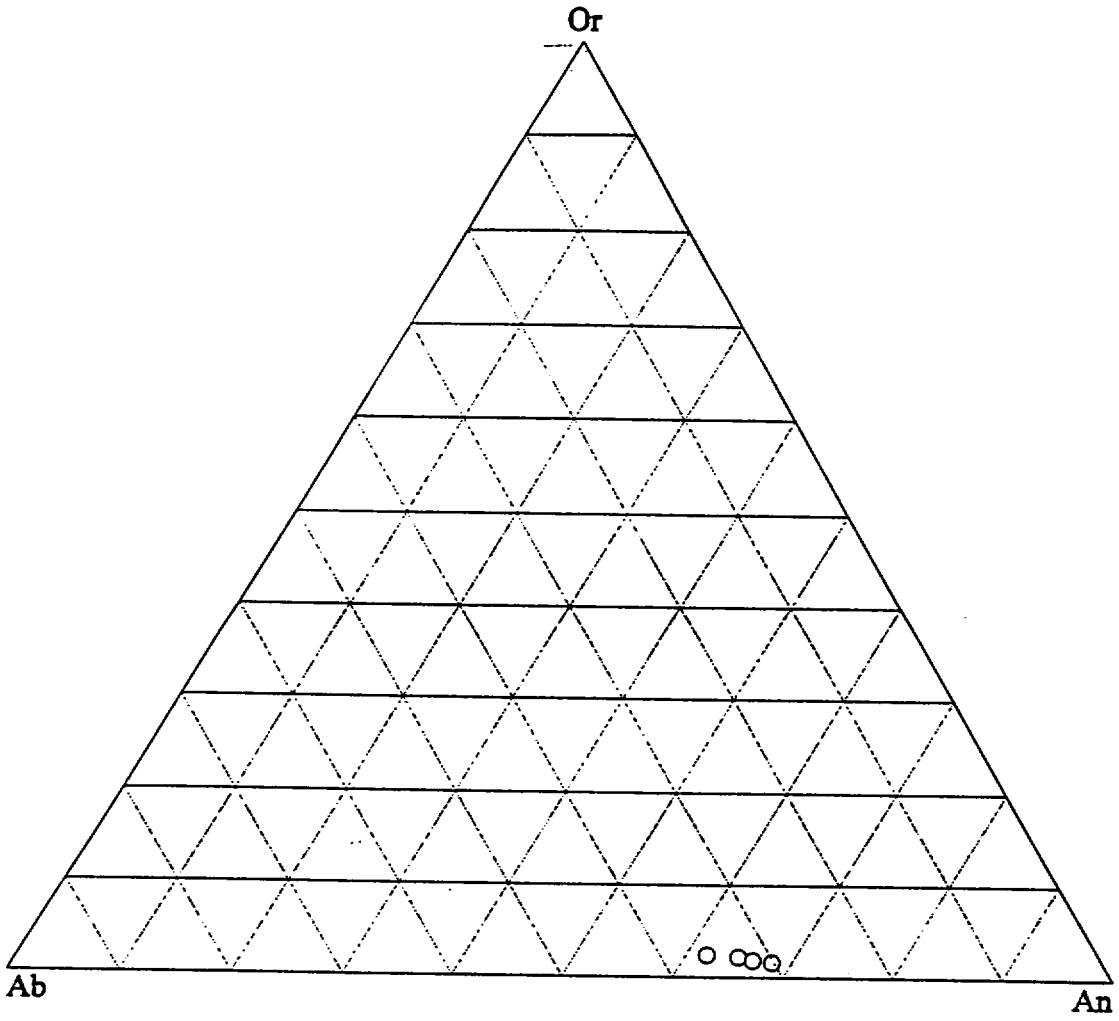

Figure 22

LW21FVP pyroxene compositions

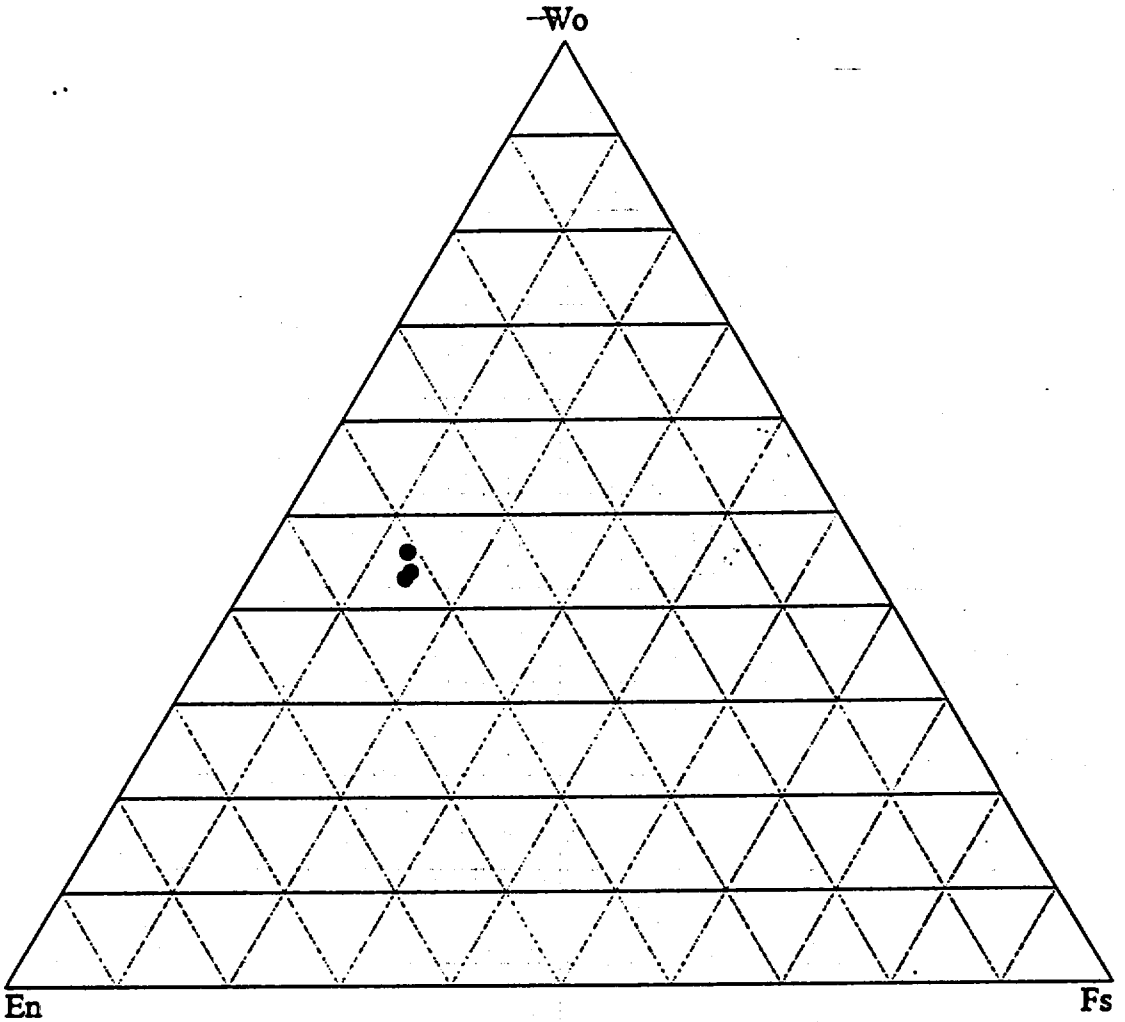

Figure 23

LW40FVP pyroxene compositions

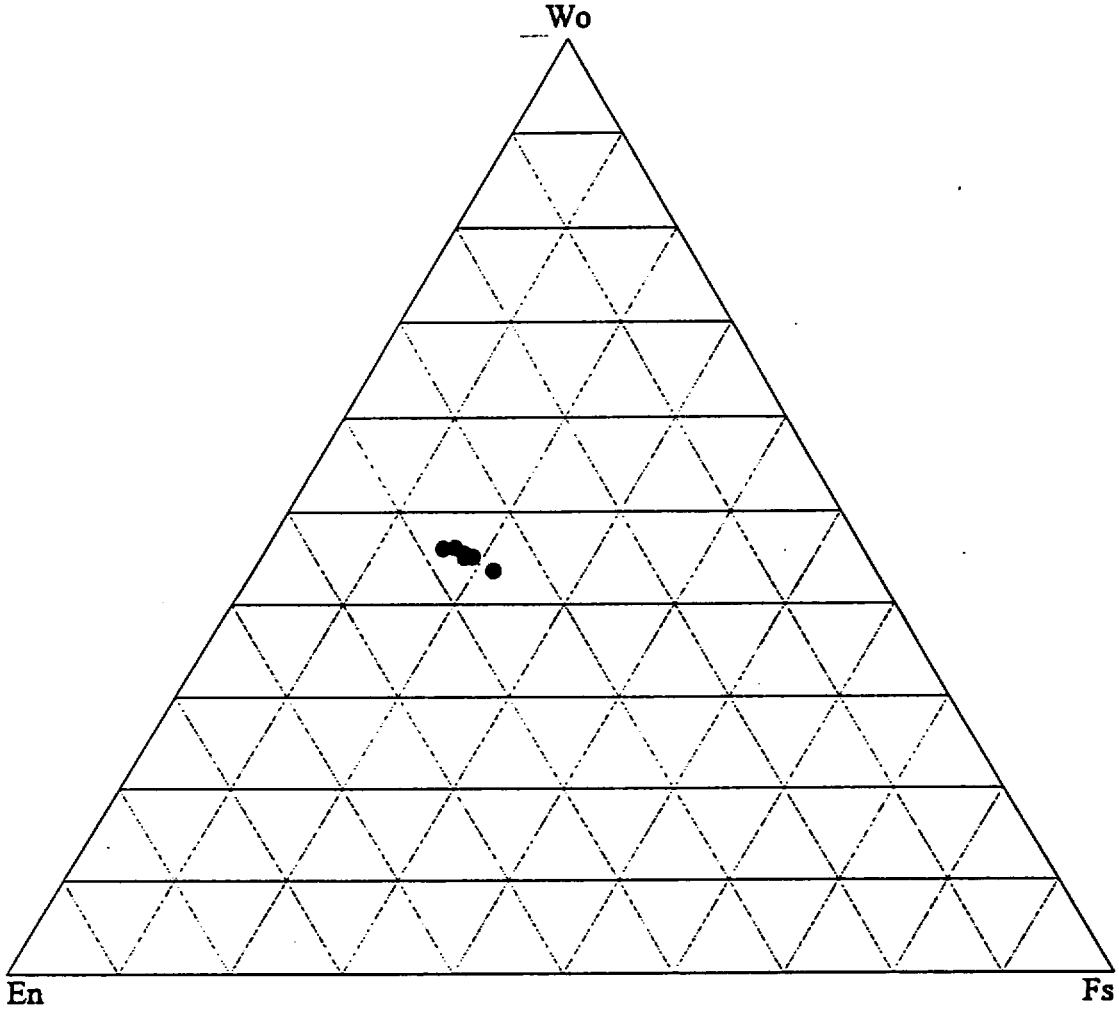

Figure 24

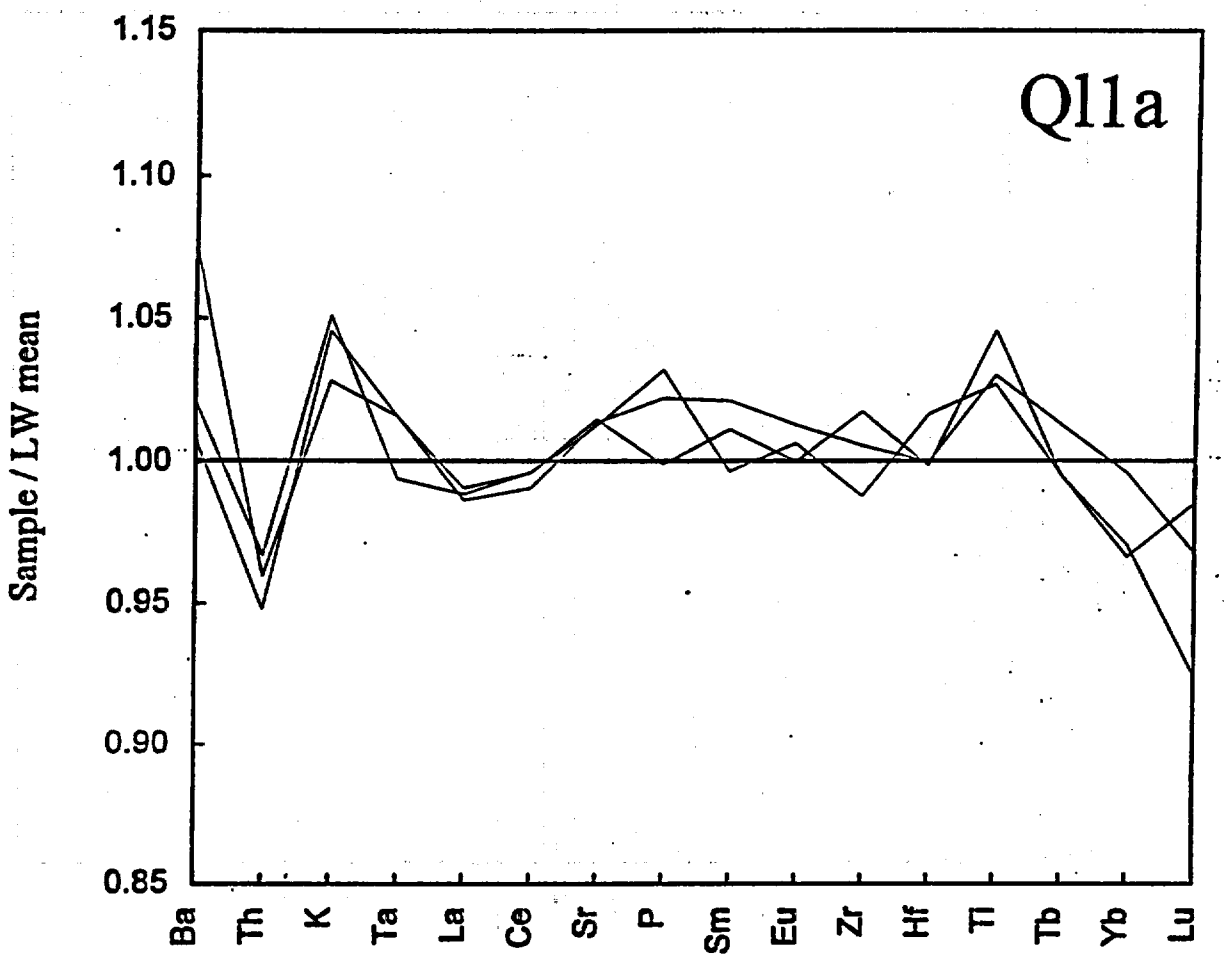
Ql1a
Sample / LW mean
1.15
1.10
1.05
1.00
0.95
0.90
0.85
Ba
Th
K
Ta
La
Ce
Sr
P
Sm
Eu
Zr
Hf
Ti
Tb
Yb
Lu

Figure 25

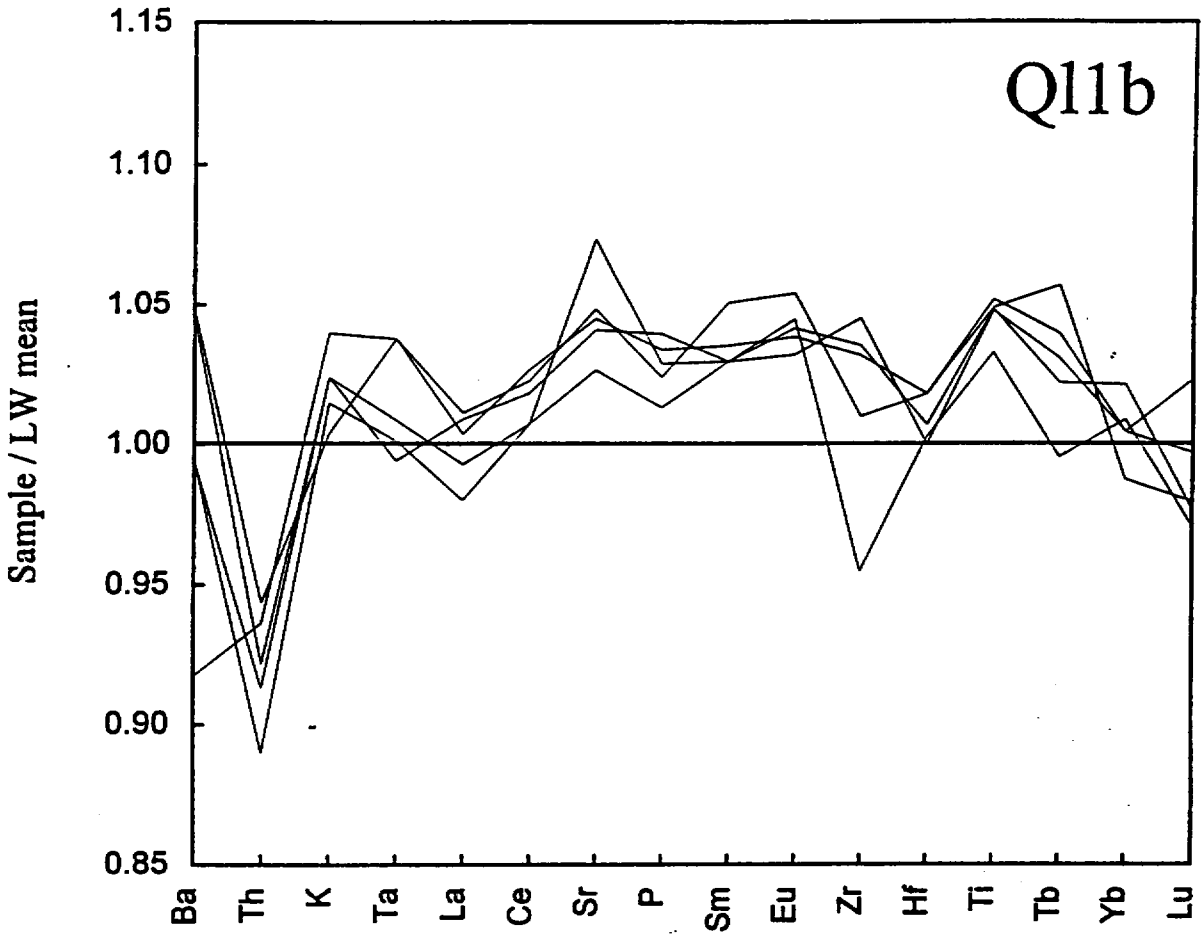
Ql1b
Sample / LW mean
1.15
1.10
1.05
1.00
0.95
0.90
0.85
Ba
Th
K
Ta
La
Ce
Sr
P
Sm
Eu
Zr
Hf
Ti
Tb
Yb
Lu

Figure 26

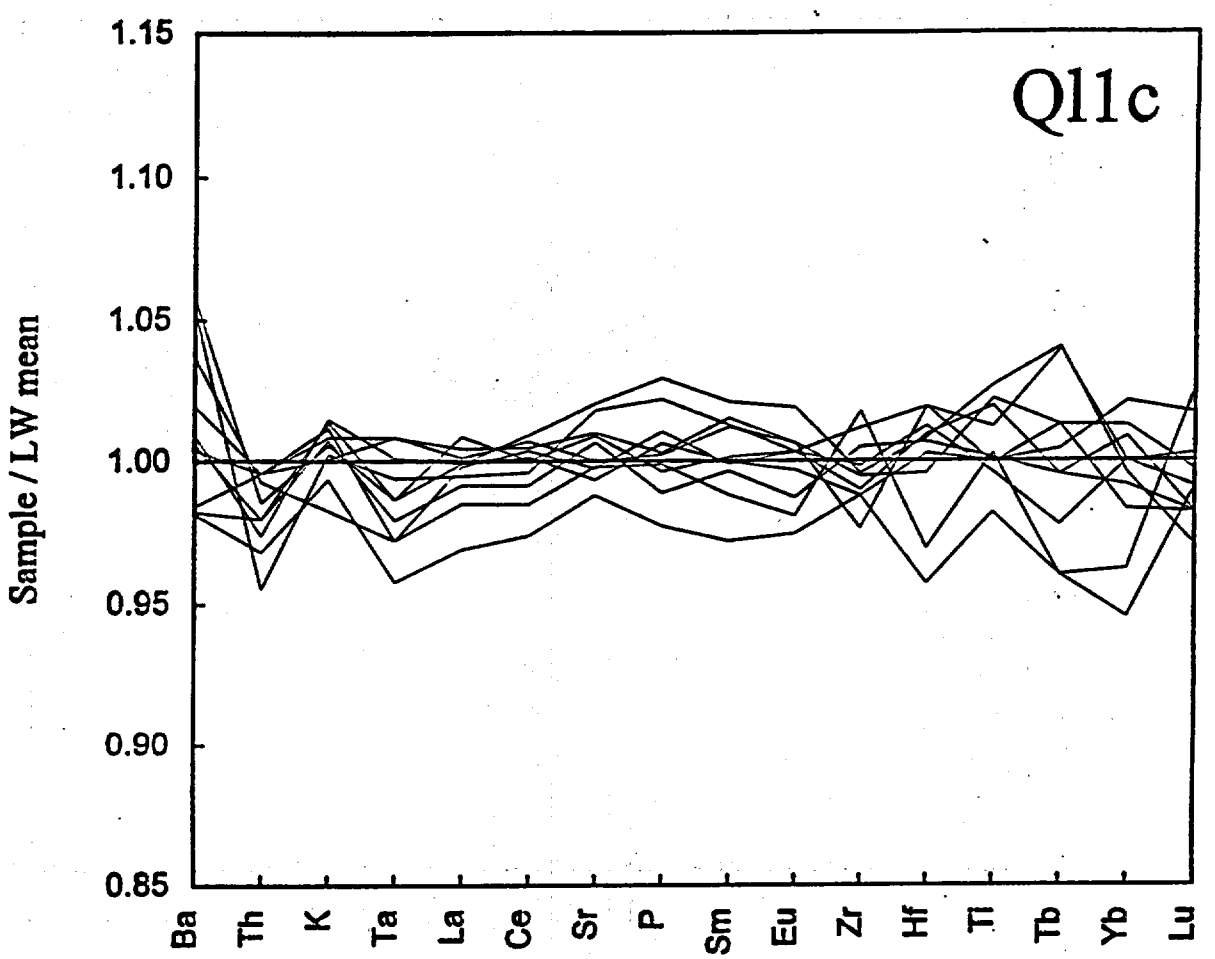
Ql1c
Sample / LW mean
1.15
1.10
1.05
1.00
0.95
0.90
0.85
Ba
Th
K
Ta
La
Ce
Sr
P
Sm
Eu
Zr
Hf
Ti
Tb
Yb
Lu

Figure 27

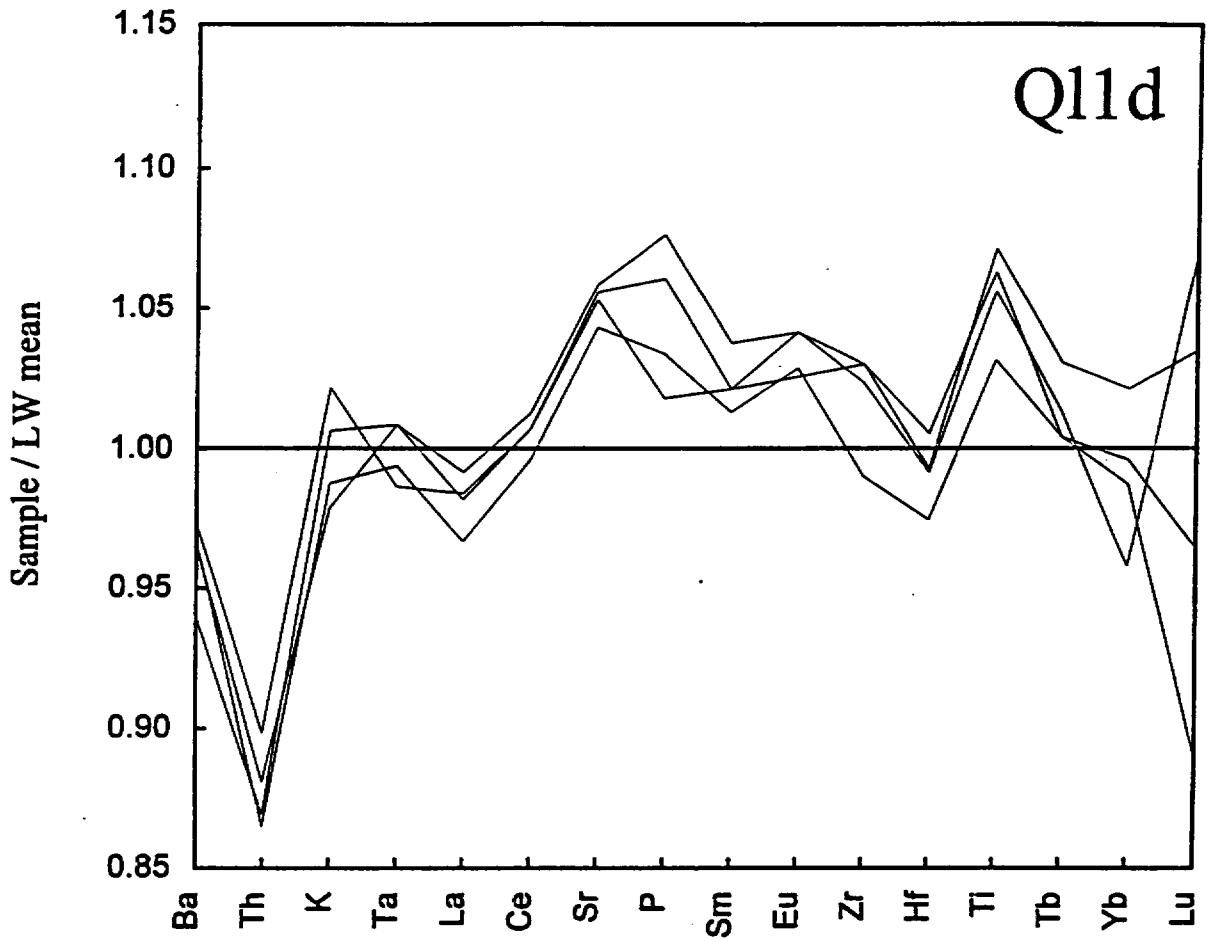
Ql1d
Sample / LW mean
1.15
1.10
1.05
1.00
0.95
0.90
0.85
Ba
Th
K
Ta
La
Ce
Sr
P
Sm
Eu
Zr
Hf
Ti
Tb
Yb
Lu

Figure 28

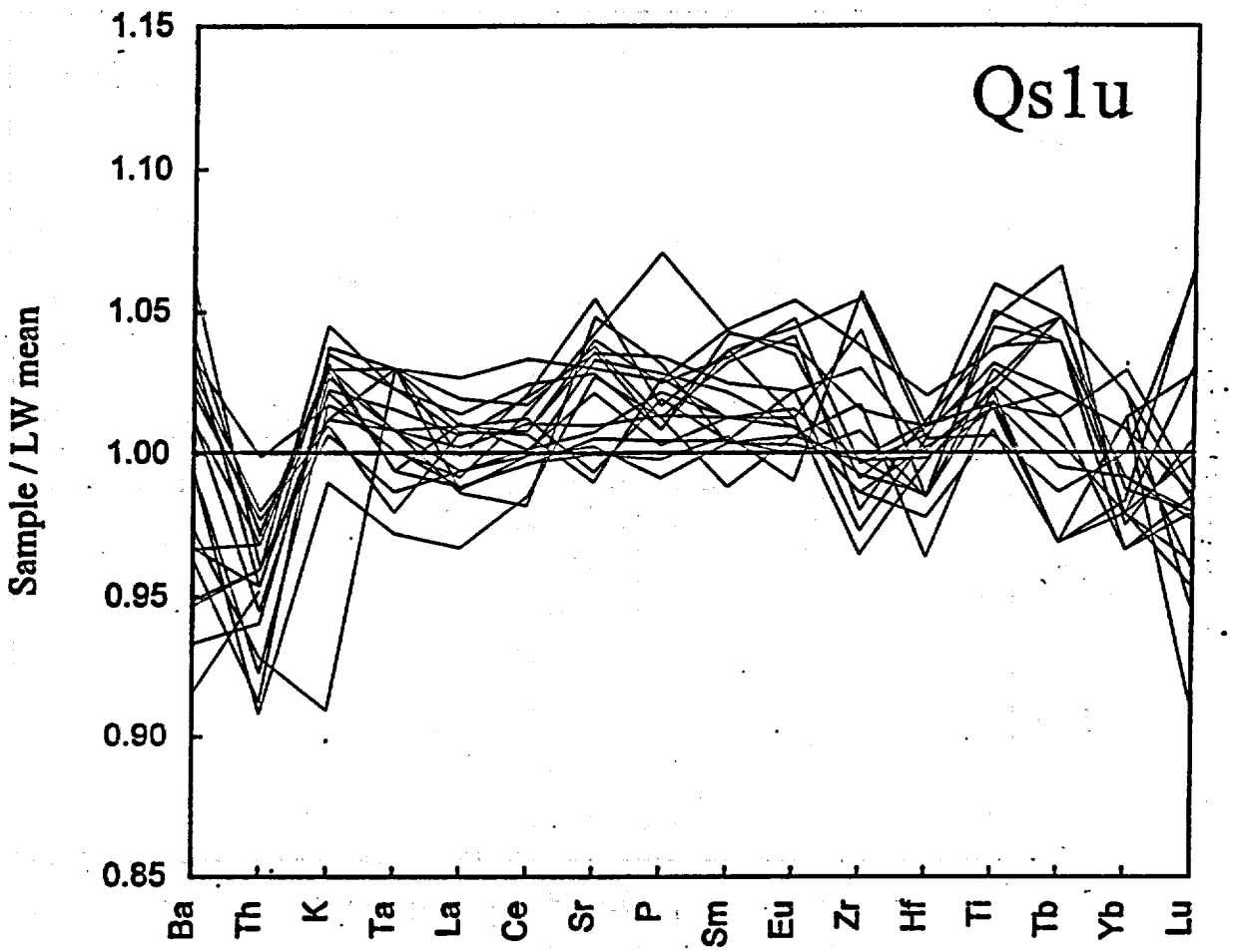
Qs1u
Sample / LW mean
1.15
1.10
1.05
1.00
0.95
0.90
0.85
Ba
Th
K
Ta
La
Ce
Sr
P
Sm
Eu
Zr
Hf
Ti
Tb
Yb
Lu

Figure 29

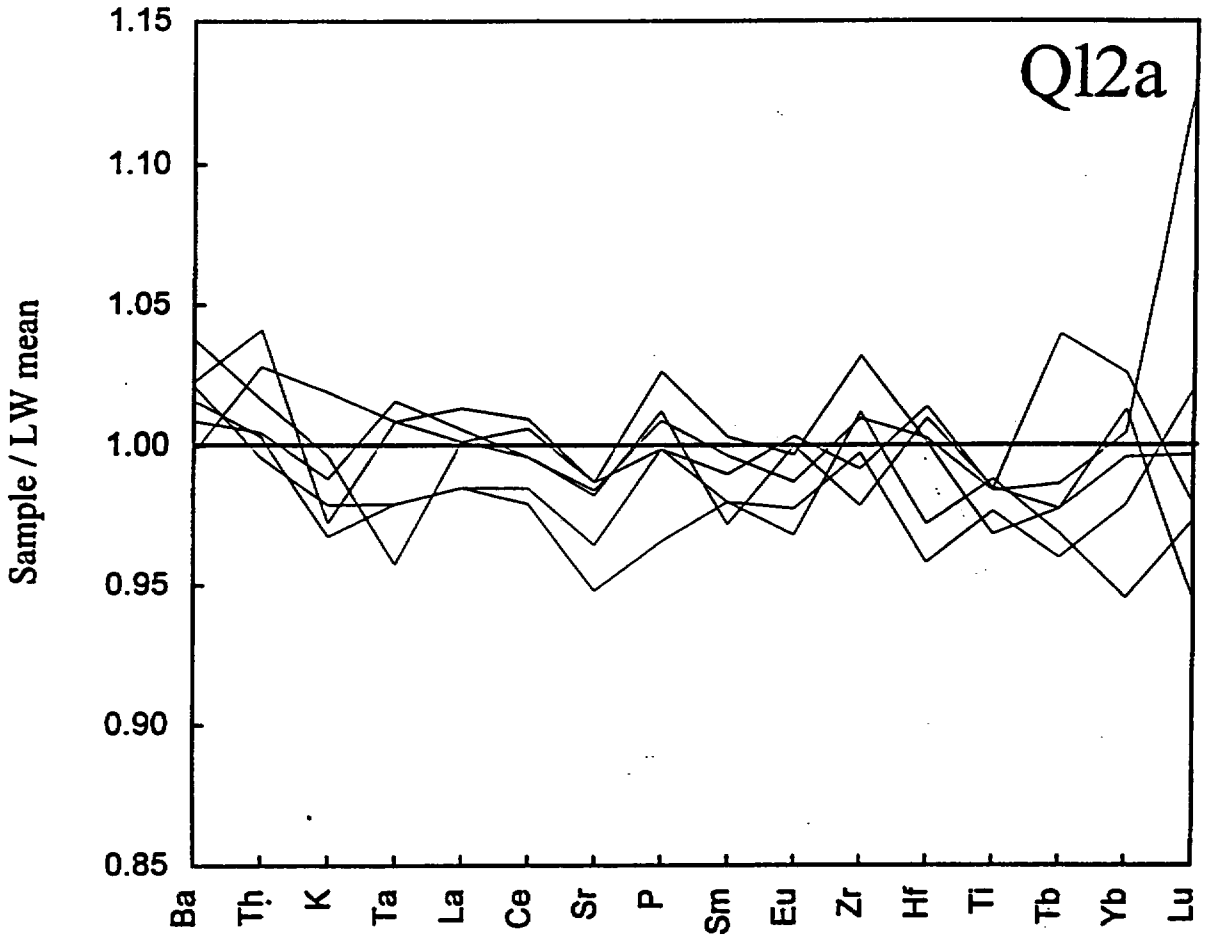
Q12a
Sample / LW mean
1.15
1.10
1.05
1.00
0.95
0.90
0.85
Ba
Th
K
Ta
La
Ce
Sr
P
Sm
Eu
Zr
Hf
Ti
Tb
Yb
Lu

Figure 30

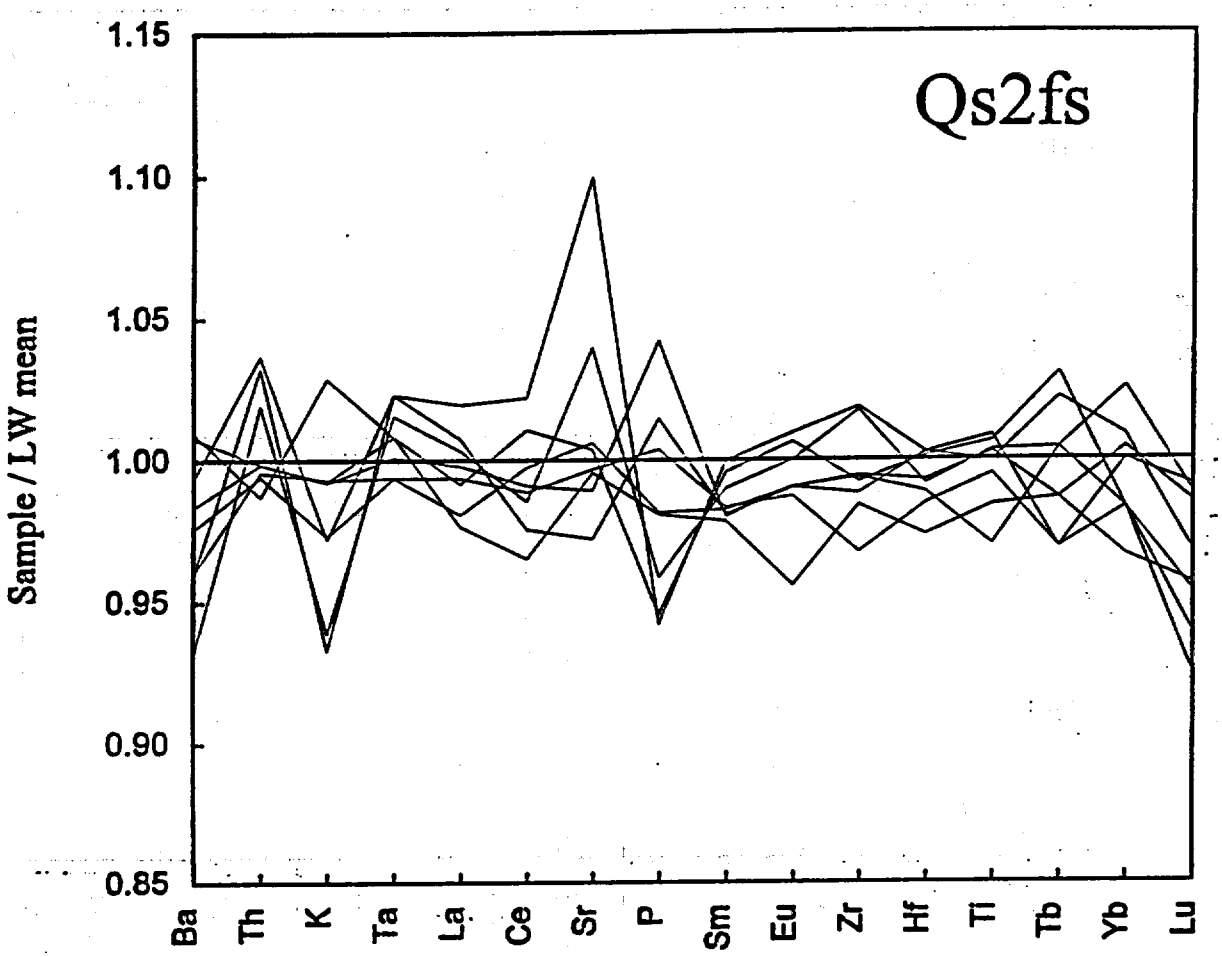
Qs2fs
Sample / LW mean
1.15
1.10
1.05
1.00
0.95
0.90
0.85
Ba
Th
K
Ta
La
Ce
Sr
P
Sm
Eu
Zr
Hf
Ti
Tb
Yb
Lu

Figure 31

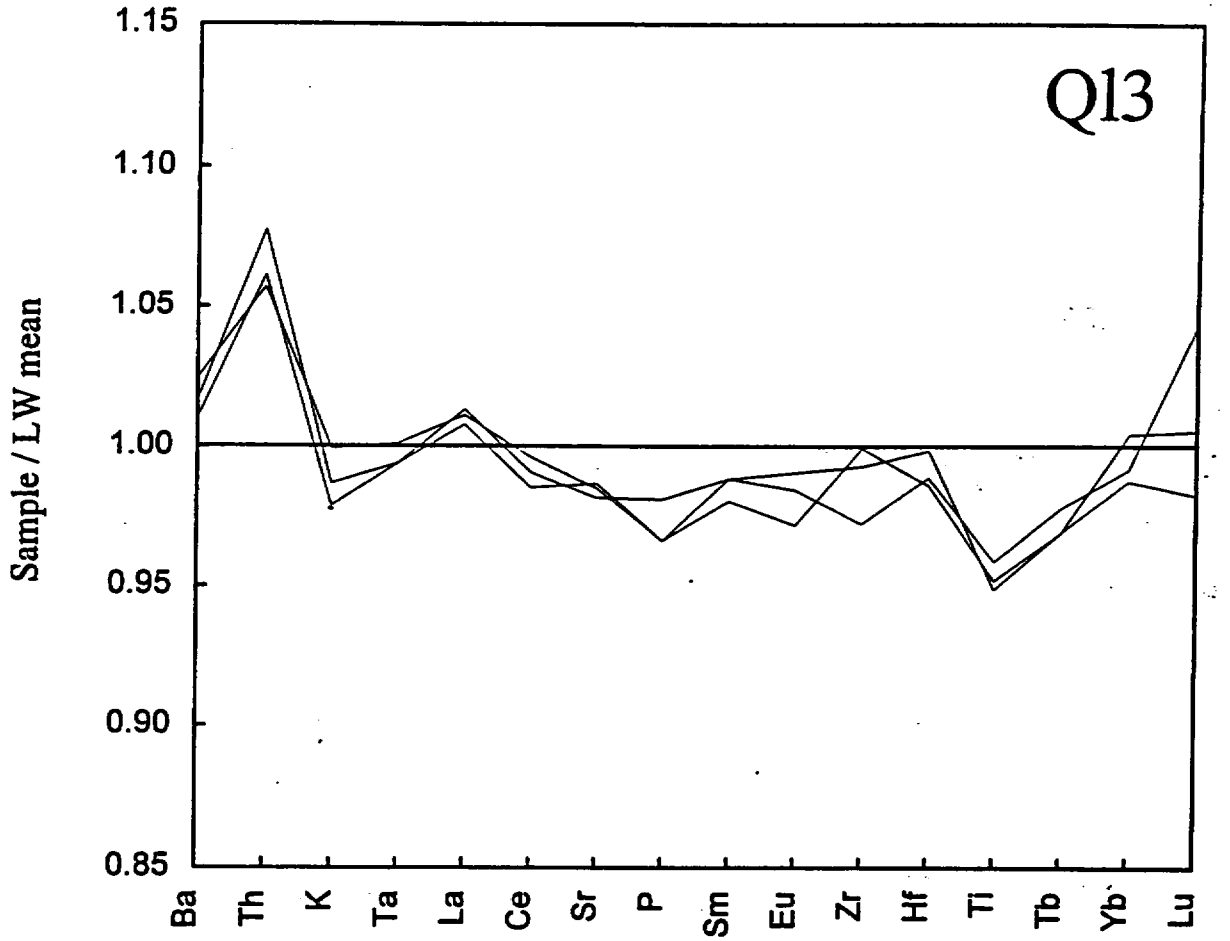
Q13
Sample / LW mean
1.15
1.10
1.05
1.00
0.95
0.90
0.85
Ba
Th
K
Ta
La
Ce
Sr
P
Sm
Eu
Zr
Hf
Ti
Tb
Yb
Lu

Figure 32

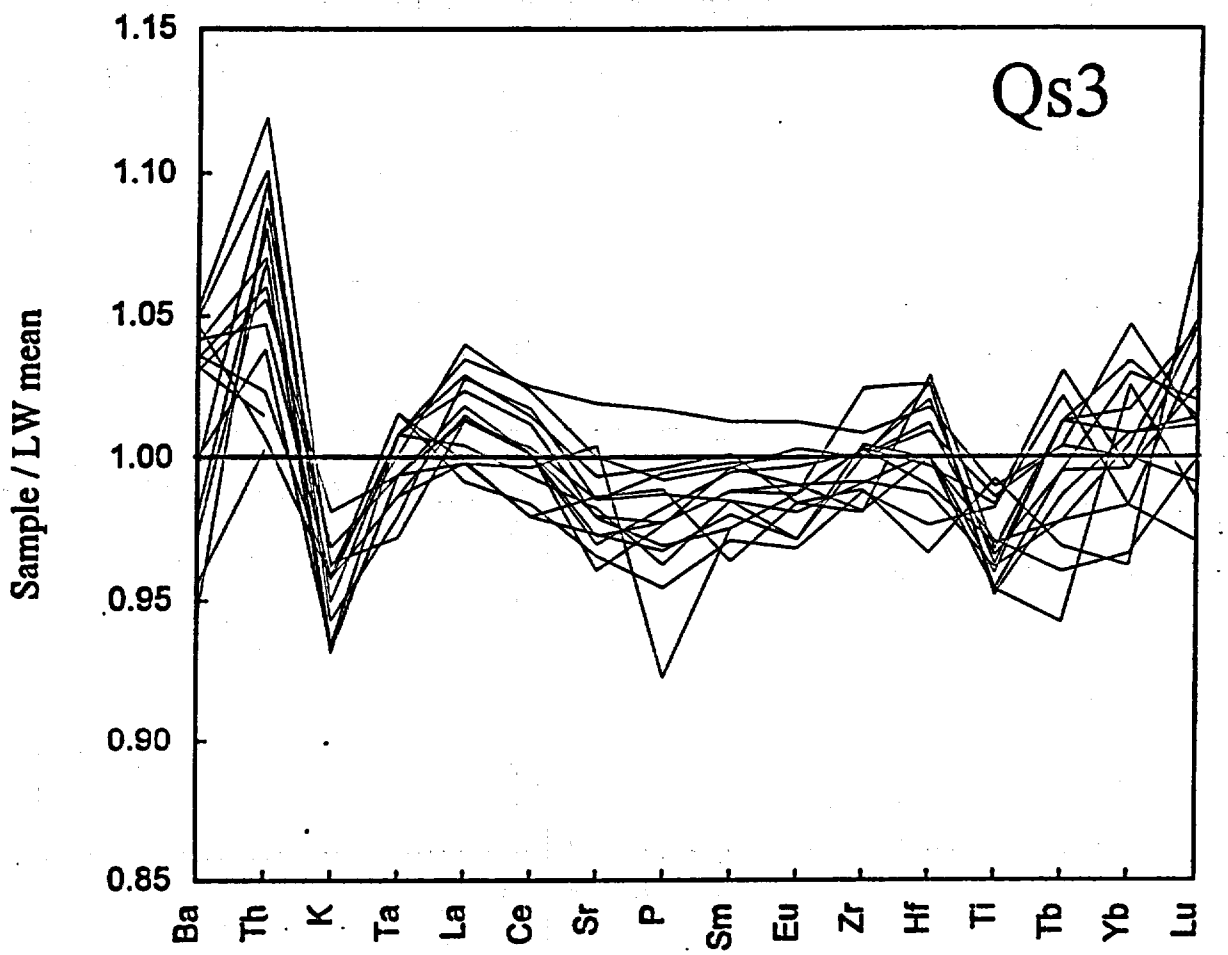
Qs3
Sample / LW mean
1.15
1.10
1.05
1.00
0.95
0.90
0.85
Ba
Th
K
Ta
La
Ce
Sr
P
Sm
Eu
Zr
Hf
Ti
Tb
Yb
Lu

Figure 33

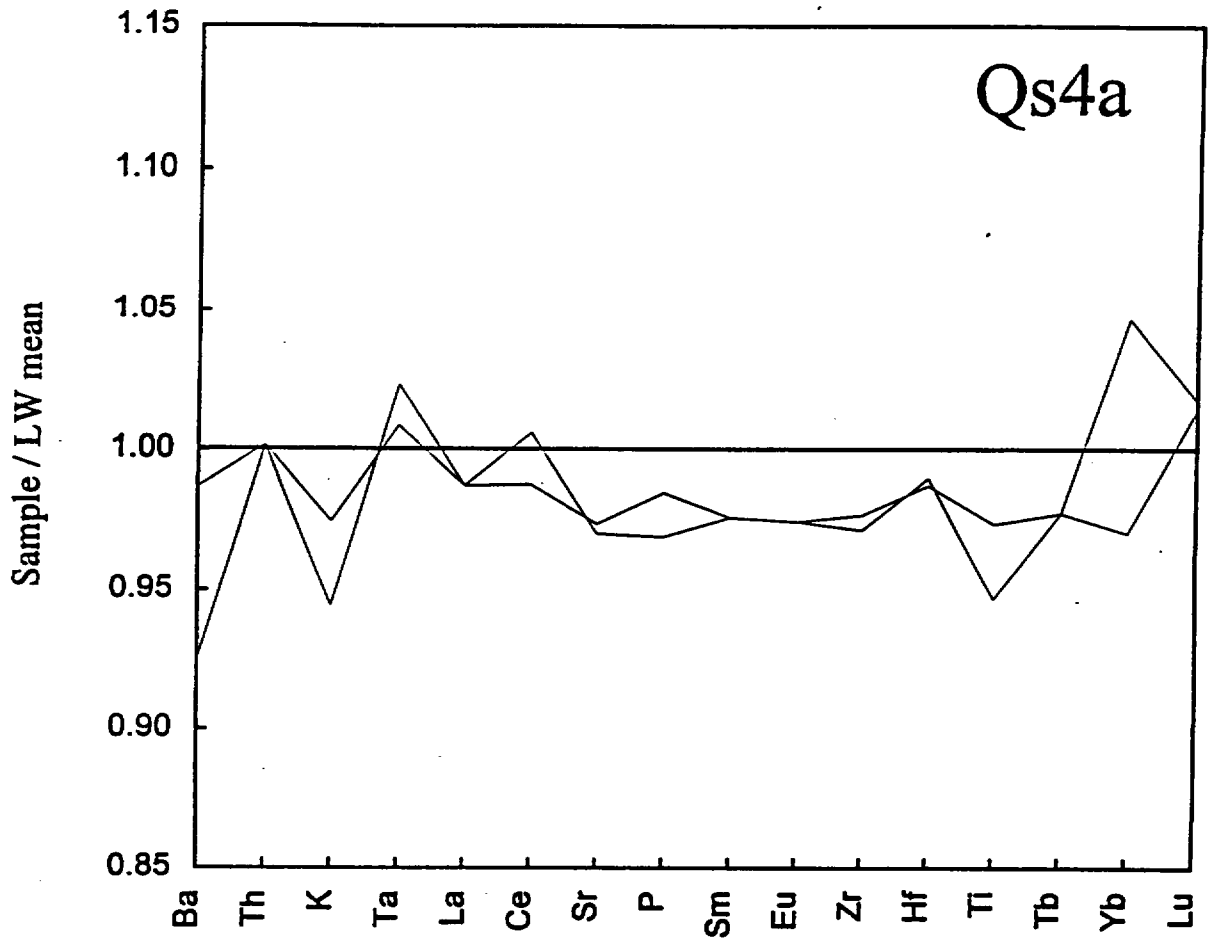
Qs4a
Sample / LW mean
1.15
1.10
1.05
1.00
0.95
0.90
0.85
Ba
Th
K
Ta
La
Ce
Sr
P
Sm
Eu
Zr
Hf
Ti
Tb
Yb
Lu

Figure 34

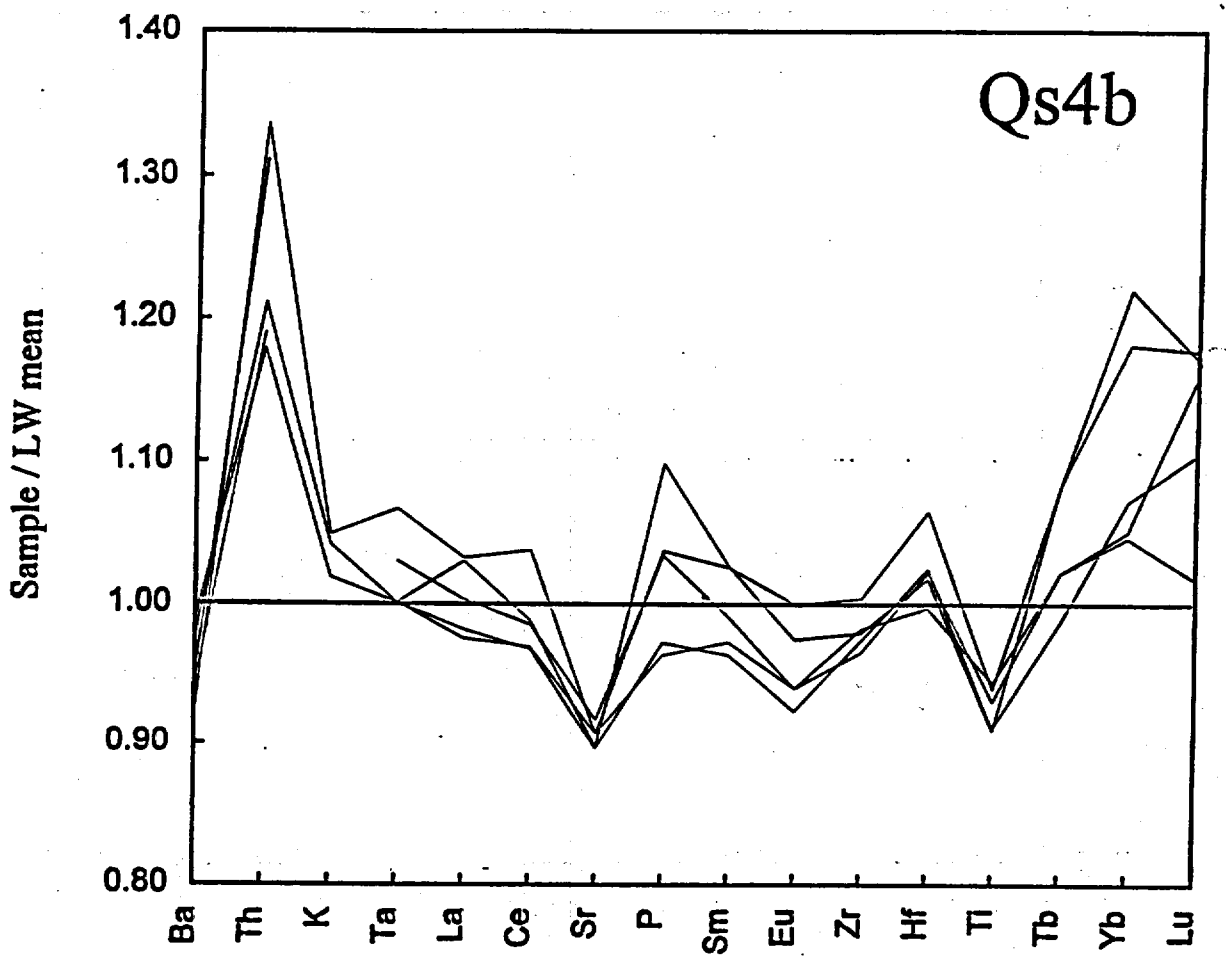
Qs4b
Sample / LW mean
1.40
1.30
1.20
1.10
1.00
0.90
0.80
Ba
Th
K
Ta
La
Ce
Sr
P
Sm
Eu
Zr
Hf
Ti
Tb
Yb
Lu

Figure 35

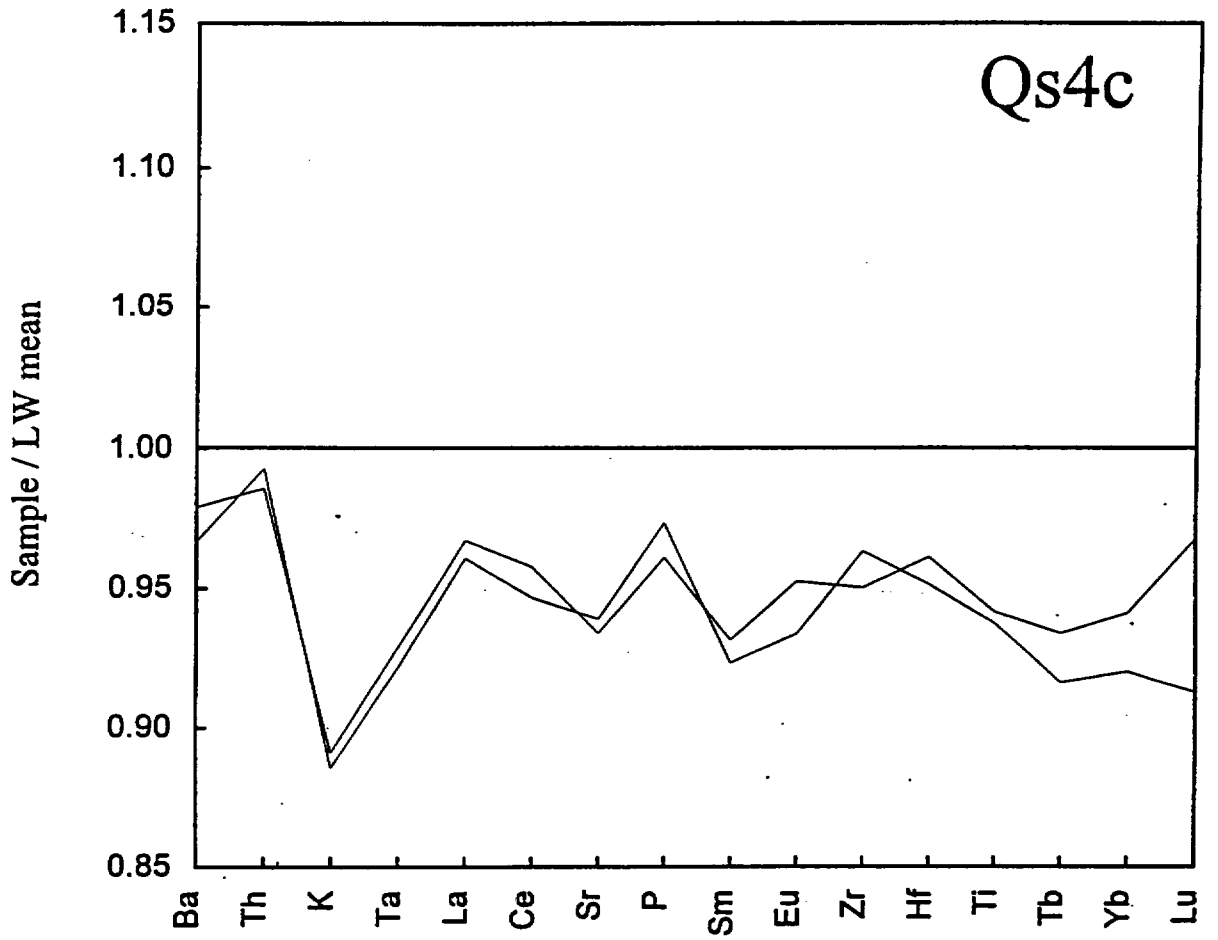
Qs4c
Sample / LW mean
1.15
1.10
1.05
1.00
0.95
0.90
0.85
Ba
Th
K
Ta
La
Ce
Sr
P
Sm
Eu
Zr
Hf
Ti
Tb
Yb
Lu

Figure 36

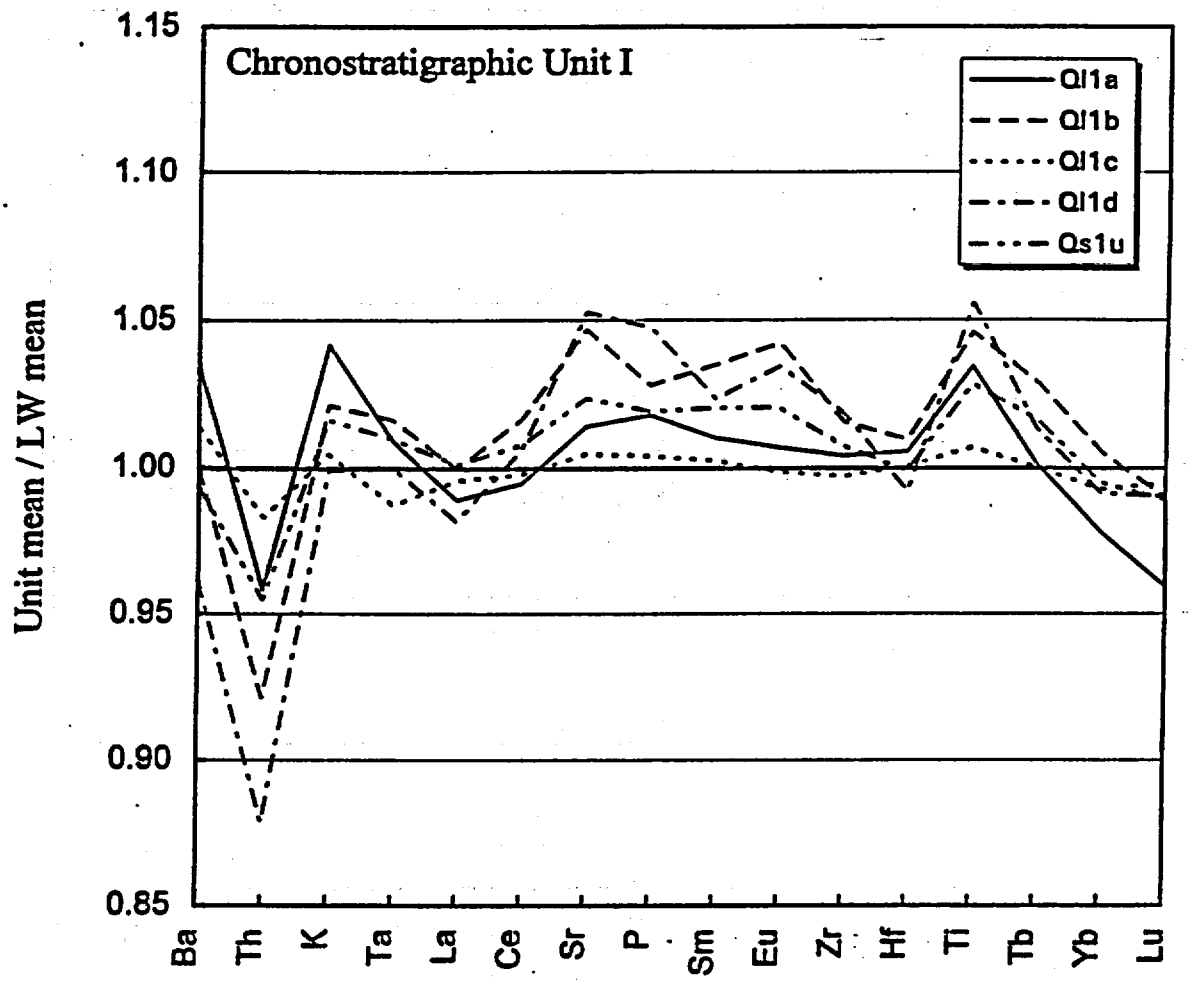
Chronostratigraphic Unit I
Ql1a
Ql1b
Ql1c
Ql1d
Qs1u
Unit mean / LW mean
1.15
1.10
1.05
1.00
0.95
0.90
0.85
Ba
Th
K
Ta
La
Ce
Sr
P
Sm
Eu
Zr
Hf
Ti
Tb
Yb
Lu

Figure 37

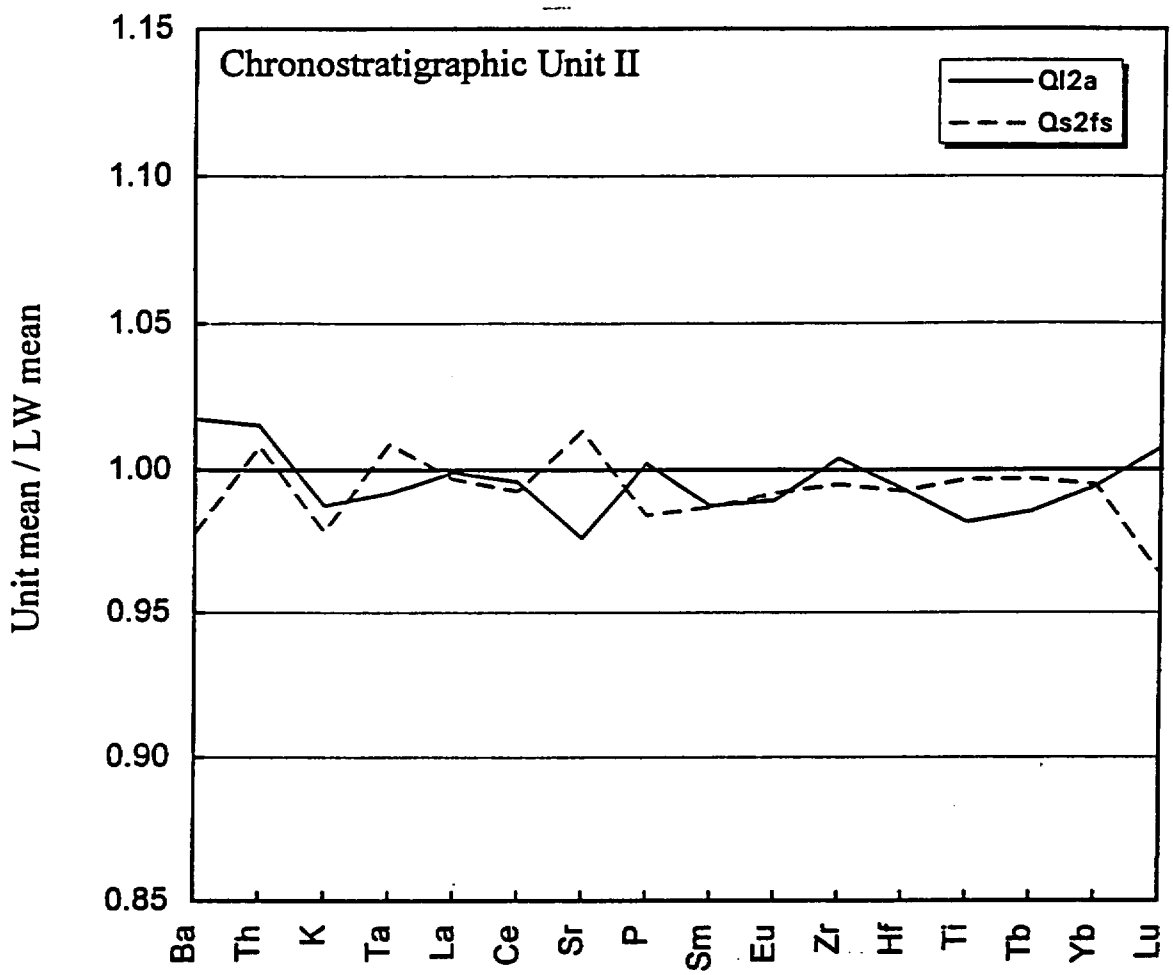
Chronostratigraphic Unit II
Ql2a
Qs2fs
Unit mean / LW mean
1.15
1.10
1.05
1.00
0.95
0.90
0.85
Ba
Th
K
Ta
La
Ce
Sr
P
Sm
Eu
Zr
Hf
Ti
Tb
Yb
Lu

Figure 38

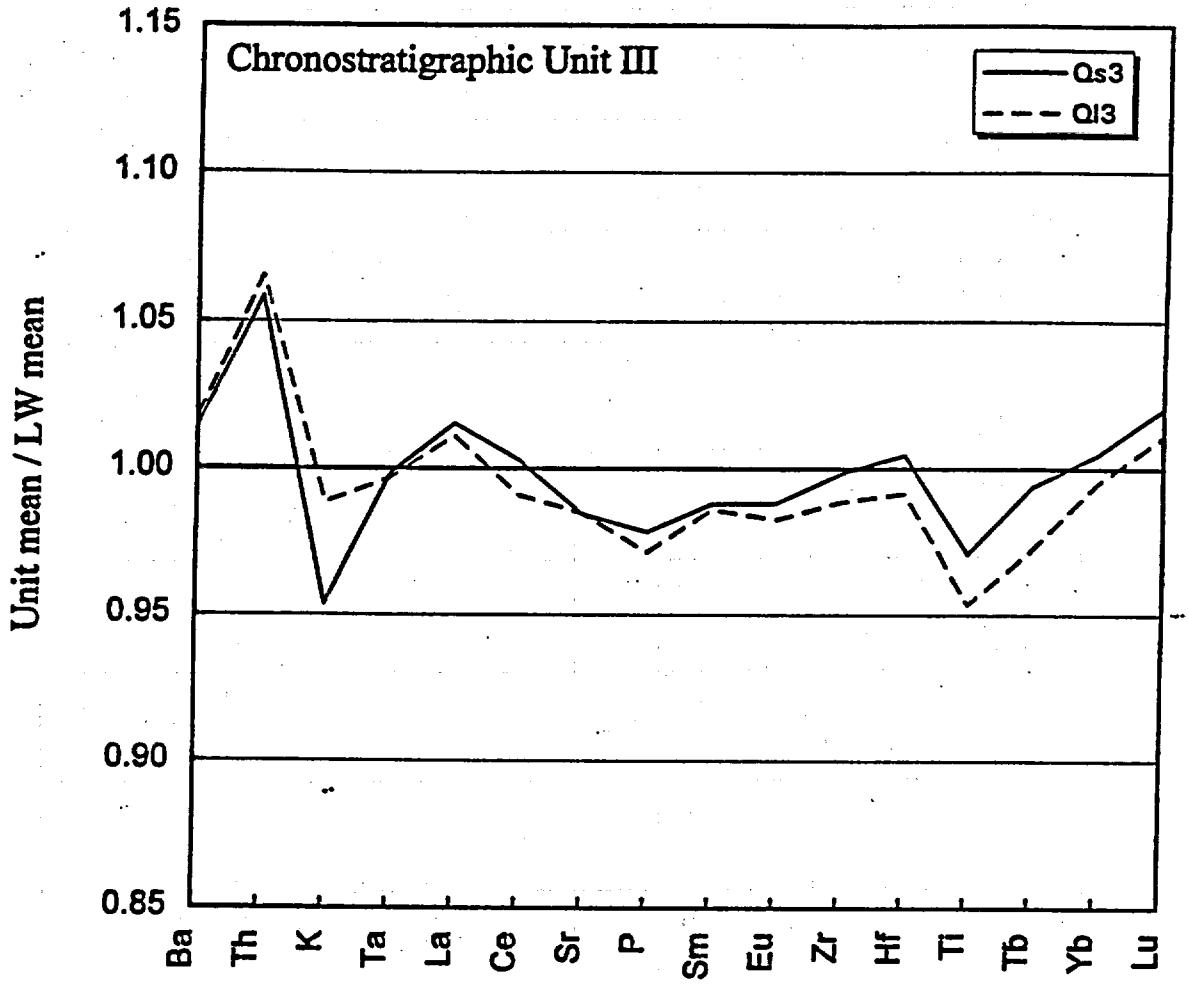
Chronostratigraphic Unit III
Qs3
Ql3
Unit mean / LW mean
1.15
1.10
1.05
1.00
0.95
0.90
0.85
Ba
Th
K
Ta
La
Ce
Sr
P
Sm
Eu
Zr
Hf
Ti
Tb
Yb
Lu

Figure 39

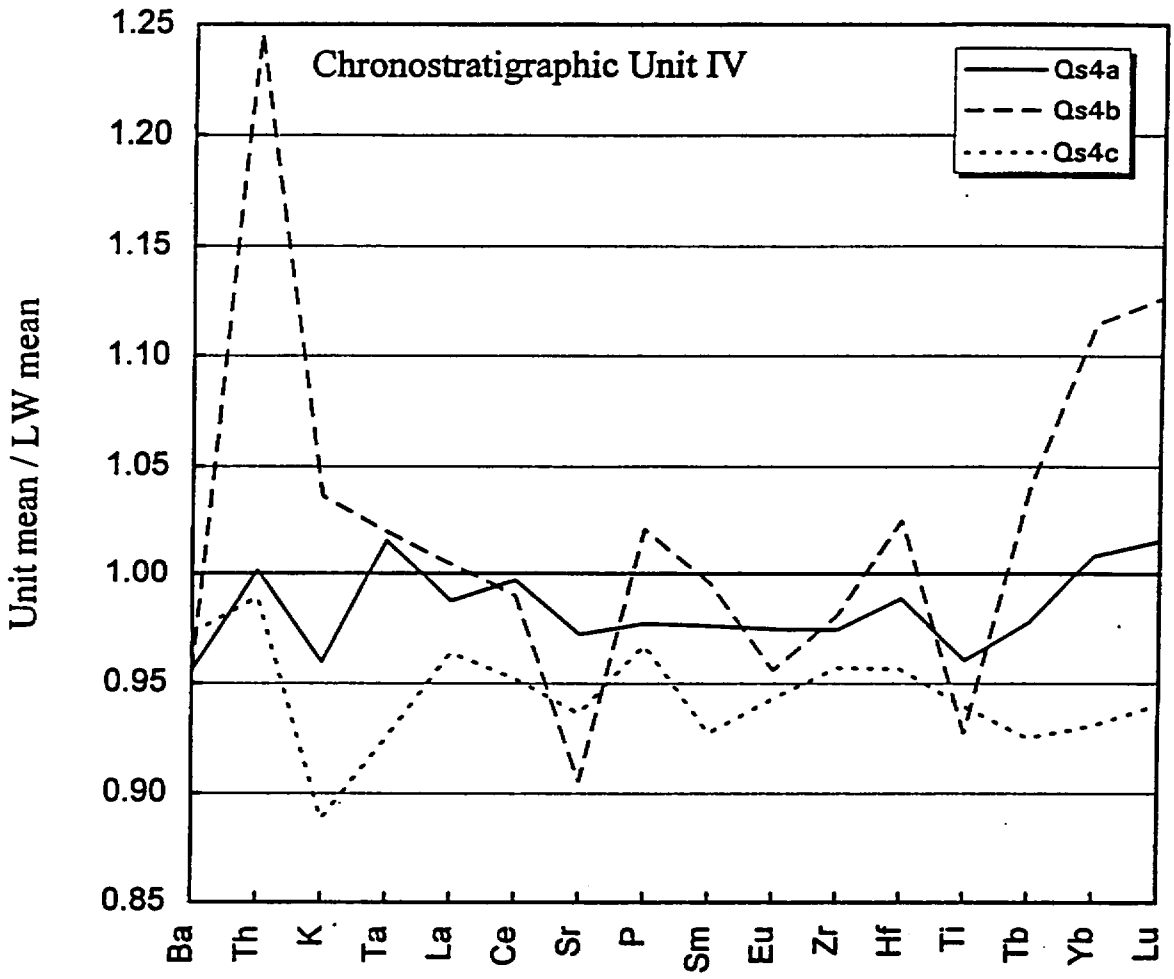
Chronostratigraphic Unit IV
Qs4a
Qs4b
Qs4c
Unit mean / LW mean
1.25
1.20
1.15
1.10
1.05
1.00
0.95
0.90
0.85
Ba
Th
K
Ta
La
Ce
Sr
P
Sm
Eu
Zr
Hf
Ti
Tb
Yb
Lu

Figure 40

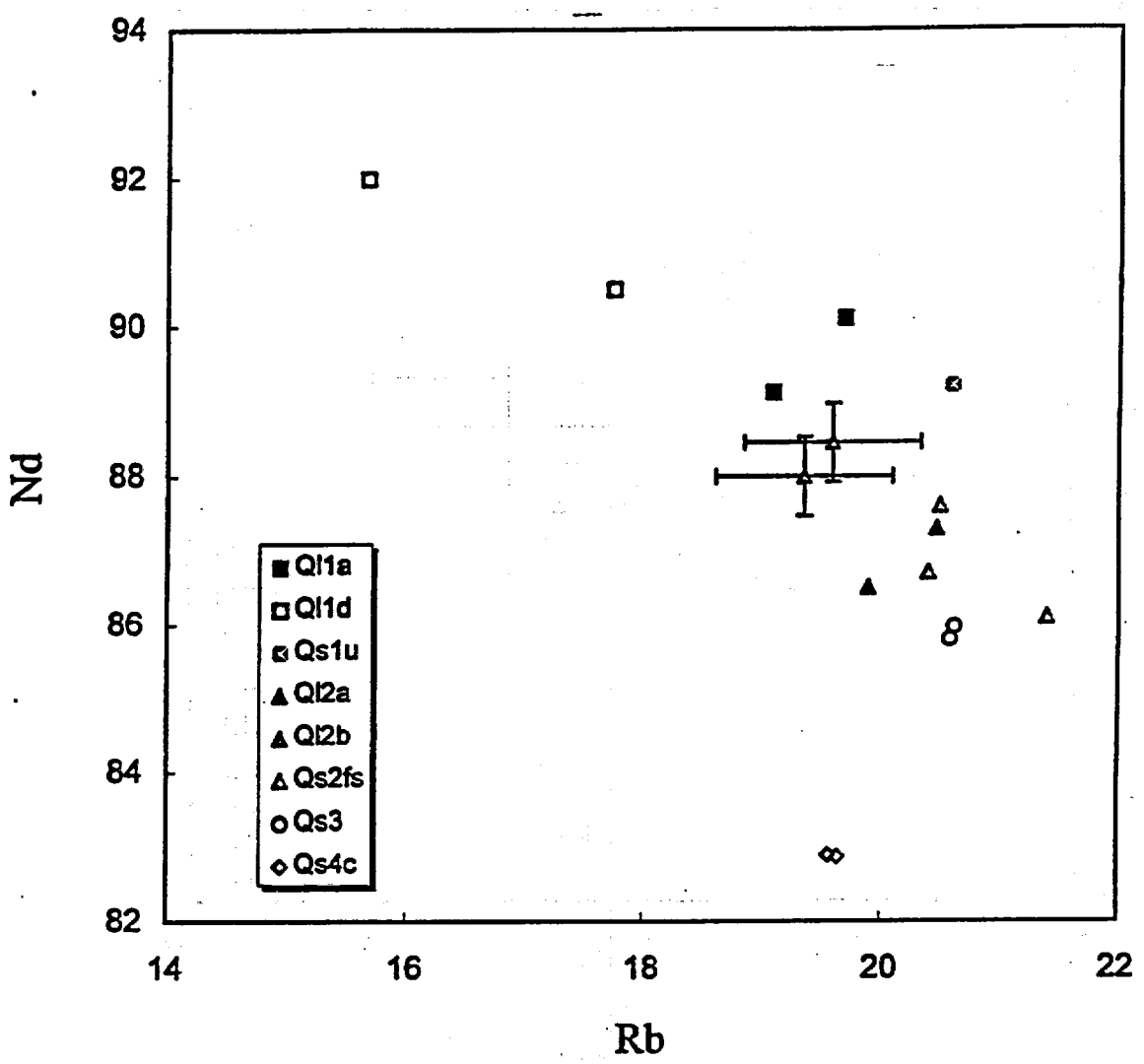
94
92
90
88
86
84
82
Nd
14
16
18
20
22
Rb
Ql1a
Ql1d
Qs1u
Ql2a
Ql2b
Qs2fs
Qs3
Qs4c

Figure 41

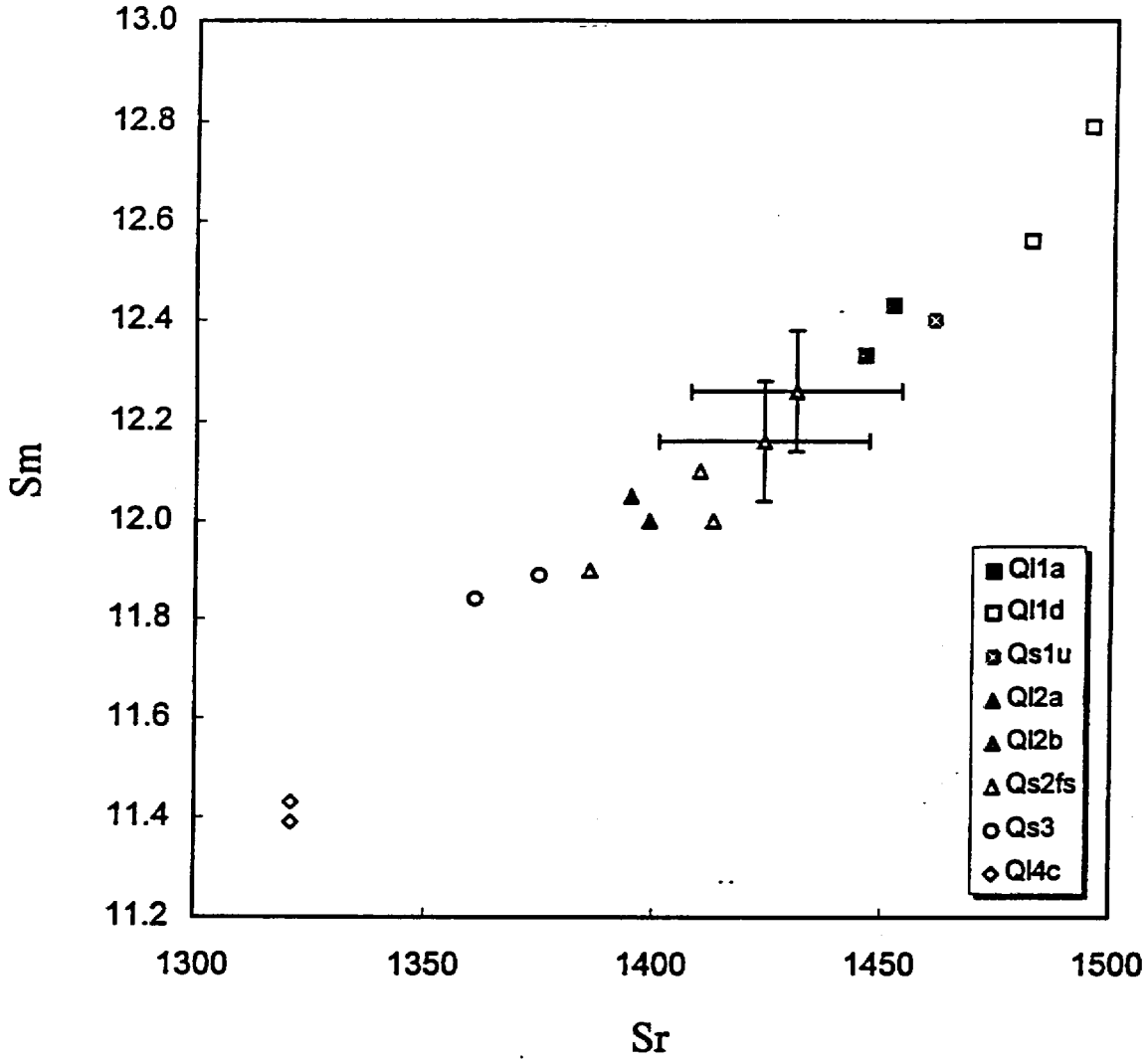
13.0
12.8
12.6
12.4
12.2
12.0
11.8
11.6
11.4
11.2
Sm
1300
1350
1400
1450
1500
Sr
Ql1a
Ql1d
Qs1u
Ql2a
Ql2b
Qs2fs
Qs3
Ql4c

Figure 42

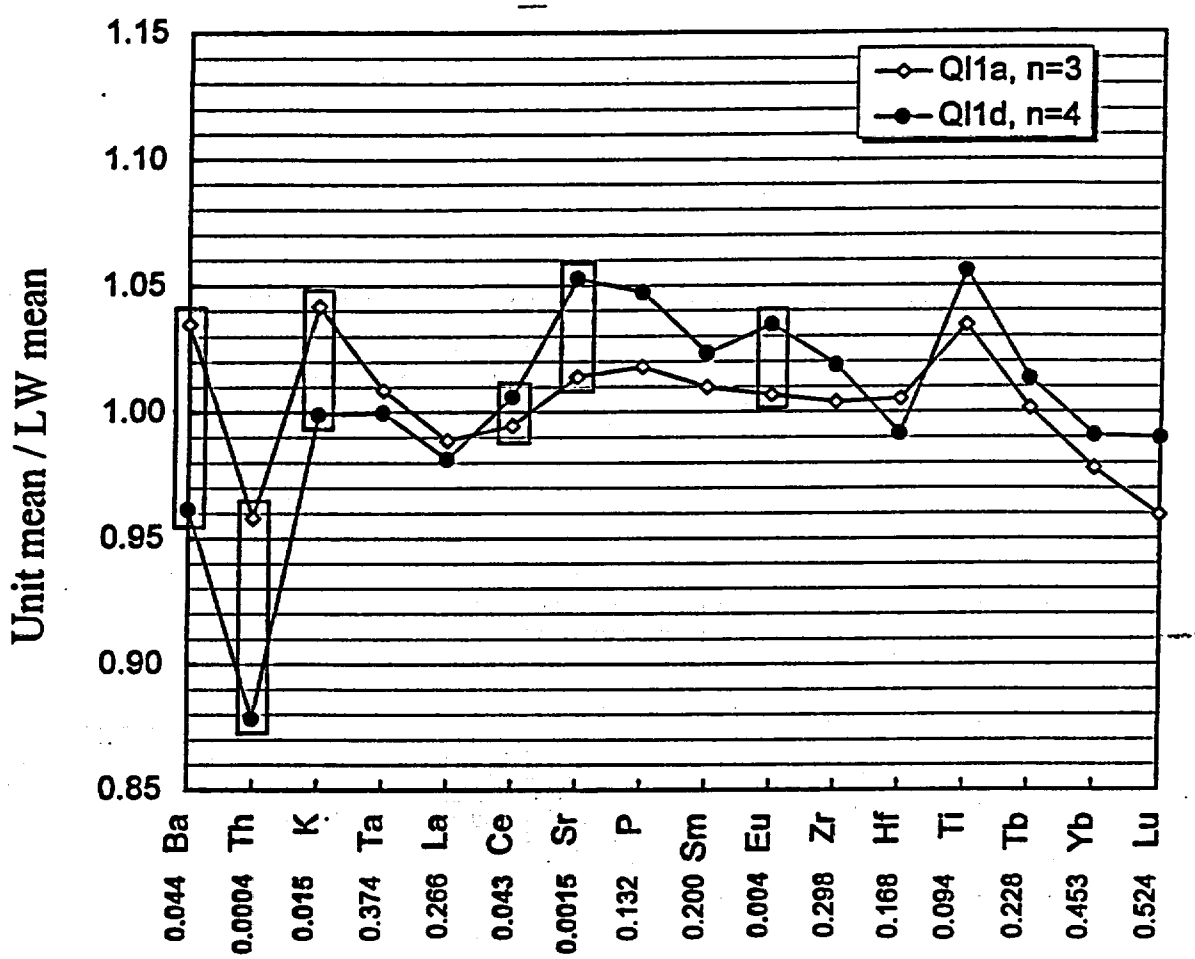
Unit mean / LW mean
1.15
1.10
1.05
1.00
0.95
0.90
0.85
Ql1a, n=3
Ql1d, n=4
Ba 0.044
Th 0.0004
K 0.015
Ta 0.374
La 0.266
Ce 0.043
Sr 0.0015
P 0.132
Sm 0.200
Eu 0.004
Zr 0.298
Hf 0.168
Ti 0.094
Tb 0.228
Yb 0.453
Lu 0.524

Figure 43

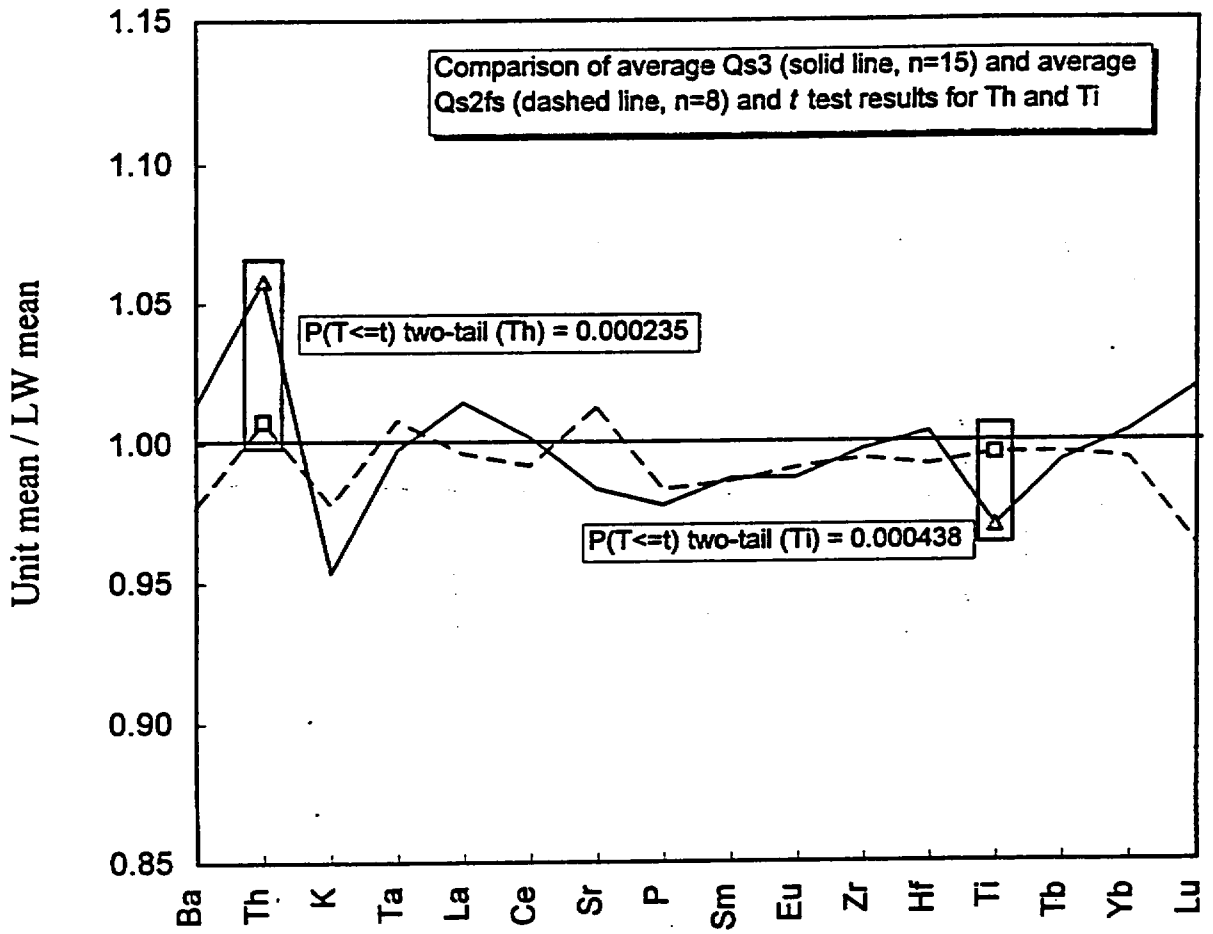
Comparison of average Qs3 (solid line, n=15) and average Qs2fs (dashed line, n=8) and t test results for Th and Ti
P(T<=t) two-tail (Th) = 0.000235
P(T<=t) two-tail (Ti) = 0.000438
Unit mean / LW mean
1.15
1.10
1.05
1.00
0.95
0.90
0.85
Ba
Th
K
Ta
La
Ce
Sr
P
Sm
Eu
Zr
Hf
Ti
Tb
Yb
Lu

Figure 44

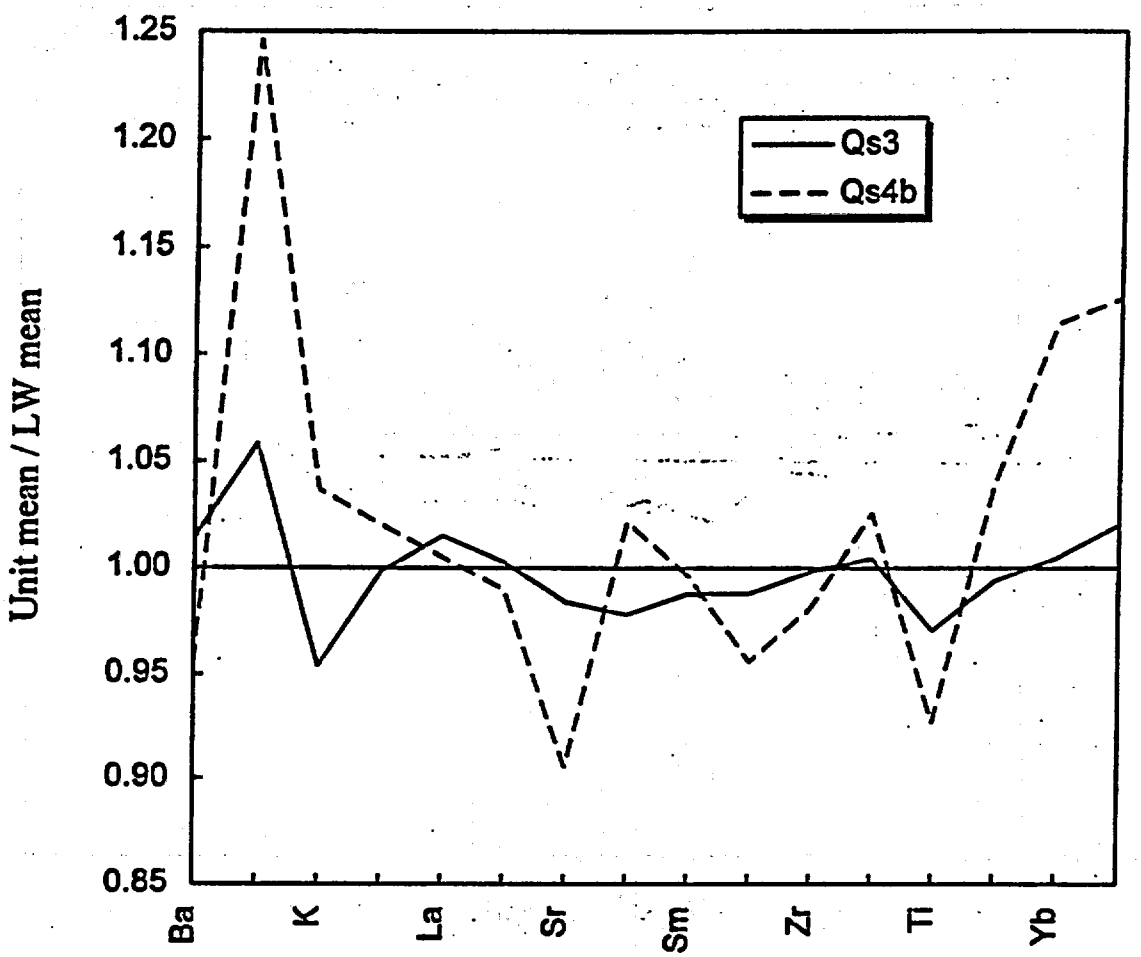
Unit mean / LW mean
1.25
1.20
1.15
1.10
1.05
1.00
0.95
0.90
0.85
Qs3
Qs4b
Ba
K
La
Sr
Sm
Zr
Ti
Yb

Figure 45

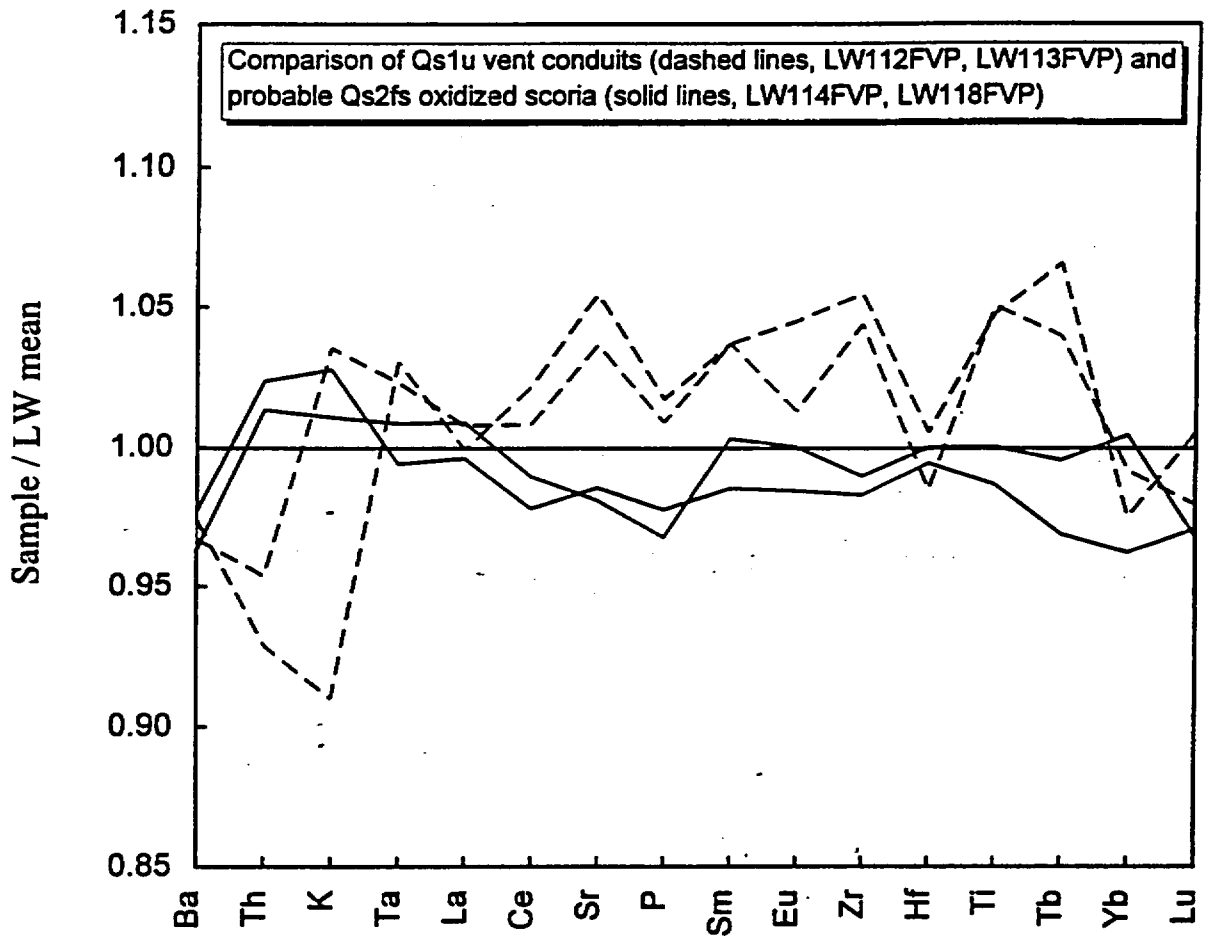
Comparison of Qs1u vent conduits (dashed lines, LW112FVP, LW113FVP) and probable Qs2fs oxidized scoria (solid lines, LW114FVP, LW118FVP)
Sample / LW mean
1.15
1.10
1.05
1.00
0.95
0.90
0.85
Ba
Th
K
Ta
La
Ce
Sr
P
Sm
Eu
Zr
Hf
Ti
Tb
Yb
Lu

Figure 46

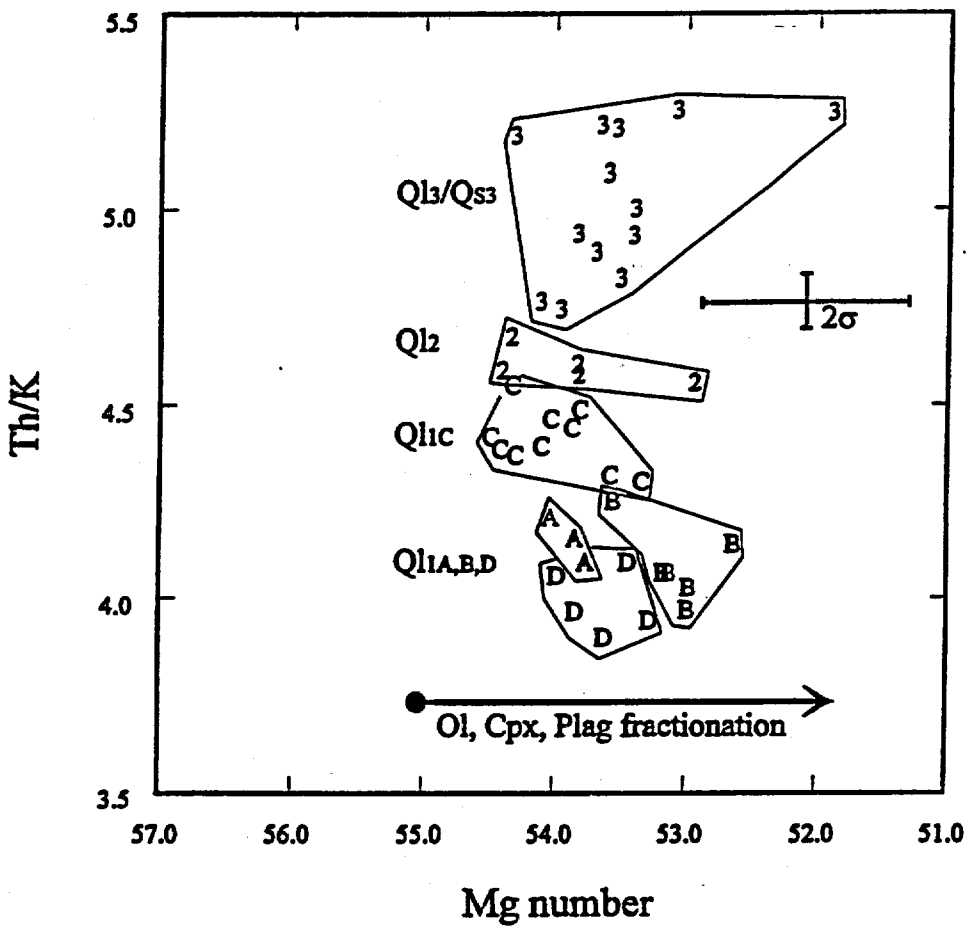
5.5
5.0
4.5
4.0
3.5
Th/K
57.0
56.0
55.0
54.0
53.0
52.0
51.0
Mg number
Ql3/Qs3
Ql2
Ql1C
Ql1A,B,D
2σ
Ol, Cpx, Plag fractionation

Figure 47

Table 1. Major, trace-element (determined by XRF) and normative compositions of Lathrop Wells basalts

Sample	LW11FVP	LW12FVP	LW74FVP	LW45FVP	LW72FVP	LW73FVP	LW100FVP	LW120FVP	LW121FVP	LW101FVP	LW30FVP	LW31FVP	LW32FVP	LW63FVP
Unit	Qlla	Qlla	Qlla	Qllb	Qllb	Qllb	Qllb	Qllb	Qllb	Qslb	Qllc	Qllc	Qllc	Qllc
SiO_2	48.59	48.63	48.49	47.83	47.89	48.47	48.55	48.25	48.62	48.94	47.55	48.82	48.25	48.31
TiO_2	1.98	1.97	2.01	2.02	1.99	2.02	2.02	2.04	2.01	2.01	1.89	1.93	1.96	1.92
Al_2O_3	16.80	16.95	16.64	16.45	16.60	16.71	16.61	16.87	16.74	16.79	16.26	16.74	16.79	16.65
Fe_2O_3T	11.78	11.82	11.72	11.91	11.80	11.85	11.88	11.95	11.80	11.88	11.36	11.58	11.70	11.56
Fe_2O_3	1.77	1.77	1.76	1.79	1.77	1.78	1.78	1.79	1.77	1.78	1.70	1.74	1.75	1.73
FeO	9.01	9.04	8.97	9.11	9.03	9.07	9.09	9.14	9.03	9.09	8.69	8.86	8.95	8.84
MnO	0.18	0.17	0.17	0.18	0.17	0.18	0.18	0.18	0.18	0.18	0.17	0.17	0.17	0.18
MgO	5.89	5.93	5.93	5.81	5.72	5.88	5.80	5.80	5.88	5.77	5.84	5.82	5.75	5.92
CaO	8.29	8.41	8.55	8.42	8.66	8.48	8.68	8.46	8.59	8.43	9.36	8.54	8.50	8.45
Na_2O	3.57	3.48	3.66	3.65	3.57	3.58	3.59	3.61	3.59	3.59	3.44	3.58	3.53	3.60
K_2O	1.92	1.93	1.89	1.88	1.88	1.84	1.91	1.90	1.86	1.91	1.83	1.86	1.84	1.81
P_2O_5	1.24	1.25	1.21	1.26	1.25	1.26	1.24	1.27	1.26	1.25	1.19	1.21	1.24	1.23
Total	100.24	100.56	100.27	99.40	99.52	100.27	100.46	100.31	100.53	100.75	98.87	100.24	99.73	99.61
Mg#	53.82	53.90	54.08	53.19	53.03	53.60	53.23	53.05	53.73	53.10	54.48	53.92	53.40	54.38
V	179.1	179.5	175.9	192.1	183.0	186.9	190.6	164.7	203.5	183.8	168.4	180.5	183.7	177.9
Cr	112.8	115.0	119.4	108.7	106.4	101.0	106.6	122.9	127.0	123.2	113.7	142.2	110.0	131.0
Ni	60.0	60.7	57.4	49.1	53.1	62.2	56.5	59.0	56.3	55.0	54.8	64.0	57.4	57.2
Zn	128.9	124.9	138.3	139.5	133.6	84.1	143.2	145.7	143.8	140.8	126.9	127.4	127.7	131.0
Rb	19.4	19.9	15.7	19.8	19.7	15.3	18.7	17.2	14.1	19.8	19.7	18.7	14.6	19.1
Sr	1490	1488	1492	1530	1578	1536	1541	1540	1521	1519	1453	1467	1497	1466
Y	27.9	30.8	36.0	23.1	27.2	24.6	21.4	30.9	23.5	29.9	29.9	19.2	28.0	27.0
Zr	372.8	366.2	377.2	383.8	354.0	382.4	374.4	386.0	370.7	368.0	366.3	377.3	367.0	370.2
Nb	30.8	27.1	30.6	29.7	27.2	37.6	34.4	28.5	32.4	35.6	30.1	34.3	31.0	30.1
Ba	1373	1391	1464	1424	1354	1428	1249	1280	1309	1312	1337	1389	1435	1412
Or	11.36	11.42	11.17	11.13	11.13	10.90	11.30	11.22	10.99	11.27	10.80	10.99	10.89	10.68
Ab	29.65	29.36	28.45	27.97	27.57	29.37	28.45	28.53	29.21	30.15	25.16	29.86	29.17	29.34
An	24.26	25.02	23.52	23.06	23.84	24.17	23.67	24.32	24.18	24.16	23.61	24.24	24.65	24.03
Ne	0.29	0.07	1.34	1.57	1.40	0.52	1.04	1.10	0.63	0.13	2.15	0.21	0.36	0.62
Di	7.94	7.76	9.78	9.37	9.77	8.75	10.02	8.43	9.15	8.55	13.10	9.11	8.49	8.84
Hy	0.00	0.00	0.00	0.00	0.00	0.00	0.00	0.00	0.00	0.00	0.00	0.00	0.00	0.00
Ol	16.81	16.99	16.11	16.23	15.86	16.51	15.96	16.56	16.35	16.45	14.55	16.12	16.31	16.39
Mt	2.56	2.57	2.55	2.59	2.57	2.58	2.58	2.60	2.57	2.58	2.47	2.52	2.54	2.51
Il	3.76	3.75	3.82	3.83	3.77	3.84	3.83	3.87	3.82	3.81	3.59	3.66	3.72	3.64
Ap	2.97	3.00	2.91	3.02	2.99	3.01	2.98	3.04	3.01	2.99	2.84	2.91	2.97	2.94

FeO, Fe_2O_3 and Mg# calculated assuming Fe^{3+}/Fe total = 0.15. K_2O values in parentheses are from oxidized scoria that has probably been affected by alteration.

Analytical uncertainties (2 sigma) are 1% for CaO, 2% for TiO_2, Al_2O_3, Fe_2O_3, MgO, K_2O, P_2O_5 and Sr, 3% for SiO_2 and Na_2O, 4% for Ba, 8% for MnO and Zr, 10% for Cr and Zn, 13% for V, 20% for Ni, Rb, Y and Nb.

Table 1. Major, trace-element (determined by XRF) and normative compositions of Lathrop Wells basalts

LW64FVP	LW65FVP	LW66FVP	LW67FVP	LW110FVP	LW115FVP	LW93FVP	LW109FVP	LW20FVP	LW21FVP	LW22FVP	LW23FVP	LW79FVP	LW01FVP	LW71FVP
Qllc	Qllc	Qllc	Qllc	Qllc	Qllc	Qslc	Qslc	Qlld	Qlld	Qlld	Qlld	Qsld	Qslr	Qslr
48.24	48.57	48.55	48.56	49.67	49.46	49.03	48.70	48.58	46.53	47.43	47.74	48.41	48.66	48.45
1.93	1.97	1.92	1.92	1.97	1.95	1.97	1.92	2.04	1.98	2.06	2.03	2.04	1.97	2.04
16.76	16.94	16.98	16.64	17.03	17.16	16.93	16.60	16.69	16.06	16.60	16.39	16.72	16.77	16.77
11.52	11.66	11.53	11.65	11.71	11.71	11.68	11.55	12.02	11.88	12.15	12.02	12.12	11.78	11.94
1.73	1.75	1.73	1.75	1.76	1.76	1.75	1.73	1.80	1.78	1.82	1.80	1.82	1.77	1.79
8.81	8.92	8.82	8.91	8.96	8.96	8.94	8.84	9.20	9.09	9.30	9.20	9.27	9.01	9.14
0.17	0.17	0.17	0.17	0.17	0.17	0.17	0.17	0.18	0.18	0.18	0.17	0.17	0.17	0.17
5.84	5.79	5.78	6.00	5.92	5.99	5.94	5.82	6.03	5.83	6.13	5.98	5.99	5.84	5.81
8.54	8.31	8.51	8.41	8.42	8.40	8.34	8.50	8.53	9.12	8.40	8.61	8.28	8.41	8.36
3.51	3.61	3.62	3.63	3.70	3.64	3.59	3.72	3.61	3.51	3.55	3.58	3.50	3.53	3.68
1.85	1.87	1.84	1.85	1.85	1.86	1.87	1.99	1.88	1.82	1.80	1.85	1.87	1.84	1.93
1.20	1.25	1.22	1.22	1.22	1.21	1.22	1.18	1.29	1.26	1.31	1.24	1.30	1.24	1.26
99.56	100.13	100.12	100.06	101.65	101.55	100.73	100.14	100.85	98.15	99.60	99.61	100.39	100.20	100.40
54.16	53.63	53.86	54.54	54.09	54.36	54.22	53.98	53.90	53.34	54.04	53.68	53.50	53.60	53.13
183.5	178.2	178.4	177.8	182.1	193.7	173.7	180.9	173.1	180.6	184.6	185.9	176.7	186.5	184.2
124.9	109.3	103.3	124.7	121.7	120.6	119.3	113.9	103.8	119.6	106.2	109.3	123.4	115.8	113.6
54.9	54.8	51.6	59.8	52.2	47.5	51.2	58.6	61.5	61.3	61.7	66.9	66.2	52.3	59.5
128.5	137.2	131.0	134.9	137.1	131.8	142.9	137.8	132.6	130.5	123.3	135.8	134.2	133.8	135.0
18.7	16.2	19.4	17.3	20.8	19.1	18.9	18.7	14.5	18.6	14.0	14.4	18.4	17.1	17.0
1480	1500	1485	1460	1470	1483	1471	1470	1552	1533	1556	1547	1532	1516	1577
28.6	31.3	28.6	30.6	30.6	31.6	25.6	25.2	31.4	29.9	23.5	26.1	27.5	25.9	29.4
372.6	369.2	362.0	366.3	368.8	375.1	375.9	376.4	381.8	367.2	381.8	379.4	367.6	381.4	365.8
27.0	29.3	36.6	35.2	31.6	32.4	34.4	35.3	26.6	27.4	29.4	33.6	26.0	37.1	28.4
1370	1375	1368	1440	1341	1338	1325	1289	1326	1318	1315	1280	1354	1428	1306
10.95	11.03	10.88	10.93	10.96	11.02	11.04	11.77	11.10	10.73	10.64	10.93	11.06	10.86	11.40
28.78	30.04	29.34	29.39	31.28	30.81	30.37	28.22	28.93	23.82	27.58	27.15	29.59	29.88	28.84
24.61	24.63	24.75	23.77	24.50	25.08	24.68	22.83	23.89	22.81	24.15	23.28	24.51	24.59	23.63
0.50	0.26	0.71	0.70	0.00	0.00	0.00	1.75	0.88	3.17	1.32	1.71	0.00	0.00	1.26
8.87	7.66	8.55	8.95	8.37	7.89	7.89	10.30	8.99	12.47	8.13	10.10	7.38	8.20	8.67
0.00	0.00	0.00	0.00	0.21	0.07	0.41	0.00	0.00	0.00	0.00	0.00	0.55	0.58	0.00
16.20	16.61	16.22	16.58	16.50	16.91	16.52	15.68	16.84	15.16	17.43	16.36	17.04	16.21	16.48
2.51	2.54	2.51	2.53	2.55	2.55	2.54	2.51	2.61	2.58	2.64	2.61	2.64	2.56	2.60
3.66	3.75	3.65	3.65	3.73	3.70	3.74	3.65	3.88	3.77	3.91	3.86	3.87	3.74	3.87
2.88	3.00	2.92	2.93	2.92	2.90	2.92	2.82	3.09	3.00	3.13	2.96	3.12	2.96	3.01

Table 1. Major, trace-element (determined by XRF) and normative compositions of Lathrop Wells basalts

LW53FVP	LW112FVP	LW08FVPA	LW09FVP	LW10FVPA	LW33FVP	LW34FVP	LW35FVP	LW42FVP	LW43FVP	LW46FVP	LW47FVP	LW49FVP	LW50FVP	LW51FVP
Qllu	Qllu	Qslu	Qslu	Qslu	Qslu	Qslu	Qslu	Qslu	Qslu	Qslu	Qslu	Qslu	Qslu	Qslu
48.12	49.51	48.78	48.27	48.42	48.95	48.80	48.80	46.60	47.52	48.32	48.60	48.56	48.50	48.71
2.04	2.02	2.00	1.97	1.98	1.95	1.94	1.94	1.96	2.01	1.96	1.96	1.97	1.95	1.97
16.80	16.84	16.65	16.57	16.52	17.10	16.90	16.93	16.09	16.24	16.80	16.75	16.68	16.62	16.87
11.99	11.43	11.80	11.67	11.68	11.69	11.73	11.64	11.53	11.88	11.67	11.72	11.74	11.58	11.58
1.80	1.71	1.77	1.75	1.75	1.75	1.76	1.75	1.73	1.78	1.75	1.76	1.76	1.74	1.74
9.17	8.74	9.03	8.93	8.94	8.94	8.97	8.91	8.82	9.09	8.93	8.97	8.98	8.86	8.86
0.18	0.19	0.17	0.17	0.18	0.17	0.18	0.18	0.17	0.17	0.17	0.17	0.17	0.17	0.17
5.98	6.01	5.79	5.86	5.67	5.86	5.98	5.78	5.51	5.76	5.82	5.91	5.96	5.87	5.86
8.46	8.36	8.66	8.58	8.69	8.37	8.29	8.45	8.56	8.29	8.41	8.37	8.39	8.29	8.36
3.72	3.25	3.58	3.56	3.48	3.65	3.58	3.59	3.63	3.62	3.52	3.52	3.48	3.54	3.59
1.81	1.67	1.86	1.88	1.89	1.86	1.86	1.89	1.82	1.86	1.90	1.87	1.88	1.85	1.89
1.27	1.24	1.23	1.26	1.25	1.25	1.24	1.24	1.23	1.23	1.21	1.23	1.22	1.20	1.22
100.37	100.51	100.52	99.78	99.76	100.85	100.49	100.43	97.09	98.59	99.77	100.10	100.04	99.56	100.22
53.75	55.06	53.34	53.91	53.09	53.85	54.30	53.65	52.69	53.04	53.76	54.00	54.18	54.13	54.09
182.7	208.9	184.6	179.6	177.0	185.7	188.0	185.0	176.9	174.0	167.4	190.1	180.3	179.1	171.3
110.6	112.1	121.5	117.1	116.2	120.3	132.0	121.3	107.3	98.9	115.6	123.9	113.4	120.1	118.6
69.1	56.3	58.9	57.0	51.3	53.0	54.8	52.6	53.8	54.1	53.8	56.0	62.2	56.7	57.2
113.0	157.9	142.4	136.0	142.1	120.6	122.1	125.7	148.9	139.5	136.2	107.6	141.1	137.1	139.7
14.4	17.1	19.5	18.9	18.1	12.4	16.8	19.5	13.8	17.2	17.5	17.4	18.6	18.0	21.0
1572	1550	1525	1522	1541	1455	1460	1481	1510	1509	1470	1485	1478	1474	1502
25.9	24.1	26.9	35.6	27.2	33.2	25.6	22.8	22.4	24.8	29.8	29.0	22.8	16.5	26.5
364.7	386.9	363.4	382.0	369.9	365.7	360.7	365.8	377.3	387.4	391.9	370.0	373.8	369.9	357.7
30.3	34.2	29.7	27.7	31.2	28.5	30.5	37.8	28.0	23.2	33.2	30.6	32.7	30.8	33.5
1399	1326	1292	1378	1272	1391	1401	1378	1353	1354	1418	1408	1411	1444	1396
10.72	9.89	11.00	11.11	11.16	10.97	11.00	11.18	10.76	11.02	11.21	11.05	11.10	10.94	11.20
28.23	27.46	29.40	28.60	29.07	30.31	30.30	29.87	26.13	28.07	29.03	29.79	29.48	29.91	29.83
23.90	26.56	23.96	23.81	23.96	24.88	24.65	24.61	22.35	22.68	24.56	24.49	24.44	24.12	24.43
1.76	0.00	0.49	0.80	0.22	0.33	0.01	0.26	2.46	1.36	0.40	0.00	0.00	0.00	0.30
8.83	6.38	9.77	9.45	9.74	7.72	7.64	8.29	10.69	9.33	8.33	8.16	8.32	8.24	8.21
0.00	11.72	0.00	0.00	0.00	0.00	0.00	0.00	0.00	0.00	0.00	0.19	0.41	0.50	0.00
16.79	8.63	15.97	16.12	15.68	16.77	17.09	16.41	14.92	16.12	16.46	16.58	16.47	16.12	16.47
2.61	2.48	2.57	2.54	2.54	2.54	2.55	2.53	2.51	2.58	2.54	2.55	2.55	2.52	2.52
3.87	3.83	3.79	3.73	3.76	3.71	3.67	3.68	3.72	3.82	3.72	3.71	3.73	3.71	3.74
3.04	2.96	2.95	3.01	3.00	2.99	2.97	2.97	2.95	2.95	2.90	2.95	2.92	2.89	2.92

Table 1. Major, trace-element (determined by XRF) and normative compositions of Lathrop Wells basalts

LW52FVP	LW98FVP	LW99FVP	LW103FVP	LW113FVP	LW116FVP	LW117FVP	LW06FVP	LW07FVP	LW40FVP	LW41FVP	LW55FVP	LW56FVP	LW19FVP	LW25FVP
Qslu	Qslu	Qslu	Qslu	Qslu	Qslu	Qslu	Ql2a	Ql2a	Ql2a	Ql2a	Ql2a	Ql2a	Ql2a	Ql2b
48.60	48.94	48.89	48.91	49.02	48.37	47.92	48.58	48.89	49.74	48.78	48.71	48.30	48.96	48.26
1.95	1.97	1.99	1.97	2.01	1.98	1.97	1.90	1.89	1.89	1.89	1.84	1.90	1.86	1.93
16.75	16.84	16.92	16.60	16.96	16.81	16.49	16.92	17.10	17.06	16.87	16.76	16.65	16.69	16.96
11.73	11.75	11.81	11.84	11.88	11.81	11.57	11.45	11.50	11.38	11.48	11.43	11.56	11.40	11.90
1.76	1.76	1.77	1.78	1.78	1.77	1.74	1.72	1.72	1.71	1.72	1.71	1.73	1.71	1.78
8.97	8.99	9.04	9.06	9.09	9.04	8.85	8.76	8.80	8.71	8.78	8.74	8.84	8.72	9.10
0.17	0.17	0.17	0.17	0.17	0.17	0.17	0.17	0.17	0.17	0.17	0.17	0.17	0.18	0.18
5.91	5.78	5.94	5.93	5.87	5.75	5.69	5.86	5.76	5.50	5.75	5.79	5.88	5.79	5.81
8.31	8.47	8.66	8.29	8.32	8.28	9.11	8.50	8.55	8.74	8.48	8.66	8.77	8.61	8.38
3.51	3.57	3.52	3.44	3.60	3.78	3.37	3.52	3.44	3.61	3.56	3.38	3.52	3.43	3.54
1.94	1.92	1.89	1.94	1.90	(2.12)	1.77	1.78	1.83	1.87	1.82	1.86	1.84	1.79	1.86
1.22	1.23	1.25	1.22	1.23	1.25	1.21	1.21	1.23	1.21	1.23	1.20	1.18	1.25	1.23
100.09	100.63	101.05	100.31	100.96	100.31	99.26	99.90	100.36	101.18	100.03	99.80	99.77	99.94	100.03
53.98	53.39	53.96	53.83	53.53	53.14	53.38	54.37	53.86	52.97	53.85	54.13	54.24	54.18	53.19
186.3	193.1	177.7	173.1	160.3	170.8	172.3	181.1	168.9	179.7	184.2	177.1	173.9	176.7	175.3
136.9	102.6	121.5	109.8	123.8	119.7	150.6	128.7	109.1	93.3	106.4	112.8	110.8	99.5	116.4
59.2	57.7	58.5	57.5	54.3	57.5	55.2	51.8	50.1	40.5	48.4	46.6	54.0	56.5	63.3
130.6	138.7	147.2	138.0	130.4	132.6	138.5	124.2	128.3	141.6	133.4	128.9	126.0	127.0	127.3
17.1	19.4	17.9	20.5	17.2	18.7	15.8	17.2	17.5	19.6	17.2	22.9	18.6	18.7	18.3
1481	1512	1514	1498	1523	1529	1530	1418	1444	1451	1447	1438	1449	1451	1456
31.8	29.8	35.4	27.1	27.5	28.5	35.6	25.0	24.1	22.7	30.0	27.1	29.1	24.7	32.4
373.0	376.6	384.7	377.6	391.0	369.4	373.5	375.1	362.9	367.7	374.3	366.3	367.6	382.4	378.7
28.0	32.4	32.6	26.1	31.3	33.0	30.2	25.6	29.4	31.7	25.6	27.2	28.6	30.8	39.4
1464	1290	1317	1328	1318	1248	1256	1384	1413	1359	1374	1374	1407	1393	1450
11.46	11.36	11.19	11.46	11.25	(12.53)	10.47	10.52	10.83	11.07	10.74	11.01	10.90	10.57	10.97
29.55	29.90	29.21	29.12	30.36	(27.27)	27.62	29.80	29.06	30.53	30.10	28.62	27.98	28.99	29.07
24.34	24.37	24.87	24.23	24.63	(22.73)	24.73	25.21	25.94	24.93	24.81	25.15	24.27	24.99	25.02
0.07	0.15	0.32	0.00	0.03	(2.56)	0.49	0.00	0.00	0.00	0.00	0.00	0.99	0.00	0.48
8.11	8.66	8.94	8.09	7.84	(9.11)	11.05	8.16	7.70	9.39	8.37	8.97	10.21	8.61	7.77
0.00	0.00	0.00	2.44	0.00	(0.00)	0.00	0.56	2.58	1.42	0.62	1.92	0.00	3.84	0.00
16.76	16.33	16.55	15.09	16.86	(16.15)	15.13	16.03	14.60	14.26	15.76	14.67	15.85	13.34	16.89
2.55	2.55	2.57	2.57	2.58	(2.57)	2.52	2.49	2.50	2.47	2.50	2.48	2.51	2.48	2.59
3.71	3.74	3.78	3.75	3.82	(3.77)	3.74	3.61	3.60	3.59	3.59	3.50	3.61	3.54	3.67
2.92	2.93	2.98	2.92	2.93	(2.98)	2.90	2.91	2.94	2.90	2.93	2.86	2.82	2.98	2.94

Table 1. Major, trace-element (determined by XRF) and normative compositions of Lathrop Wells basalts

LW26FVP	LW27FVP	LW28FVP	LW29FVP	LW04FVPA	LW54FVP	LW57FVP	LW58FVP	LW39FVP	LW48FVP	LW44FVP	LW96FVP	LW97FVP	LW104FVP	LW119FVP
Ql2b	Ql2b	Ql2b	Ql2b	Ql2c	Ql2c	Ql2c	Ql2c	Ql2u	Ql2u	Qs2a	Qs2fs	Qs2fs	Qs2fs	Qs2fs
48.26	48.87	48.62	48.66	49.04	48.41	48.79	48.53	48.20	48.28	47.49	48.84	49.32	49.30	49.22
1.93	1.96	1.86	1.97	1.85	1.87	1.85	1.91	1.91	1.91	1.88	1.93	1.91	1.94	1.87
16.68	16.78	16.74	16.73	16.73	16.77	16.80	16.39	16.68	16.67	16.23	16.71	16.80	16.91	16.87
11.56	11.74	11.40	11.72	11.47	11.40	11.55	11.39	11.46	11.39	11.43	11.63	11.76	11.61	11.53
1.73	1.76	1.71	1.76	1.72	1.71	1.73	1.71	1.72	1.71	1.71	1.74	1.76	1.74	1.73
8.84	8.98	8.72	8.97	8.78	8.72	8.84	8.71	8.77	8.71	8.74	8.90	9.00	8.88	8.82
0.17	0.17	0.17	0.17	0.17	0.17	0.18	0.17	0.17	0.17	0.17	0.17	0.17	0.17	0.17
5.83	5.88	5.86	5.89	5.75	5.78	5.68	5.84	5.88	5.85	5.86	5.92	6.13	5.85	5.90
8.62	8.51	8.67	8.38	8.94	8.72	8.92	8.80	8.41	8.64	8.36	8.56	8.38	8.33	8.70
3.47	3.60	3.44	3.61	3.40	3.44	3.47	3.55	3.60	3.53	3.42	3.48	3.32	3.37	3.32
1.80	1.85	1.81	1.83	1.83	1.78	1.76	1.79	1.86	1.86	1.80	1.82	1.83	1.79	1.79
1.19	1.21	1.21	1.22	1.21	1.18	1.23	1.20	1.18	1.20	1.17	1.27	1.22	1.19	1.23
99.50	100.57	99.77	100.18	100.40	99.52	100.22	99.56	99.35	99.50	97.81	100.32	100.84	100.46	100.59
54.01	53.84	54.47	53.91	53.88	54.15	53.40	54.43	54.45	54.46	54.44	54.26	54.85	53.99	54.36
182.0	172.4	181.8	172.1	179.5	175.2	177.4	169.5	170.6	186.1	180.7	179.7	178.8	181.1	177.0
127.5	113.0	110.0	115.6	112.4	94.4	103.7	104.6	109.8	124.2	117.5	110.5	126.5	118.2	104.1
60.2	58.3	49.4	53.6	50.4	42.9	49.9	50.8	56.8	53.0	53.7	51.2	54.1	57.5	49.9
125.4	128.3	126.8	119.4	135.9	129.9	115.8	129.6	127.1	133.2	135.1	135.5	141.7	129.6	135.6
18.6	15.8	17.0	18.3	20.3	21.0	19.8	17.6	20.8	18.2	17.7	20.0	17.5	19.7	19.1
1453	1489	1426	1496	1454	1450	1423	1486	1455	1467	1394	1454	1465	1479	1429
24.3	25.0	27.9	31.9	28.0	30.6	23.7	29.8	21.9	27.2	30.9	26.4	32.4	32.8	26.8
386.4	377.5	367.0	372.1	374.7	379.1	370.7	368.7	366.9	379.3	369.9	368.7	358.7	366.4	368.5
25.2	32.0	32.9	33.4	32.4	22.7	27.5	29.1	30.7	23.9	25.5	33.0	33.8	34.5	31.6
1403	1399	1395	1392	1322	1377	1410	1312	1455	1435	1391	1373	1308	1329	1353
10.66	10.92	10.72	10.84	10.84	10.53	10.40	10.57	10.98	11.02	10.64	10.78	10.79	10.58	10.56
29.02	29.88	29.07	30.01	28.77	29.12	29.36	29.14	28.70	28.49	28.67	29.45	28.07	28.51	28.06
24.73	24.26	25.00	24.12	25.07	25.15	25.17	23.61	23.96	24.26	23.74	24.69	25.66	25.84	25.97
0.17	0.33	0.00	0.30	0.00	0.00	0.00	0.47	0.97	0.72	0.12	0.00	0.00	0.00	0.00
9.20	8.98	9.05	8.53	10.10	9.28	9.85	10.79	9.03	9.58	9.00	8.53	7.23	7.07	8.24
0.00	0.00	1.11	0.00	1.75	0.30	0.65	0.00	0.00	0.00	0.00	1.74	6.64	6.92	5.73
16.09	16.38	15.31	16.54	14.35	15.68	15.22	15.40	16.17	15.84	16.16	15.29	12.68	11.85	12.41
2.51	2.55	2.48	2.55	2.49	2.48	2.51	2.48	2.49	2.48	2.48	2.53	2.56	2.52	2.51
3.66	3.73	3.53	3.74	3.52	3.55	3.51	3.62	3.63	3.63	3.57	3.66	3.63	3.68	3.54
2.84	2.91	2.89	2.93	2.89	2.82	2.94	2.86	2.82	2.88	2.81	3.03	2.92	2.86	2.95

Table 1. Major, trace-element (determined by XRF) and normative compositions of Lathrop Wells basalts

LW126FVP	LW130FVP	LW132FVP	LW135FVP	LW114FVP	LW118FVP	LW127FVP	LW128FVP	LW36FVP	LW37FVP	LW38FVP	LW05FVPA	LW59FVP	LW60FVP
Qs2fs	Qs2fs	Qs2fs	Qs2fs	Qs2fs	Qs2fs	Qs2fs	Qs2fs	Qs2u	Qs2u	Qs2u	Ql3	Ql3	Ql3
49.01	49.04	49.46	49.22	48.87	49.50	49.17	49.12	48.61	48.82	48.77	49.31	49.03	48.88
1.92	1.93	1.89	1.94	1.92	1.90	1.95	1.94	1.92	1.91	1.94	1.91	1.86	1.84
17.02	16.95	16.91	16.80	17.00	17.18	17.02	16.87	16.89	16.60	16.45	16.76	16.95	16.75
11.76	11.82	11.66	11.54	11.62	11.48	11.74	11.58	11.63	11.63	11.69	11.59	11.42	11.37
1.76	1.77	1.75	1.73	1.74	1.72	1.76	1.74	1.74	1.74	1.75	1.74	1.71	1.71
9.00	9.04	8.92	8.83	8.89	8.78	8.98	8.86	8.90	8.90	8.94	8.87	8.74	8.70
0.17	0.17	0.17	0.17	0.17	0.17	0.18	0.17	0.18	0.17	0.17	0.17	0.18	0.17
5.75	5.87	5.89	5.78	5.94	5.81	5.99	5.74	5.81	5.84	5.86	5.95	5.60	5.76
8.40	8.39	8.46	8.26	8.39	8.54	8.14	8.12	8.45	8.34	8.32	8.84	8.64	8.74
3.04	3.27	3.28	3.27	3.45	3.45	3.46	3.60	3.43	3.48	3.58	3.53	3.43	3.41
1.71	1.73	1.82	1.89	1.86	1.89	1.89	(2.24)	1.88	1.89	1.94	1.83	1.88	1.84
1.14	1.16	1.19	1.15	1.18	1.19	1.19	1.19	1.23	1.19	1.21	1.19	1.23	1.17
99.93	100.33	100.74	100.01	100.39	101.10	100.71	100.56	100.03	99.87	99.91	101.07	100.22	99.93
53.23	53.62	54.07	53.84	54.35	54.09	54.29	53.59	53.80	53.93	53.86	54.46	53.30	54.15
175.9	179.0	179.3	166.9	175.5	183.3	178.8	180.9	178.0	186.7	186.5	181.6	185.6	182.0
106.4	116.6	113.2	110.8	122.1	109.5	110.0	111.7	132.8	123.7	134.8	112.5	86.8	95.0
50.4	53.9	53.4	48.6	47.5	47.0	58.0	58.3	54.6	57.4	55.9	52.3	46.8	44.8
141.6	137.5	141.2	136.2	134.1	136.8	140.5	138.4	124.9	126.5	124.5	127.8	130.9	139.3
16.7	19.8	22.8	19.9	19.0	21.6	21.1	26.1	18.9	19.9	19.7	20.9	18.0	19.3
1616	1528	1464	1476	1442	1449	1482	1469	1447	1456	1484	1486	1425	1448
33.7	28.5	30.5	28.1	25.8	29.3	30.6	26.2	21.3	26.1	28.5	26.2	29.4	21.5
377.6	377.2	364.9	367.9	366.9	364.4	387.5	371.5	368.0	371.0	365.3	356.4	377.6	360.4
33.7	37.0	32.5	36.9	33.6	28.8	28.1	27.1	34.2	33.9	32.2	26.8	32.0	31.0
1307	1268	1340	1376	1312	1331	1343	1353	1388	1406	1433	1280	1426	1395
10.14	10.20	10.79	11.18	10.98	11.17	11.17	(13.24)	11.11	11.16	11.50	10.80	11.12	10.86
25.72	27.69	27.77	27.62	29.15	29.18	29.25	(28.94)	29.01	29.44	29.87	29.88	29.05	28.83
27.85	26.57	26.13	25.71	25.54	25.93	25.46	(23.38)	25.25	24.21	23.19	24.58	25.39	25.09
0.00	0.00	0.00	0.00	0.00	0.00	0.00	(0.81)	0.00	0.00	0.22	0.00	0.00	0.00
6.00	6.88	7.34	7.14	7.62	7.88	6.57	(8.24)	7.84	8.46	9.14	10.16	8.50	9.46
12.55	7.79	7.82	7.84	2.08	3.39	3.93	(0.00)	1.62	1.86	0.00	0.06	2.63	1.92
8.09	11.53	11.28	10.97	15.39	14.00	14.59	(16.29)	15.45	15.11	16.28	15.97	13.95	14.40
2.56	2.57	2.54	2.51	2.53	2.50	2.55	(2.52)	2.53	2.53	2.54	2.52	2.48	2.47
3.65	3.66	3.59	3.67	3.65	3.60	3.70	(3.68)	3.65	3.62	3.67	3.62	3.53	3.50
2.74	2.79	2.85	2.75	2.81	2.84	2.86	(2.85)	2.94	2.86	2.89	2.85	2.95	2.81

Table 1. Major, trace-element (determined by XRF) and normative compositions of Lathrop Wells basalts

LW61FVP	LW62FVP	LW02FVP	LW03FVP	LW68FVP	LW69FVP	LW70FVP	LW75FVP	LW76FVP	LW80FVP	LW81FVP	LW82FVP-B	LW82FVP-R	LW86FVP	LW87FVP
Ql3	Ql3	Qs3	Qs3	Qs3	Qs3	Qs3	Qs3	Qs3	Qs3	Qs3	Qs3	Qs3	Qs3	Qs3
48.65	48.19	48.55	48.68	48.62	49.02	48.74	48.67	48.46	48.50	48.78	49.09	48.04	49.62	49.33
1.83	1.82	1.83	1.83	1.90	1.87	1.87	1.90	1.89	1.91	1.85	1.83	1.85	1.86	1.86
16.87	16.87	16.96	16.87	16.86	16.96	16.81	16.86	16.94	16.73	16.84	16.91	16.51	17.08	16.95
11.45	11.22	11.25	11.50	11.45	11.43	11.40	11.57	11.66	11.48	11.52	11.34	11.43	11.49	11.50
1.72	1.68	1.69	1.72	1.72	1.71	1.71	1.74	1.75	1.72	1.73	1.70	1.71	1.72	1.72
8.76	8.58	8.61	8.80	8.76	8.74	8.72	8.85	8.92	8.78	8.81	8.68	8.74	8.79	8.80
0.18	0.17	0.17	0.18	0.17	0.17	0.17	0.17	0.17	0.17	0.17	0.17	0.17	0.17	0.17
5.70	5.62	5.22	5.67	5.90	5.69	5.77	5.72	5.74	5.78	5.88	5.64	5.65	5.69	5.59
8.79	8.93	8.83	8.52	8.59	8.65	8.70	8.20	8.30	8.62	8.57	8.59	8.67	8.81	8.94
3.39	3.31	3.47	3.35	3.50	3.43	3.44	3.22	2.99	3.47	3.39	3.28	3.50	3.09	3.19
1.80	1.81	1.77	1.76	1.84	1.78	1.80	1.76	1.72	1.76	1.71	1.75	(1.43)	1.72	1.73
1.17	1.19	1.21	1.18	1.21	1.19	1.19	1.17	1.12	1.20	1.19	1.18	1.19	1.21	1.21
99.82	99.15	99.25	99.53	100.04	100.19	99.89	99.24	98.99	99.62	99.90	99.77	98.45	100.74	100.47
53.72	53.87	51.93	53.44	54.54	53.69	54.11	53.54	53.43	53.99	54.34	53.69	53.53	53.57	53.12
187.6	175.5	181.4	178.4	179.9	180.2	181.1	181.3	164.0	168.4	174.7	181.0	172.8	182.4	187.5
110.3	108.3	63.1	107.3	111.7	105.0	105.3	106.6	96.9	107.4	106.9	84.0	111.5	102.8	97.9
46.9	47.4	32.5	42.2	45.3	45.3	48.1	55.0	58.1	50.2	49.9	45.3	54.3	48.0	40.7
137.6	131.8	124.9	132.1	133.9	133.0	128.2	115.9	135.0	141.3	138.0	124.0	133.3	134.2	136.5
19.8	23.9	21.7	18.3	19.5	20.2	19.7	20.8	19.9	20.3	20.1	18.2	14.5	20.5	17.9
1450	1443	1470	1431	1480	1430	1440	1444	1476	1450	1412	1439	1426	1460	1449
22.6	22.2	34.2	28.8	26.1	26.5	25.9	26.7	23.9	18.3	22.3	26.5	25.2	29.9	27.9
370.5	368.1	370.8	372.5	372.4	371.8	363.9	370.8	372.0	366.6	367.6	379.8	371.3	363.6	371.0
36.6	27.1	26.9	29.9	31.0	29.9	30.1	35.5	32.4	36.5	30.6	30.1	31.5	32.6	33.1
1376	1385	1433	1419	1361	1410	1404	1412	1362	1426	1417	1429	1406	1334	1357
10.63	10.72	10.45	10.42	10.90	10.53	10.66	10.40	10.15	10.41	10.13	10.32	(8.45)	10.16	10.25
28.65	28.03	29.39	28.31	29.41	29.03	29.08	27.24	25.27	29.32	28.68	27.77	(29.62)	26.16	27.02
25.63	25.91	25.57	25.92	24.94	25.73	25.22	26.48	27.87	25.00	25.78	26.37	(25.22)	27.76	26.90
0.00	0.00	0.00	0.00	0.12	0.00	0.00	0.00	0.00	0.00	0.00	0.00	(0.00)	0.00	0.00
9.21	9.47	9.29	7.89	8.77	8.51	9.12	6.13	5.67	8.89	8.10	7.77	(8.96)	7.33	8.59
1.63	0.89	1.38	4.67	0.00	3.28	1.49	8.99	12.15	1.21	4.07	7.53	(3.37)	12.20	8.48
14.69	14.77	13.78	12.91	16.29	13.64	14.84	10.47	8.44	15.18	13.66	10.66	(13.36)	7.59	9.70
2.49	2.44	2.45	2.50	2.49	2.48	2.48	2.52	2.54	2.50	2.51	2.47	(2.48)	2.50	2.50
3.48	3.46	3.48	3.48	3.61	3.54	3.55	3.60	3.59	3.62	3.51	3.48	(3.52)	3.53	3.53
2.81	2.85	2.89	2.81	2.89	2.84	2.84	2.80	2.69	2.88	2.84	2.82	(2.86)	2.90	2.89

Table 1. Major, trace-element (determined by XRF) and normative compositions of Lathrop Wells basalts

LW88FVP	LW95FVP	LW123FVP	LW133FVP-B	LW133FVP-R	LW78FVP-B	LW78FVP-R	LW124FVP-B	LW124FVP-R	LW134FVP	LW15FVP	LW16FVP	LW14FVP
Qs3	Qs3	Qs3	Qs4a	Qs4a	Qs4b	Qs4b	Qs4b	Qs4b	Qs4b	Qs4c	Qs4c	?
49.43	48.98	49.04	49.36	48.90	49.77	49.34	50.37	49.46	50.11	48.20	48.65	49.13
1.85	1.90	1.89	1.87	1.82	1.75	1.75	1.79	1.81	1.81	1.81	1.80	1.88
16.84	17.08	16.79	16.70	16.45	16.63	16.68	16.88	16.85	16.79	16.07	16.24	16.82
11.50	11.80	11.60	11.81	11.90	10.87	10.98	11.09	11.21	11.21	12.05	12.13	11.61
1.72	1.77	1.74	1.77	1.78	1.63	1.65	1.66	1.68	1.68	1.81	1.82	1.74
8.80	9.03	8.87	9.04	9.10	8.32	8.40	8.48	8.58	8.58	9.22	9.28	8.88
0.17	0.18	0.18	0.18	0.17	0.17	0.17	0.16	0.18	0.19	0.18	0.18	0.17
5.71	5.86	5.99	6.21	6.32	5.63	5.36	5.62	5.13	5.70	7.09	7.14	5.71
8.86	8.66	8.44	8.57	8.43	8.40	8.29	8.08	8.11	7.98	8.20	8.18	7.98
3.32	3.15	3.52	3.20	3.49	3.05	3.13	3.47	3.66	3.08	3.18	3.17	3.06
1.77	(1.48)	(1.61)	1.79	(1.74)	1.91	(1.77)	1.87	(1.55)	1.93	1.64	1.63	1.67
1.20	1.24	1.16	1.20	1.18	1.18	1.33	1.17	1.26	1.26	1.17	1.18	1.07
100.64	100.32	100.21	100.89	100.40	99.37	98.81	100.51	99.21	100.04	99.57	100.30	99.09
53.63	53.66	54.61	55.07	55.30	54.70	53.23	54.16	51.60	54.23	57.80	57.82	53.41
193.1	181.0	174.4	167.9	181.4	164.1	160.4	165.9	169.1	163.5	171.7	169.4	161.5
105.2	106.3	113.0	297.0	406.1	103.2	102.2	110.3	106.9	128.0	187.0	193.0	106.2
49.4	46.4	55.9	62.5	76.8	53.0	47.8	48.8	39.4	52.0	110.4	106.5	57.8
127.7	142.0	133.5	137.9	144.1	134.5	145.9	134.3	184.0	140.5	94.3	99.0	100.8
18.7	19.0	22.6	20.6	17.9	30.7	32.5	30.8	28.6	32.6	16.8	15.8	16.5
1449	1498	1420	1432	1427	1317	1318	1334	1349	1334	1372	1380	1414
25.2	30.8	24.3	25.4	26.7	32.0	32.0	30.5	27.6	28.1	17.6	25.4	32.0
367.4	374.0	366.3	362.2	360.2	361.0	363.1	357.9	364.2	372.2	352.3	357.1	368.2
30.4	27.7	36.4	31.8	32.0	31.4	32.8	33.2	38.7	30.8	31.0	26.6	29.9
1284	1324	1301	1344	1259	1330	1292	1347	1282	1251	1334	1317	1383
10.47	(8.73)	(9.53)	10.59	(10.26)	11.32	(10.48)	11.08	(9.17)	11.40	9.68	9.62	9.86
28.06	(26.62)	(29.76)	27.09	(29.53)	25.76	(26.46)	29.35	(30.92)	26.03	26.87	26.85	25.90
25.94	(28.24)	(25.37)	26.01	(24.19)	26.16	(26.35)	25.06	(25.09)	26.42	24.86	25.37	27.35
0.00	(0.00)	(0.00)	0.00	(0.00)	0.00	(0.00)	0.00	(0.00)	0.00	0.00	0.00	0.00
9.10	(6.23)	(8.04)	7.86	(8.88)	7.10	(5.67)	6.76	(6.39)	4.71	7.41	6.84	5.04
6.09	(12.16)	(4.14)	7.98	(1.78)	14.51	(15.66)	10.27	(9.28)	17.51	6.05	7.72	15.65
11.49	(8.57)	(13.86)	11.72	(16.21)	5.42	(4.71)	8.78	(8.85)	4.47	15.17	14.34	6.02
2.50	(2.57)	(2.52)	2.57	(2.59)	2.36	(2.39)	2.41	(2.44)	2.44	2.62	2.64	2.52
3.50	(3.61)	(3.59)	3.56	(3.46)	3.33	(3.32)	3.40	(3.44)	3.43	3.44	3.42	3.56
2.87	(2.96)	(2.78)	2.86	(2.82)	2.83	(3.19)	2.80	(3.01)	3.02	2.80	2.83	2.56

Table 1. Major, trace-element (determined by XRF) and normative compositions of Lathrop Wells basalts

LW129FVP	LW131FVP-B
?	?
49.06	49.13
2.02	1.84
16.79	16.79
11.93	11.40
1.79	1.71
9.13	8.72
0.18	0.18
5.89	5.73
7.84	8.41
3.32	3.47
1.96	1.86
1.21	1.23
100.19	100.05
53.49	53.95
180.9	181.2
108.2	107.2
51.5	47.6
138.7	136.2
19.6	22.8
1503	1398
25.7	27.5
382.0	369.6
37.3	27.7
1298	1320
11.58	11.03
28.11	29.36
25.23	24.83
0.00	0.00
5.45	8.01
7.65	3.68
12.20	13.61
2.59	2.48
3.83	3.50
2.90	2.94

Table 2. Trace-element compositions of Lathrop Wells basalts determined by INAA

Sample	LW11FVP	LW12FVP	LW74FVP	LW45FVP	LW72FVP	LW73FVP	LW100FVP	LW101FVP	LW30FVP
Unit	Qlla	Qlla	Qlla	Qllb	Qllb	Qllb	Qllb	Qslb	Qllc
Rb	20	21	22	21	18	19	19	20	22
Sc	18.8	18.9	18.87	19.1	18.7	19	19.04	18.7	18.8
Co	30.8	31.1	30.6	31	30.5	30.5	30.7	30.4	29.8
Sr	1430	1440	1420	1480	1400	1460	1470	1460	1470
Ba	1410	1420	1430	1380	1370	1430	1430	1420	1410
La	92.1	92.3	92.5	94.2	92.7	93.7	94.4	92.2	90.5
Ce	180	181	181	185	183	186.5	185.8	181.6	177
Nd	72	74	80	78	72	80	84	76	72
Sm	12.5	12.2	12.38	12.6	12.6	12.67	12.86	12.51	11.9
Eu	3.19	3.17	3.15	3.28	3.29	3.27	3.32	3.18	3.07
Tb	1.15	1.13	1.13	1.16	1.13	1.18	1.2	1.18	1.09
Yb	2.36	2.3	2.29	2.42	2.39	2.38	2.34	2.29	2.24
Lu	0.333	0.318	0.339	0.336	0.334	0.352	0.337	0.337	0.341
Hf	7.22	7.34	7.21	7.27	7.24	7.35	7.35	7.12	6.91
Ta	1.40	1.37	1.40	1.37	1.39	1.43	1.43	1.42	1.32
Th	6.51	6.64	6.59	6.33	6.27	6.48	6.43	6.27	6.65

Table 2. Trace-element compositions of Lathrop Wells basalts determined by INAA

LW31FVP	LW32FVP	LW63FVP	LW64FVP	LW65FVP	LW66FVP	LW67FVP	LW110FVP	LW115FVP	LW93FVP	LW20FVP
Qllc	Qllc	Qllc	Qllc	Qllc	Qllc	Qllc	Qllc	Qllc	Qslc	Qlld
21	18	22.1	23	20.2	22	21	22	26	20	22
19	18.9	19.4	19.11	19.13	19.46	19.42	19.52	19.66	19.01	18.6
30.2	30.6	31.56	30.27	30.58	30.58	31.32	30.8	31.2	30.74	30.3
1410	1390	1410	1450	1490	1450	1420	1420	1450	1410	1460
1430	1450	1430	1430	1460	1450	1450	1510	1500	1470	1370
92	92.9	93.2	92.6	93.3	93.8	93.3	93.5	94.2	92.8	91.9
179	181	182.4	180.2	183.4	182.6	182	183	181.8	181.3	183
71	80	74	74	75	73	74	79	78	75	77
12.1	12.4	12.23	12.2	12.5	12.43	12.24	12.39	12.26	12.29	12.5
3.09	3.16	3.16	3.11	3.21	3.17	3.14	3.17	3.16	3.11	3.23
1.09	1.13	1.11	1.13	1.181	1.15	1.14	1.15	1.18	1.19	1.14
2.28	2.35	2.37	2.39	2.36	2.4	2.42	2.33	2.37	2.37	2.36
0.353	0.338	0.345	0.338	0.334	0.343	0.35	0.338	0.341	0.346	0.332
7	7.29	7.31	7.27	7.28	7.36	7.24	7.19	7.36	7.34	7.26
1.34	1.37	1.34	1.35	1.38	1.39	1.36	1.39	1.36	1.39	1.36
6.84	6.56	6.82	6.73	6.69	6.84	6.77	6.84	6.73	6.59	6.17

Table 2. Trace-element compositions of Lathrop Wells basalts determined by INAA

LW21FVP	LW22FVP	LW23FVP	LW79FVP	LW01FVP	LW71FVP	LW8FVP	LW9FVP	LW10FVP	LW33FVP	LW34FVP
Qlld	Qlld	Qlld	Qsld	Qslr	Qslr	Qslu	Qslu	Qslu	Qslu	Qslu
19.3	19	20	20	22	20	23	21	20	20	21
18.3	18.7	18.4	18.68	19.1	19	19.27	19.13	18.67	19.5	19.5
30.4	31.5	30.9	31.3	30.7	31	31.2	30.9	30.3	30.6	31.8
1520	1500	1490	1490	1420	1420	1540	1450	1470	1400	1390
1320	1350	1330	1360	1430	1400	1430	1430	1400	1420	1460
90.3	92.6	91.7	92.6	93.1	94.6	95.2	94	92.1	94.1	94.3
181	184	183	184.4	183	187	184.9	185.4	178.4	183	184
78	73	81	78	74	73	79	76	80	77	70
12.4	12.7	12.5	12.77	12.5	12.9	12.64	12.55	12.29	12.4	12.3
3.24	3.28	3.28	3.26	3.18	3.31	3.28	3.22	3.17	3.18	3.22
1.14	1.17	1.15	1.19	1.14	1.16	1.18	1.19	1.15	1.1	1.12
2.34	2.42	2.27	2.42	2.36	2.47	2.32	2.32	2.29	2.4	2.37
0.306	0.356	0.368	0.338	0.346	0.354	0.328	0.331	0.339	0.354	0.366
7.04	7.17	7.16	7.29	7.35	7.29	7.31	7.23	7.11	7.24	7.26
1.37	1.39	1.39	1.38	1.36	1.43	1.42	1.40	1.39	1.35	1.39
5.94	6.05	5.97	6.34	6.64	6.12	6.59	6.49	6.46	6.71	6.73

Table 2. Trace-element compositions of Lathrop Wells basalts determined by INAA

LW35FVP	LW42FVP	LW43FVP	LW46FVP	LW47FVP	LW49FVP	LW50FVP	LW51FVP	LW98FVP	LW99FVP	LW103FVP
Qslu	Qslu	Qslu	Qslu	Qslu	Qslu	Qslu	Qslu	Qslu	Qslu	Qslu
20	19	21	21	22	20	19.1	22	21	18	22
19.3	18.2	18.5	18.86	19.31	19	19.02	19.1	19.28	19.41	19.05
30.8	29.4	30.6	30.31	31.05	31.1	30.53	30.8	31	31.1	30.73
1350	1430	1410	1430	1400	1430	1440	1430	1460	1430	1460
1420	1340	1360	1430	1450	1420	1440	1450	1470	1450	1450
94.4	90.3	91.5	92.3	93.6	92.3	92.8	92.8	94.7	95.9	93.7
182	179	183	181.1	183.7	181	181.6	182	186.2	187.8	183.8
73	79	79	76	81	73	73	77	79	79	77
12.4	12.1	12.6	12.32	12.4	12.3	12.29	12.4	12.76	12.78	12.59
3.18	3.17	3.25	3.12	3.2	3.15	3.16	3.19	3.27	3.32	3.22
1.1	1.1	1.17	1.13	1.15	1.1	1.16	1.14	1.19	1.19	1.16
2.33	2.4	2.38	2.35	2.44	2.32	2.39	2.32	2.34	2.42	2.38
0.367	0.313	0.343	0.336	0.34	0.355	0.339	0.344	0.337	0.325	0.336
7.06	6.96	7.22	7.29	7.3	7.11	7.21	7.2	7.29	7.37	7.4
1.37	1.34	1.38	1.37	1.39	1.38	1.36	1.39	1.41	1.42	1.37
6.65	6.24	6.11	6.67	6.86	6.55	6.6	6.68	6.59	6.65	6.66

Table 2. Trace-element compositions of Lathrop Wells basalts determined by INAA

LW113FVP	LW116FVP	LW112FVP	LW06FVP	LW07FVP	LW19FVP	LW40FVP	LW41FVP	LW44FVP	LW25FVP	LW27FVP
Qs1u	Qs1u	Ql1u	Ql2a	Ql2a	Ql2a	Ql2a	Ql2a	Ql2a	Ql2b	Ql2b
23	19	18	19	22	23	23	21	20	21	21
19.12	19.09	18.9	19.4	19.9	20.1	19.75	19.8	19.3	19	19.3
30.9	31.3	32.9	30.6	30.5	30.4	29.5	30.1	30.4	30.6	30.7
1470	1440	1490	1310	1310	1390	1403	1330	1400	1470	1450
1420	1420	1460	1460	1440	1480	1450	1430	1390	1420	1400
94.1	94.3	93.3	92	93.5	94.6	93.5	93.9	92	93.2	93.6
183.2	183.2	185.6	179	181	183.4	182.8	181	178	183	183
82	88	77	73	70	74	75	71	72	76	79
12.69	12.66	12.69	12	11.9	12.28	12.12	12.2	12	12.1	12.1
3.29	3.3	3.19	3.05	3.15	3.14	3.16	3.11	3.08	3.13	3.19
1.21	1.16	1.18	1.1	1.11	1.11	1.18	1.12	1.09	1.11	1.08
2.31	2.39	2.35	2.24	2.4	2.36	2.43	2.38	2.32	2.32	2.38
0.346	0.33	0.337	0.335	0.325	0.343	0.337	0.388	0.351	0.327	0.342
7.26	7.27	7.11	7.02	7.29	7.23	7.32	7.24	6.92	7.1	7.22
1.41	1.42	1.42	1.35	1.32	1.39	1.39	1.40	1.35	1.39	1.36
6.55	6.54	6.38	6.89	6.98	7.15	7.06	6.9	6.84	6.59	6.51

Table 2. Trace-element compositions of Lathrop Wells basalts determined by INAA

LW28FVP	LW29FVP	LW96FVP	LW97FVP	LW104FVP	LW114FVP	LW118FVP	LW119FVP	LW126FVP	LW127FVP
Ql2b	Ql2b	Qs2fs	Qs2fs	Qs2fs	Qs2fs	Qs2fs	Qs2fs	Qs2fs	Qs2fs
22	21	21.6	20	22	24	23	25	20	22
19.7	19.3	19.29	19.37	19.15	19.83	19.53	19.82	20.2	19.11
29.7	30.9	30.48	31.13	30.76	31.2	30.2	30.4	30.7	30.6
1390	1370	1400	1380	1460	1410	1380	1370	1530	1470
1410	1400	1410	1400	1430	1450	1410	1430	1460	1470
93.8	93.8	93.2	92.8	91.6	94.2	93	94.1	95.2	92.1
180	183	180.1	179.7	181.3	179.8	177.7	177.3	185.7	180.6
78	76	75	75	79	80	75	81	76	74
11.9	12.4	12	12.04	12.03	12.28	12.06	12.01	12.24	12.12
3.1	3.21	3.12	3.11	3.12	3.15	3.1	3.12	3.18	3.12
1.11	1.13	1.12	1.1	1.1	1.13	1.1	1.14	1.16	1.15
2.33	2.35	2.38	2.37	2.33	2.38	2.28	2.43	2.39	2.24
0.334	0.348	0.339	0.341	0.328	0.333	0.334	0.34	0.333	0.349
7.16	7.31	7.17	7.11	7.24	7.22	7.18	7.14	7.24	7.13
1.37	1.34	1.38	1.37	1.37	1.39	1.37	1.41	1.41	1.40
7.12	6.61	6.86	6.84	6.83	6.96	7.03	7.12	7.09	6.66

Table 2. Trace-element compositions of Lathrop Wells basalts determined by INAA

LW130FVP	LW132FVP	LW135FVP	LW36FVP	LW37FVP	LW38FVP	LW60FVP	LW61FVP	LW62FVP	LW02FVP	LW03FVP
Qs2fs	Qs2fs	Qs2fs	Qs2u	Qs2u	Qs2u	Ql3	Ql3	Ql3	Qs3	Qs3
22	19	25	22	22	23	20.3	21	22	23	23
19.75	19.34	19.51	19.6	19.7	19.5	19.9	19.7	19.9	20.3	19.7
31.4	30.8	30.7	30.9	31.1	31.2	30	29.8	29.9	28.1	30.3
1400	1410	1410	1320	1310	1380	1330	1460	1330	1330	1340
1420	1440	1490	1460	1430	1400	1410	1430	1380	1410	1410
93.7	91.2	92.6	94.2	95	94.1	94.4	94.1	94.6	97.1	93.3
179.1	175.4	183.7	184	185	184	181	179	180	186	178
82	75	78	72	72	71	65	74	71	77	68
12.12	11.98	12.19	12.2	12.3	12.3	12.1	12	12.1	12.2	12
3.15	3.01	3.17	3.16	3.18	3.22	3.1	3.06	3.12	3.16	3.06
1.14	1.12	1.17	1.11	1.11	1.14	1.11	1.1	1.1	1.13	1.07
2.33	2.29	2.33	2.36	2.35	2.37	2.35	2.34	2.38	2.36	2.43
0.323	0.329	0.318	0.352	0.344	0.331	0.359	0.338	0.346	0.36	0.339
7.16	7.03	7.23	7.28	7.34	7.2	7.14	7.12	7.21	7.41	7.22
1.40	1.39	1.39	1.37	1.36	1.34	1.38	1.37	1.37	1.38	1.40
7	6.86	6.78	6.78	6.93	6.66	7.26	7.29	7.4	7.69	7.19

Table 2. Trace-element compositions of Lathrop Wells basalts determined by INAA

LW69FVP	LW70FVP	LW75FVP	LW76FVP	LW80FVP	LW81FVP	LW82BFVP	LW82RFVP	LW86FVP	LW87FVP	LW88FVP
Qs3	Qs3	Qs3	Qs3	Qs3	Qs3	Qs3	Qs3	Qs3	Qs3	Qs3
23	21	21.6	20.2	21	24	24	20	21	22.4	23
19.9	19.9	19.71	19.84	19.5	19.9	20.03	19.92	20.13	20.07	19.84
29.4	30	30.62	30.66	30	30.3	29.77	30.54	29.83	29.68	29.68
1400	1390	1380	1410	1410	1370	1400	1370	1410	1430	1400
1400	1420	1400	1400	1430	1420	1460	1420	1430	1431	1420
94.6	95.1	93.8	93.2	93.2	94.7	95.6	94.8	96.1	96	94.6
182	182	180.5	181.1	178	182	183.9	181.9	184.4	184.9	182.4
80	72	75	75	78	76	75	74	70	74	72
12.1	12.1	12.06	11.94	11.8	12.2	11.94	12.18	12.26	12.22	12.06
3.11	3.12	3.06	3.11	3.1	3.12	3.11	3.14	3.1	3.15	3.09
1.11	1.09	1.14	1.17	1.1	1.11	1.12	1.15	1.15	1.13	1.15
2.38	2.29	2.37	2.36	2.28	2.33	2.39	2.39	2.41	2.44	2.45
0.361	0.344	0.341	0.353	0.37	0.357	0.348	0.349	0.36	0.351	0.349
7.15	7.22	7.29	7.2	6.98	7.13	7.41	7.37	7.43	7.31	7.23
1.37	1.37	1.39	1.37	1.36	1.37	1.39	1.36	1.39	1.35	1.34
7.28	7.25	7.03	7.13	6.92	7.35	7.56	6.97	7.42	7.53	7.47

Table 2. Trace-element compositions of Lathrop Wells basalts determined by INAA

LW95FVP	LW123FVP	LW133FVP-R	LW133FVP-B	LW78FVP-B	LW78FVP-R	LW124FVP-B	LW124FVP-R	LW134FVP
Qs3	Qs3	Qs4a	Qs4a	Qs4b	Qs4b	Qs4b	Qs4b	Qs4b
18	21	21	21	34	34.4	32	28	36
20.28	19.57	19.57	19.57	18.76	19.03	19.15	19.29	19.09
30.65	30.6	32.8	32	28.88	28.89	28.9	28.7	29.5
1460	1340	1390	1340	1290	1250	1300	1270	1260
1390	1450	1410	1450	1360	1330	1430	1380	1410
96.6	92.6	92.2	92.2	91.7	96.2	91.1	93.7	96.4
186.3	178.8	182.8	179.5	175.9	179.6	176.2	179.1	188.6
77	77	74	80	73	75	71	73	75
12.4	11.89	11.95	11.95	11.8	12.57	11.91	12.13	12.56
3.19	3.05	3.07	3.07	2.91	3.07	2.96	2.96	3.15
1.14	1.16	1.11	1.11	1.12	1.23	1.16	1.16	1.23
2.48	2.33	2.48	2.3	2.54	2.8	2.48	2.49	2.89
0.348	0.334	0.35	0.349	0.38	0.405	0.35	0.399	0.403
7.35	7.05	7.15	7.13	7.4	7.35	7.38	7.2	7.69
1.39	1.40	1.41	1.39	1.38	1.38	1.38	1.42	1.47
7.34	6.89	6.88	6.88	8.32	9.01	8.1	8.18	9.18

Table 2. Trace-element compositions of Lathrop Wells basalts determined by INAA

LW15FVP	LW16FVP	LW14FVP
Qs4c	Qs4c	?
18	21	20
19.4	19.1	19.5
36.5	35.8	30
1240	1230	1280
1350	1310	1390
90.3	89.7	90.3
174	172	178
67	66	68
11.4	11.3	11.2
3	2.94	2.99
1.06	1.04	1.03
2.23	2.18	2.23
0.333	0.314	0.334
6.94	6.87	7.22
1.28	1.27	1.30
6.77	6.82	6.8

Table 3. Replicate INAA analyses of LW27FVP

Sample	Sc	Co	Rb	Sr	Ba	La	Ce	Nd
LW27FVP[1]	19.3	30.7	21	1450	1400	93.6	183	79
NM18FVP[1]	19.4	31.1	18	1370	1430	93.9	183	71
NM19FVP[1]	19.2	30.7	23	1410	1430	92.8	181	73
NM20FVP[1]	19.3	30.8	19	1420	1440	93.3	183	78
NM30FVP[2]	19.23	30.81	21	1430	1430	93.4	183.4	77
NM33FVP[2]	19.2	30.64	20.3	1440	1430	92.9	183.8	78
NM34FVP[2]	19.24	30.66	21	1440	1460	93.1	182.7	77
NM41FVP[2]	19.15	30.66	21	1430	1440	92.6	182.5	77
NM42FVP[3]	19.13	30.6	20	1410	1470	92.8	181.3	77
NM43FVP[3]	19.44	31.2	20	1430	1500	94.2	183.7	78
NM45FVP[3]	19.36	30.7	17	1440	1480	93.8	183	75
NM48FVP[3]	19.42	31	18	1360	1470	93.7	183.7	73
Mean	19.28	30.80	19.94	1419.17	1448.33	93.34	182.84	76.08
Standard Deviation	0.11	0.20	1.68	28.11	27.91	0.51	0.89	2.50
Percent Standard Deviation (100·s/mean)	0.55	0.64	8.42	1.98	1.93	0.55	0.49	3.29

Sample	Sm	Eu	Tb	Yb	Lu	Hf	Ta	Th
LW27FVP[1]	12.1	3.19	1.08	2.38	0.340	7.22	1.36	6.51
NM18FVP[1]	12.4	3.19	1.13	2.35	0.350	7.22	1.38	6.65
NM19FVP[1]	12.4	3.16	1.14	2.33	0.360	7.23	1.4	6.68
NM20FVP[1]	12.4	3.19	1.13	2.25	0.360	7.14	1.37	6.56
NM30FVP[2]	12.33	3.17	1.12	2.39	0.332	7.37	1.36	6.71
NM33FVP[2]	12.36	3.19	1.14	2.41	0.340	7.36	1.37	6.77
NM34FVP[2]	12.47	3.19	1.16	2.39	0.342	7.27	1.38	6.76
NM41FVP[2]	12.26	3.19	1.17	2.33	0.341	7.3	1.36	6.80
NM42FVP[3]	12.39	3.16	1.18	2.31	0.336	7.33	1.42	6.68
NM43FVP[3]	12.64	3.22	1.19	2.35	0.335	7.33	1.4	6.63
NM45FVP[3]	12.56	3.24	1.19	2.31	0.353	7.34	1.34	6.60
NM48FVP[3]	12.33	3.28	1.17	2.33	0.339	7.39	1.34	6.87
Mean	12.39	3.20	1.15	2.34	0.344	7.29	1.37	6.69
Standard Deviation	0.14	0.03	0.03	0.04	0.009	0.08	0.02	0.10
Percent Standard Deviation (100·s/mean)	1.11	1.08	2.85	1.89	2.76	1.04	1.77	1.55

[1,2,3] Sample group

Table 4. Isotopic and trace-element compositions of Lathrop Wells Basalts determined by solid-source mass spectrometry

Sample	LW11FVP	LW12FVP	LW20FVP	LW22FVP	LW113FVP	LW7FVP	LW41FVP	LW27FVP	LW29FVP	LW96FVP	LW97FVP	LW118FVP
Unit	Ql1a	Ql1a	Ql1d	Ql1d	Qs1u	Ql2a	Ql2a	Ql2b	Ql2b	Qs2fs	Qs2fs	Qs2fs
Rb	19.70	19.10	17.76	15.68	20.60	19.90	20.47	19.36	19.60	20.50	20.40	21.40
Sr	1452	1446	1482	1495	1461	1399	1395	1424	1431	1410	1413	1386
$^{87}Sr/^{86}Sr$	0.707021	0.707047	0.707084	0.707077	0.707039	0.707006	0.707011	0.707033	0.707034	0.706978	0.707044	0.707003
Sm	12.43	12.33	12.56	12.79	12.40	12.00	12.05	12.16	12.26	12.10	12.00	11.90
Nd	90.10	89.11	90.50	91.99	89.20	86.50	87.30	87.99	88.44	87.60	86.70	86.10
$^{143}Nd/^{144}Nd$	0.512135	0.512110	0.512142	0.512142	0.512130	0.512123	0.512125	0.512114	0.512124	0.512120	0.512123	0.512113
ε_{Nd}	-9.81	-10.30	-9.68	-9.68	-9.91	-10.00	-10.01	-10.22	-10.03	-10.10	-10.00	-10.20
Pb	11.0	11.1	10.1	10.2	11.1	11.7	10.8	11.0	11.0	12.3	12.2	11.8
$^{208}Pb/^{204}Pb$	38.264	38.323	38.32	38.343	38.288	38.296	38.222	38.316	38.365	38.36	38.328	38.323
$^{207}Pb/^{204}Pb$	15.514	15.528	15.52	15.527	15.519	15.527	15.505	15.528	15.542	15.545	15.536	15.535
$^{206}Pb/^{204}Pb$	18.345	18.353	18.372	18.389	18.355	18.336	18.312	18.343	18.354	18.352	18.341	18.361

Table 4. Isotopic and trace-element compositions of Lathrop Wells Basalts determined by solid-source mass spectrometry

Sample	LW80FVP	LW81FVP	LW15FVP	LW16FVP
Unit	Qs3	Qs3	Qs4c	Qs4c
Rb	20.62	20.59	19.57	19.64
Sr	1375	1361	1321	1321
$^{87}Sr/^{86}Sr$	0.707024	0.707022	0.707062	0.707062
Sm	11.89	11.84	11.43	11.39
Nd	85.97	85.80	82.90	82.88
$^{143}Nd/^{144}Nd$	0.512126	0.512138	0.512120	0.512132
ε_{Nd}	-9.99	-9.75	-10.10	-9.87
Pb	14.9	13.1	12.4	11.2
$^{208}Pb/^{204}Pb$	38.032	38.288	38.269	38.33
$^{207}Pb/^{204}Pb$	15.486	15.54	15.52	15.537
$^{206}Pb/^{204}Pb$	18.17	18.522	18.332	18.349

Table 5. Replicate solid-source mass spectroscopy analyses of LW41FVP

Sample	Rb	Sr	$^{87}Sr/^{86}Sr$	Sm	Nd	$^{143}Nd/^{144}Nd$	ε_{Nd}	Pb	$^{208}Pb/^{204}Pb$	$^{207}Pb/^{204}Pb$	$^{206}Pb/^{204}Pb$
LW41FVP	20.47	1395.00	0.707011	12.1	87.3	0.512125	-10.01	10.8	38.222	15.505	18.312
LW13FVP	19.54	1380.00	0.707042	12.0	87.1	0.512125	-10.01	10.8	38.231	15.51	18.322
DP3FVP	20.50	1407.00	0.707018	12.0	87.2	0.512118	-10.14	10.7	38.282	15.524	18.335
DP4FVP	20.50	1412.00	0.707002	11.9	87.2	0.512134	-9.83	10.8	38.329	15.538	18.343
DP5FVP	20.20	1398.00	0.707013	12.1	86.9	0.512127	-9.97	10.0	38.217	15.504	18.33
DP8FVP	20.20	1407.00	0.707007	12.0	86.6	0.512132	-9.87	10.5	38.24	15.511	18.328
Mean	20.24	1399.83	0.707016	12.01	87.04	0.512127	-9.97	10.59	38.254	15.515	18.328
Standard Deviation	0.37	11.58	0.000014	0.06	0.26	0.000006	0.11	0.34	0.044	0.013	0.011
Percent Standard Deviation (100·s/mean)	1.828	0.827	0.002	0.479	0.296	0.001	1.11	3.166	0.114	0.085	0.058

Table 6. Composition of olivine phenocrysts and groundmass (gm) from LW21FVP of Ql1d

Point	lw21fvp_#1ab	lw21fvp_#1a	lw21fvp_#1a	lw21fvp_#1a	lw21fvp_#1a	lw21fvp_#1a	lw21fvp_#1ae	lw21fvp_#1bb	lw21fvp_#1b	lw21fvp_#1b
SiO_2	38.04	38.80	38.26	37.99	38.26	38.09	37.96	38.16	38.00	38.10
MgO	36.91	40.19	38.85	38.75	39.21	40.09	39.73	39.74	39.98	40.12
FeO	24.46	20.70	22.04	22.35	21.78	20.96	21.32	21.00	20.59	20.65
CaO	0.19	0.14	0.15	0.13	0.13	0.13	0.17	0.16	0.14	0.14
MnO	0.35	0.30	0.32	0.29	0.31	0.28	0.30	0.26	0.32	0.27
NiO	0.13	0.29	0.16	0.18	0.21	0.25	0.23	0.24	0.27	0.23
TOTAL	100.08	100.42	99.76	99.69	99.90	99.79	99.70	99.56	99.29	99.50
Cations based on 4 oxygens										
Si	1.00	1.00	1.00	0.99	1.00	0.99	0.99	0.99	0.99	0.99
Mg	1.45	1.54	1.51	1.51	1.52	1.55	1.54	1.54	1.55	1.56
Fe	0.54	0.45	0.48	0.49	0.47	0.46	0.46	0.46	0.45	0.45
Ca	0.01	0.00	0.00	0.00	0.00	0.00	0.01	0.00	0.00	0.00
Mn	0.01	0.01	0.01	0.01	0.01	0.01	0.01	0.01	0.01	0.01
Ni	0.00	0.01	0.00	0.00	0.00	0.01	0.01	0.01	0.01	0.01
Fo	72.81	77.48	75.75	75.45	76.11	77.22	76.80	77.08	77.46	77.51
Fa	27.06	22.39	24.11	24.41	23.73	22.65	23.12	22.85	22.38	22.39

Table 6. Composition of olivine phenocrysts and groundmass (gm) from LW21FVP of Ql1d

lw21fvp_#1be	lw21fvp_#2b	lw21fvp_#2	lw21fvp_#2	lw21fvp_#2	lw21fvp_#2	lw21fvp_#2	lw21fvp_#2e	lw21fvp_3b	lw21fvp_3	lw21fvp_3	lw21fvp_3
37.62	37.64	37.73	38.08	38.62	38.26	38.17	37.63	35.92	37.81	37.41	37.46
39.17	38.18	40.02	40.24	40.43	40.10	39.97	38.27	32.51	40.34	40.35	40.15
21.57	23.24	21.16	20.59	20.99	20.94	21.08	22.90	29.51	20.82	20.92	20.61
0.19	0.25	0.13	0.12	0.14	0.14	0.14	0.19	0.29	0.14	0.12	0.13
0.28	0.30	0.25	0.27	0.33	0.29	0.32	0.34	0.55	0.23	0.26	0.26
0.16	0.05	0.23	0.23	0.24	0.26	0.22	0.16	0.04	0.31	0.29	0.26
98.98	99.68	99.51	99.53	100.75	100.01	99.90	99.48	98.82	99.64	99.36	98.86
0.99	0.99	0.98	0.99	0.99	0.99	0.99	0.99	0.99	0.98	0.98	0.98
1.53	1.50	1.56	1.56	1.55	1.55	1.55	1.50	1.33	1.56	1.57	1.57
0.47	0.51	0.46	0.45	0.45	0.45	0.46	0.50	0.68	0.45	0.46	0.45
0.01	0.01	0.00	0.00	0.00	0.00	0.00	0.01	0.01	0.00	0.00	0.00
0.01	0.01	0.01	0.01	0.01	0.01	0.01	0.01	0.01	0.01	0.01	0.01
0.00	0.00	0.01	0.01	0.01	0.01	0.01	0.00	0.00	0.01	0.01	0.01
76.37	74.55	77.05	77.60	77.30	77.24	77.05	74.78	66.11	77.50	77.37	77.55
23.59	25.46	22.86	22.27	22.52	22.63	22.80	25.10	33.68	22.44	22.51	22.34

Table 6. Composition of olivine phenocrysts and groundmass (gm) from LW21FVP of Ql1d

lw21fvp_3	lw21fvp_3	lw21fvp_3e	lw21fvp_#4ab	lw21fvp_#4a	lw21fvp_#4a	lw21fvp_#4a	lw21fvp_#4a	lw21fvp_#4a	lw21fvp_#4ae	lw21fvp_#4bb
37.19	37.03	36.80	37.32	37.60	37.81	37.73	37.66	37.89	37.81	38.19
39.97	39.64	38.96	38.07	40.06	39.47	39.40	39.58	40.05	40.12	40.29
20.39	21.28	21.71	23.02	20.73	21.53	21.26	21.39	20.62	20.14	20.72
0.14	0.17	0.17	0.26	0.15	0.16	0.15	0.14	0.12	0.15	0.12
0.26	0.30	0.31	0.36	0.28	0.26	0.28	0.33	0.26	0.33	0.28
0.28	0.22	0.11	0.12	0.21	0.19	0.18	0.22	0.22	0.16	0.20
98.23	98.63	98.06	99.15	99.04	99.42	98.99	99.32	99.16	98.70	99.80
0.98	0.98	0.98	0.99	0.98	0.99	0.99	0.99	0.99	0.99	0.99
1.57	1.56	1.55	1.50	1.56	1.54	1.54	1.54	1.56	1.57	1.56
0.45	0.47	0.48	0.51	0.45	0.47	0.47	0.47	0.45	0.44	0.45
0.00	0.01	0.01	0.01	0.00	0.00	0.00	0.00	0.00	0.00	0.00
0.01	0.01	0.01	0.01	0.01	0.01	0.01	0.01	0.01	0.01	0.01
0.01	0.01	0.00	0.00	0.00	0.00	0.00	0.01	0.01	0.00	0.00
77.68	76.78	76.10	74.64	77.43	76.52	76.68	76.61	77.50	77.91	77.50
22.23	23.13	23.79	25.33	22.47	23.42	23.22	23.22	22.39	21.94	22.36

Table 6. Composition of olivine phenocrysts and groundmass (gm) from LW21FVP of Ql1d

lw21fvp_#4b	lw21fvp_#4b	lw21fvp_#4be	lw21fvp_#5ab	lw21fvp_#5a	lw21fvp_#5a	lw21fvp_#5a	lw21fvp_#5a	lw21fvp_#5a	lw21fvp_#5ae	lw21fvp_#6b
38.08	38.23	36.36	37.88	38.19	38.35	38.27	38.28	38.24	38.00	36.97
40.38	40.21	34.10	39.35	39.72	39.98	39.68	39.82	39.97	38.41	34.98
20.57	20.68	27.65	21.79	20.96	21.60	21.52	21.58	21.22	22.94	26.54
0.15	0.14	0.48	0.21	0.17	0.13	0.13	0.13	0.12	0.17	0.25
0.27	0.25	0.44	0.32	0.29	0.25	0.23	0.26	0.30	0.34	0.40
0.27	0.23	0.15	0.07	0.18	0.29	0.16	0.26	0.24	0.11	0.12
99.72	99.75	99.17	99.61	99.50	100.60	100.00	100.33	100.08	99.95	99.25
0.99	0.99	0.99	0.99	0.99	0.99	0.99	0.99	0.99	0.99	0.99
1.56	1.55	1.38	1.53	1.54	1.54	1.54	1.54	1.54	1.50	1.40
0.45	0.45	0.63	0.48	0.46	0.47	0.47	0.47	0.46	0.50	0.60
0.00	0.00	0.01	0.01	0.01	0.00	0.00	0.00	0.00	0.01	0.01
0.01	0.01	0.01	0.01	0.01	0.01	0.01	0.01	0.01	0.01	0.01
0.01	0.01	0.00	0.00	0.00	0.01	0.00	0.01	0.01	0.00	0.00
77.71	77.54	68.86	76.25	77.09	76.67	76.61	76.60	76.92	74.80	70.07
22.21	22.37	31.33	23.69	22.82	23.24	23.31	23.29	22.92	25.06	29.84

Table 6. Composition of olivine phenocrysts and groundmass (gm) from LW21FVP of Ql1d

lw21fvp_#6	lw21fvp_#6	lw21fvp_#6	lw21fvp_#6e	lw21fvp_7a	lw21fvp_7a	lw21fvp_7a	lw21fvp_7a	lw21fvp_7a	lw21fvp_7b	lw21fvp_7b	lw21fvp_7b
38.20	37.54	38.15	37.83	37.61	38.16	38.10	38.24	38.25	38.33	38.26	38.20
39.85	39.96	40.27	37.93	37.39	40.26	40.36	40.14	40.24	40.20	40.24	40.07
21.06	20.89	20.97	23.43	23.52	21.20	21.13	21.12	20.89	21.25	21.01	20.93
0.14	0.12	0.15	0.20	0.25	0.16	0.16	0.12	0.13	0.18	0.13	0.15
0.23	0.29	0.27	0.34	0.33	0.23	0.24	0.26	0.23	0.30	0.27	0.21
0.27	0.22	0.23	0.19	0.14	0.21	0.20	0.23	0.23	0.21	0.28	0.23
99.75	99.00	100.04	99.91	99.25	100.22	100.18	100.11	99.98	100.46	100.19	99.79
0.99	0.98	0.99	0.99	0.99	0.99	0.99	0.99	0.99	0.99	0.99	0.99
1.54	1.56	1.56	1.48	1.47	1.55	1.56	1.55	1.55	1.55	1.55	1.55
0.46	0.46	0.45	0.51	0.52	0.46	0.46	0.46	0.45	0.46	0.45	0.45
0.00	0.00	0.00	0.01	0.01	0.01	0.00	0.00	0.00	0.01	0.00	0.00
0.01	0.01	0.01	0.01	0.01	0.01	0.01	0.01	0.01	0.01	0.01	0.01
0.01	0.01	0.01	0.00	0.00	0.00	0.00	0.01	0.01	0.00	0.01	0.01
77.09	77.20	77.32	74.19	73.91	77.18	77.26	77.11	77.39	77.06	77.26	77.32
22.86	22.64	22.59	25.72	26.08	22.80	22.70	22.77	22.54	22.85	22.63	22.66

Table 6. Composition of olivine phenocrysts and groundmass (gm) from LW21FVP of Ql1d

lw21fvp_7b	lw21fvp_8b	lw21fvp_8	lw21fvp_8	lw21fvp_8	lw21fvp_8	lw21fvp_8e	lw21fvp_9b	lw21fvp_9	lw21fvp_9	lw21fvp_9e	lw21fvp_9ab
38.30	37.56	37.47	37.37	37.52	37.61	35.61	37.68	37.44	37.62	37.57	37.25
39.98	39.80	39.09	39.25	39.57	39.40	31.69	39.86	40.00	40.10	40.10	38.15
21.17	21.47	22.14	22.12	21.52	21.66	30.64	21.00	21.08	20.71	20.93	22.86
0.16	0.15	0.16	0.10	0.15	0.17	0.35	0.16	0.13	0.12	0.15	0.25
0.24	0.25	0.30	0.29	0.29	0.32	0.58	0.28	0.27	0.25	0.29	0.37
0.24	0.26	0.21	0.14	0.28	0.21	0.03	0.30	0.25	0.27	0.25	0.10
100.07	99.49	99.37	99.27	99.33	99.38	98.90	99.28	99.17	99.06	99.29	98.97
0.99	0.98	0.98	0.98	0.98	0.99	0.98	0.99	0.98	0.98	0.98	0.99
1.54	1.55	1.53	1.54	1.55	1.54	1.30	1.55	1.56	1.56	1.56	1.51
0.46	0.47	0.49	0.49	0.47	0.48	0.71	0.46	0.46	0.45	0.46	0.51
0.00	0.00	0.00	0.00	0.00	0.01	0.01	0.01	0.00	0.00	0.00	0.01
0.01	0.01	0.01	0.01	0.01	0.01	0.01	0.01	0.01	0.01	0.01	0.01
0.01	0.01	0.00	0.00	0.01	0.00	0.00	0.01	0.01	0.01	0.01	0.00
77.06	76.71	75.80	75.84	76.53	76.33	64.72	77.13	77.10	77.46	77.26	74.80
22.90	23.22	24.09	23.98	23.35	23.55	35.12	22.79	22.79	22.44	22.62	25.15

Table 6. Composition of olivine phenocrysts and groundmass (gm) from LW21FVP of Ql1d

lw21fvp_9a	lw21fvp_9a	lw21fvp_9a	lw21fvp_9a	lw21fvp_9ae	lw21fvp_#12b	lw21fvp_#12	lw21fvp_#12	lw21fvp_#12	lw21fvp_#12e	lw21fvp_#14b
37.78	37.64	37.53	37.43	37.55	37.87	38.45	38.26	38.24	37.43	37.87
39.69	39.70	40.13	39.94	39.89	38.41	39.92	39.92	39.81	35.52	37.91
21.31	21.05	21.26	21.09	21.34	22.77	21.31	21.46	21.28	26.02	23.90
0.15	0.15	0.15	0.15	0.20	0.42	0.17	0.16	0.15	0.24	0.19
0.22	0.26	0.29	0.26	0.27	0.33	0.27	0.29	0.28	0.53	0.32
0.21	0.21	0.18	0.20	0.21	0.07	0.16	0.20	0.16	0.14	0.11
99.36	99.01	99.54	99.07	99.45	99.85	100.27	100.29	99.92	99.88	100.30
0.99	0.99	0.98	0.98	0.98	0.99	0.99	0.99	0.99	1.00	0.99
1.55	1.55	1.56	1.56	1.55	1.50	1.54	1.54	1.54	1.41	1.48
0.47	0.46	0.46	0.46	0.47	0.50	0.46	0.47	0.46	0.58	0.52
0.00	0.00	0.00	0.00	0.01	0.01	0.01	0.00	0.00	0.01	0.01
0.01	0.01	0.01	0.01	0.01	0.01	0.01	0.01	0.01	0.01	0.01
0.00	0.00	0.00	0.00	0.00	0.00	0.00	0.00	0.00	0.00	0.00
76.83	77.01	77.01	77.08	76.90	75.20	76.90	76.75	76.84	70.69	73.81
23.14	22.91	22.89	22.84	23.08	25.02	23.04	23.15	23.05	29.05	26.11

Table 6. Composition of olivine phenocrysts and groundmass (gm) from LW21FVP of Ql1d

lw21fvp_#14	lw21fvp_#14	lw21fvp_#14e	lw21fvp_#13a gm	lw21fvp_#13a gm	lw21fvp_#13bb gm	lw21fvp_#13b gm	lw21fvp_#13be gm	lw21fvp_#14ab gm	lw21fvp_#14ae gm
38.79	38.41	37.45	35.73	36.55	35.86	35.92	35.23	36.73	36.80
38.49	39.18	35.94	30.99	32.14	29.15	31.42	28.25	35.15	35.80
21.58	21.98	25.31	30.09	29.41	32.89	30.32	32.97	25.77	25.04
0.22	0.22	0.26	1.17	0.36	0.34	0.73	1.29	0.70	0.92
0.31	0.31	0.43.	0.60	0.62	0.66	0.58	0.61	0.45	0.43
0.12	0.12	0.10	0.02	0.02	0.01	0.08	0.00	0.05	0.07
99.51	100.22	99.49	98.59	99.11	98.92	99.06	98.34	98.85	99.06
1.01	1.00	1.00	0.99	1.00	1.00	0.99	0.99	0.99	0.99
1.49	1.52	1.43	1.28	1.31	1.21	1.29	1.19	1.41	1.43
0.47	0.48	0.56	0.70	0.67	0.77	0.70	0.78	0.58	0.56
0.01	0.01	0.01	0.04	0.01	0.01	0.02	0.04	0.02	0.03
0.01	0.01	0.01	0.01	0.01	0.02	0.01	0.02	0.01	0.01
0.00	0.00	0.00	0.00	0.00	0.00	0.00	0.00	0.00	0.00
76.05	76.03	71.59	65.42	65.95	61.07	65.14	61.19	71.21	72.42
23.92	23.93	28.29	35.64	33.86	38.66	35.26	40.06	29.29	28.42

Table 6. Composition of olivine phenocrysts and groundmass (gm) from LW21FVP of Ql1d

lw21fvp_#14a gm	lw21fvp_#14bb gm	lw21fvp_#14b gm	lw21fvp_#14ba gm
37.47	35.34	35.54	35.26
35.43	27.81	28.17	27.80
25.97	33.93	33.87	34.74
0.38	0.45	0.63	0.44
0.43	0.74	0.80	0.80
0.04	0.04	0.03	0.01
99.70	98.32	99.04	99.05
1.00	1.00	1.00	0.99
1.41	1.17	1.18	1.17
0.58	0.80	0.79	0.82
0.01	0.01	0.02	0.01
0.01	0.02	0.02	0.02
0.00	0.00	0.00	0.00
70.91	59.24	59.71	58.61
29.16	40.56	40.28	41.10

Table 7. Composition of olivine phenocrysts from LW73FVP of Ql1b

Point	lw73fvp_#1b	lw73fvp_#1	lw73fvp_#1	lw73fvp_#1	lw73fvp_#1e	lw73fvp_#3b	lw73fvp_#3	lw73fvp_#3	lw73fvp_#3	lw73fvp_#3e
SiO_2	37.52	37.20	37.80	37.73	37.04	35.92	36.56	36.89	37.99	35.50
MgO	38.69	39.81	39.69	39.19	37.56	36.80	39.66	40.20	40.22	34.99
FeO	22.49	21.32	21.57	22.14	23.56	24.95	21.72	21.16	21.60	25.99
CaO	0.16	0.18	0.17	0.18	0.18	0.20	0.15	0.15	0.16	0.84
MnO	0.37	0.31	0.23	0.30	0.37	0.41	0.24	0.30	0.36	0.43
NiO	0.16	0.13	0.18	0.17	0.16	0.04	0.19	0.24	0.21	0.13
TOTAL	99.39	98.94	99.65	99.72	98.87	98.31	98.52	98.94	100.53	97.88
Cations based on 4 oxygens										
Si	0.99	0.98	0.99	0.99	0.99	0.97	0.97	0.97	0.98	0.97
Mg	1.52	1.56	1.54	1.53	1.49	1.48	1.57	1.58	1.55	1.43
Fe	0.50	0.47	0.47	0.48	0.52	0.56	0.48	0.47	0.47	0.59
Ca	0.00	0.01	0.01	0.01	0.01	0.01	0.00	0.00	0.00	0.03
Mn	0.01	0.01	0.01	0.01	0.01	0.01	0.01	0.01	0.01	0.01
Ni	0.00	0.00	0.00	0.00	0.00	0.00	0.00	0.01	0.00	0.00
Fo	75.26	76.82	76.62	75.87	73.86	72.31	76.45	77.10	76.71	71.10
Fa	24.55	23.08	23.36	24.05	25.99	27.51	23.49	22.78	23.11	29.64

Table 7. Composition of olivine phenocrysts from LW73FVP of Ql1b

lw73fvp_#4b	lw73fvp_#4	lw73fvp_#4	lw73fvp_#4	lw73fvp_#4e	lw73fvp_#5b	lw73fvp_#5	lw73fvp_#5	lw73fvp_#5	lw73fvp_#5e	lw73fvp_#6
37.60	38.14	37.34	37.20	36.10	37.05	37.12	37.12	37.86	37.17	37.79
37.61	39.74	40.50	39.31	35.60	37.44	39.75	39.46	39.44	36.61	40.31
24.14	21.21	21.17	22.31	26.30	24.03	21.92	21.91	22.19	25.60	21.25
0.21	0.13	0.13	0.15	0.28	0.20	0.15	0.15	0.15	0.19	0.19
0.41	0.27	0.23	0.34	0.41	0.32	0.30	0.31	0.34	0.40	0.23
0.22	0.23	0.19	0.23	0.08	0.22	0.30	0.19	0.16	0.06	0.10
100.19	99.73	99.56	99.55	98.77	99.26	99.54	99.14	100.15	100.03	99.87
0.99	0.99	0.98	0.98	0.98	0.98	0.97	0.98	0.99	0.99	0.98
1.47	1.54	1.58	1.54	1.43	1.48	1.55	1.55	1.53	1.45	1.56
0.53	0.46	0.46	0.49	0.59	0.53	0.48	0.48	0.48	0.57	0.46
0.01	0.00	0.00	0.00	0.01	0.01	0.00	0.00	0.00	0.01	0.01
0.01	0.01	0.01	0.01	0.01	0.01	0.01	0.01	0.01	0.01	0.01
0.01	0.01	0.00	0.01	0.00	0.01	0.01	0.00	0.00	0.00	0.00
73.40	76.87	77.27	75.72	70.66	73.46	76.28	76.14	75.88	71.69	77.18
26.44	23.01	22.66	24.12	29.28	26.46	23.60	23.73	23.96	28.13	22.83

Table 7. Composition of olivine phenocrysts from LW73FVP of Ql1b

lw73fvp_#6	lw73fvp_#6	lw73fvp_#6	lw73fvp_#6	lw73fvp_#6e
38.51	38.14	38.20	37.94	37.69
39.82	40.15	40.65	40.43	38.73
21.76	21.58	21.35	21.20	22.68
0.19	0.20	0.20	0.19	0.15
0.24	0.26	0.24	0.22	0.31
0.03	0.05	0.05	0.02	0.17
100.55	100.37	100.69	99.99	99.73
0.99	0.99	0.98	0.98	0.99
1.53	1.55	1.56	1.56	1.51
0.47	0.47	0.46	0.46	0.50
0.01	0.01	0.01	0.01	0.00
0.01	0.01	0.01	0.01	0.01
0.00	0.00	0.00	0.00	0.00
76.53	76.83	77.24	77.29	75.18
23.46	23.17	22.77	22.74	24.69

Table 8. Composition of olivine phenocrysts from LW40FVP of Ql2a

Point	lw40fvp#1a	lw40fvp#1b	lw40fvp#1c	lw40fvp#1d	lw40fvp#2b	lw40fvp#2	lw40fvp#2	lw40fvp#2	lw40fvp#2e	lw40fvp#4a	lw40fvp#4b
SiO_2	38.11	38.12	37.95	37.01	37.11	37.99	37.94	37.83	37.32	36.88	37.99
MgO	40.32	40.56	40.38	36.92	36.45	40.53	39.17	39.98	37.23	36.29	40.76
FeO	20.89	21.04	20.75	24.91	25.32	21.08	21.69	21.93	24.53	26.17	20.29
CaO	0.12	0.12	0.14	0.23	0.27	0.11	0.11	0.09	0.22	0.26	0.14
MnO	0.23	0.21	0.27	0.36	0.38	0.24	0.30	0.26	0.32	0.43	0.26
NiO	0.30	0.32	0.13	0.16	0.10	0.23	0.33	0.20	0.10	0.04	0.20
TOTAL	99.97	100.36	99.61	99.59	99.62	100.18	99.54	100.29	99.72	100.07	99.63
Cations based on 4 oxygens											
Si	0.99	0.99	0.99	0.98	0.99	0.98	0.99	0.98	0.99	0.98	0.99
Mg	1.56	1.56	1.56	1.46	1.45	1.56	1.53	1.55	1.47	1.44	1.58
Fe	0.45	0.46	0.45	0.55	0.56	0.46	0.47	0.48	0.54	0.58	0.44
Ca	0.00	0.00	0.00	0.01	0.01	0.00	0.00	0.00	0.01	0.01	0.00
Mn	0.01	0.01	0.01	0.01	0.01	0.01	0.01	0.01	0.01	0.01	0.01
Ni	0.01	0.01	0.00	0.00	0.00	0.01	0.01	0.00	0.00	0.00	0.00
Fo	77.42	77.40	77.54	72.49	71.92	77.32	76.16	76.34	72.97	71.11	78.10
Fa	22.50	22.53	22.35	27.44	28.04	22.56	23.66	23.50	26.98	28.77	21.81

Table 8. Composition of olivine phenocrysts from LW40FVP of Ql2a

lw40fvp#4c	lw40fvp#4d	lw40fvp#4e	lw40fvp#4f	lw40fvp#4g	lw40fvp#4h	lw40fvp#5b	lw40fvp#5	lw40fvp#5	lw40fvp#5	lw40fvp#5	lw40fvp#5	lw40fvp#5e
38.20	38.36	38.04	38.25	38.31	36.95	37.48	37.88	37.85	38.03	38.05	38.71	37.14
40.99	40.58	41.02	40.98	40.76	35.29	38.18	40.57	40.14	40.55	41.02	40.83	38.53
19.97	21.03	20.52	20.07	20.43	26.98	23.30	20.83	21.18	21.00	20.53	20.16	23.43
0.15	0.16	0.13	0.14	0.12	0.28	0.14	0.15	0.15	0.14	0.13	0.11	0.16
0.23	0.29	0.22	0.29	0.27	0.45	0.33	0.25	0.22	0.26	0.23	0.27	0.34
0.20	0.22	0.22	0.30	0.25	0.07	0.15	0.24	0.28	0.34	0.21	0.21	0.13
99.74	100.63	100.16	100.03	100.13	100.01	99.58	99.92	99.82	100.32	100.16	100.30	99.72
0.99	0.99	0.98	0.99	0.99	0.99	0.99	0.98	0.98	0.98	0.98	1.00	0.98
1.58	1.56	1.58	1.58	1.57	1.41	1.50	1.57	1.56	1.56	1.58	1.56	1.51
0.43	0.45	0.44	0.43	0.44	0.60	0.51	0.45	0.46	0.45	0.44	0.43	0.52
0.00	0.00	0.00	0.00	0.00	0.01	0.00	0.00	0.00	0.00	0.00	0.00	0.01
0.01	0.01	0.01	0.01	0.01	0.01	0.01	0.01	0.01	0.01	0.01	0.01	0.01
0.00	0.01	0.01	0.01	0.01	0.00	0.00	0.01	0.01	0.01	0.00	0.00	0.00
78.49	77.40	78.03	78.34	77.96	69.91	74.37	77.59	77.13	77.42	78.02	78.19	74.45
21.45	22.51	21.91	21.53	21.92	29.98	25.46	22.35	22.83	22.50	21.90	21.67	25.40

Table 8. Composition of olivine phenocrysts from LW40FVP of Ql2a

lw40fvp#6a	lw40fvp#6b	lw40fvp#6c	lw40fvp#6d	lw40fvp#6e
36.67	36.86	38.10	38.20	37.09
34.90	35.54	40.65	40.59	36.08
27.72	26.28	20.48	20.53	25.83
0.30	0.24	0.12	0.15	0.26
0.45	0.45	0.27	0.24	0.43
0.08	0.08	0.26	0.25	0.11
100.13	99.44	99.87	99.96	99.79
0.98	0.99	0.99	0.99	0.99
1.39	1.42	1.57	1.57	1.43
0.62	0.59	0.44	0.44	0.58
0.01	0.01	0.00	0.00	0.01
0.01	0.01	0.01	0.01	0.01
0.00	0.00	0.01	0.01	0.00
69.12	70.56	77.87	77.86	71.27
30.80	29.27	22.01	22.09	28.62

Table 9. Composition of olivine phenocrysts from LW135FVP of Qs2fs

Point	lw135_1b	lw135_1	lw135_1	lw135_1	lw135_1	lw135_1	lw135_1	lw135_1	lw135_1	lw135_1	lw135_1	lw135_1e	lw135_4ab
SiO_2	38.31	38.59	38.34	38.38	39.05	38.31	38.18	38.57	38.44	38.41	38.32	38.14	38.05
Cr_2O_3	0.00	0.01	0.01	0.05	0.03	0.02	0.00	0.01	0.01	0.00	0.00	0.01	0.00
FeO	21.94	21.54	21.87	21.87	21.80	22.03	22.18	22.07	21.90	21.05	21.52	22.56	21.00
MgO	39.42	39.59	39.74	39.56	39.57	39.50	39.73	39.51	39.71	39.31	39.71	39.26	39.28
MnO	0.38	0.27	0.31	0.30	0.27	0.30	0.29	0.31	0.27	0.29	0.30	0.40	0.31
CaO	0.18	0.15	0.14	0.13	0.13	0.15	0.16	0.14	0.13	0.17	0.17	0.15	0.20
NiO	0.16	0.25	0.22	0.26	0.25	0.08	0.22	0.21	0.19	0.18	0.19	0.13	0.04
TOTAL	100.39	100.39	100.63	100.54	101.11	100.38	100.76	100.82	100.65	99.40	100.21	100.65	98.87
Cations based on 4 oxygens													
Si	0.99	1.00	0.99	0.99	1.00	0.99	0.99	1.00	0.99	1.00	0.99	0.99	1.00
Cr	0.00	0.00	0.00	0.00	0.00	0.00	0.00	0.00	0.00	0.00	0.00	0.00	0.00
Fe	0.48	0.47	0.47	0.47	0.47	0.48	0.48	0.48	0.47	0.46	0.47	0.49	0.46
Mg	1.52	1.53	1.53	1.53	1.51	1.53	1.53	1.52	1.53	1.53	1.53	1.52	1.53
Mn	0.01	0.01	0.01	0.01	0.01	0.01	0.01	0.01	0.01	0.01	0.01	0.01	0.01
Ca	0.01	0.00	0.00	0.00	0.00	0.00	0.00	0.00	0.00	0.01	0.01	0.00	0.01
Ni	0.00	0.01	0.01	0.01	0.01	0.00	0.01	0.00	0.00	0.00	0.00	0.00	0.00
Fo	76.07	76.55	76.29	76.21	76.30	76.07	76.08	76.03	76.27	76.84	76.61	75.44	76.87
Fa	23.76	23.37	23.56	23.64	23.59	23.81	23.83	23.83	23.61	23.08	23.29	24.33	23.06

Table 9. Composition of olivine phenocrysts from LW135FVP of Qs2fs

lw135_4a	lw135_4a	lw135_4a	lw135_4a	lw135_4a	lw135_4a	lw135_4a	lw135_4a	lw135_4a	lw135_4ae	lw135_5b	lw135_5	lw135_5
38.39	38.26	38.73	38.92	38.65	38.27	38.09	38.01	38.13	38.31	38.52	38.63	38.36
0.01	0.01	0.02	0.02	0.00	0.00	0.14	0.02	0.01	0.02	0.00	0.00	0.01
20.69	20.52	20.88	20.83	20.85	20.69	21.34	20.72	20.86	21.14	20.53	20.64	20.51
39.96	39.89	39.95	40.13	40.01	38.92	39.87	40.09	39.91	39.33	40.14	40.05	39.97
0.27	0.32	0.28	0.24	0.24	0.22	0.22	0.31	0.27	0.28	0.22	0.30	0.26
0.17	0.14	0.13	0.13	0.15	0.15	0.14	0.13	0.17	0.17	0.16	0.15	0.16
0.22	0.17	0.24	0.20	0.17	0.26	0.19	0.23	0.18	0.11	0.19	0.20	0.19
99.70	99.30	100.24	100.48	100.07	98.50	99.99	99.52	99.53	99.34	99.76	99.97	99.46
1.00	1.00	1.00	1.00	1.00	1.01	0.99	0.99	0.99	1.00	1.00	1.00	1.00
0.00	0.00	0.00	0.00	0.00	0.00	0.00	0.00	0.00	0.00	0.00	0.00	0.00
0.45	0.45	0.45	0.45	0.45	0.45	0.46	0.45	0.45	0.46	0.44	0.45	0.45
1.55	1.55	1.54	1.54	1.54	1.52	1.54	1.56	1.55	1.53	1.55	1.54	1.55
0.01	0.01	0.01	0.01	0.01	0.01	0.01	0.01	0.01	0.01	0.01	0.01	0.01
0.01	0.00	0.00	0.00	0.00	0.00	0.00	0.00	0.01	0.01	0.00	0.00	0.00
0.01	0.00	0.01	0.00	0.00	0.01	0.00	0.01	0.00	0.00	0.00	0.00	0.00
77.44	77.49	77.22	77.39	77.33	77.00	76.87	77.40	77.28	76.77	77.68	77.48	77.59
22.50	22.36	22.65	22.54	22.61	22.97	23.09	22.45	22.67	23.16	22.29	22.40	22.34

Table 9. Composition of olivine phenocrysts from LW135FVP of Qs2fs

lw135_5	lw135_5	lw135_5	lw135_5	lw135_5	lw135_5	lw135_5	lw135_5	lw135_5e
38.40	38.46	38.48	38.46	38.50	38.30	38.63	38.42	38.39
0.00	0.01	0.01	0.02	0.04	0.00	0.00	0.00	0.01
20.24	20.33	20.56	20.12	20.57	20.37	20.26	20.57	20.20
40.14	39.96	40.01	40.00	39.96	39.91	39.81	39.95	39.59
0.25	0.25	0.23	0.21	0.27	0.28	0.28	0.24	0.24
0.14	0.15	0.16	0.16	0.14	0.17	0.14	0.18	0.16
0.22	0.18	0.23	0.24	0.12	0.23	0.27	0.24	0.14
99.39	99.34	99.69	99.21	99.61	99.26	99.39	99.60	98.73
1.00	1.00	1.00	1.00	1.00	1.00	1.00	1.00	1.00
0.00	0.00	0.00	0.00	0.00	0.00	0.00	0.00	0.00
0.44	0.44	0.45	0.44	0.45	0.44	0.44	0.45	0.44
1.55	1.55	1.55	1.55	1.54	1.55	1.54	1.55	1.54
0.01	0.01	0.01	0.01	0.01	0.01	0.01	0.01	0.01
0.00	0.00	0.00	0.01	0.00	0.01	0.00	0.01	0.00
0.01	0.00	0.01	0.01	0.00	0.01	0.01	0.01	0.00
77.89	77.73	77.60	77.99	77.51	77.69	77.70	77.57	77.70
22.04	22.19	22.37	22.01	22.39	22.24	22.19	22.41	22.25

Table 10. Composition of olivine phenocrysts from LW61FVP of Ql3

Point	lw61fvp_#1a	lw61fvp_#1b	lw61fvp_#1c	lw61fvp_#1d	lw61fvp_#1e	lw61fvp_#1f	lw61fvp_#1g	lw61fvp_#2a	lw61fvp_#2b	lw61fvp_#2c
SiO_2	37.13	38.13	38.11	38.07	38.35	36.97	36.96	37.15	38.10	38.18
MgO	36.62	40.85	40.97	40.91	40.88	36.08	35.66	36.44	41.14	41.02
FeO	25.00	20.27	20.33	20.14	20.22	26.33	26.51	25.44	20.30	20.33
CaO	0.17	0.11	0.14	0.13	0.12	0.23	0.28	0.22	0.11	0.14
MnO	0.41	0.28	0.25	0.32	0.26	0.40	0.42	0.43	0.27	0.29
NiO	0.09	0.21	0.21	0.24	0.25	0.10	0.11	0.09	0.22	0.20
TOTAL	99.42	99.86	100.00	99.81	100.07	100.11	99.93	99.77	100.14	100.15
Cations based on 4 oxygens										
Si	0.99	0.99	0.99	0.99	0.99	0.98	0.99	0.99	0.98	0.99
Mg	1.45	1.58	1.58	1.58	1.57	1.43	1.42	1.44	1.58	1.58
Fe	0.56	0.44	0.44	0.44	0.44	0.59	0.59	0.57	0.44	0.44
Ca	0.01	0.00	0.00	0.00	0.00	0.01	0.01	0.01	0.00	0.00
Mn	0.01	0.01	0.01	0.01	0.01	0.01	0.01	0.01	0.01	0.01
Ni	0.00	0.00	0.00	0.01	0.01	0.00	0.00	0.00	0.01	0.00
Fo	72.15	78.11	78.17	78.22	78.19	70.86	70.51	71.74	78.20	78.14
Fa	27.64	21.75	21.76	21.61	21.70	29.01	29.42	28.11	21.66	21.73

Table 10. Composition of olivine phenocrysts from LW61FVP of Q13

lw61fvp_-#2d	lw61fvp_#2e	lw61fvp_#2f	lw61fvp_#2g	lw61fvp_#2h	lw61fvp_#2i	lw61fvp_#2j	lw61fvp_#2k	lw61fvp_#3a	lw61fvp_#3b	lw61fvp_#3c
38.39	38.24	37.67	38.15	38.17	38.12	38.17	37.04	37.43	38.23	38.17
40.80	40.53	38.04	40.95	40.99	40.79	40.32	36.09	36.11	40.60	40.98
20.30	21.23	23.36	20.33	20.59	20.56	21.09	25.79	25.98	20.84	20.74
0.16	0.14	0.18	0.13	0.13	0.13	0.12	0.24	0.24	0.16	0.13
0.31	0.29	0.36	0.26	0.27	0.24	0.28	0.41	0.39	0.27	0.25
0.30	0.23	0.13	0.28	0.22	0.28	0.24	0.11	0.13	0.20	0.21
100.26	100.66	99.74	100.10	100.37	100.11	100.22	99.67	100.27	100.31	100.48
0.99	0.99	0.99	0.99	0.98	0.99	0.99	0.99	0.99	0.99	0.98
1.57	1.56	1.49	1.58	1.58	1.57	1.55	1.43	1.43	1.56	1.57
0.44	0.46	0.51	0.44	0.44	0.44	0.46	0.58	0.58	0.45	0.45
0.00	0.00	0.01	0.00	0.00	0.00	0.00	0.01	0.01	0.00	0.00
0.01	0.01	0.01	0.01	0.01	0.01	0.01	0.01	0.01	0.01	0.01
0.01	0.01	0.00	0.01	0.01	0.01	0.01	0.00	0.00	0.00	0.00
78.09	77.20	74.27	78.13	77.93	77.89	77.21	71.30	71.17	77.58	77.82
21.80	22.69	25.59	21.76	21.96	22.03	22.66	28.59	28.73	22.35	22.10

Table 10. Composition of olivine phenocrysts from LW61FVP of Ql3

lw61fvp_#3d	lw61fvp_#3e	lw61fvp_#4a	lw61fvp_#4b	lw61fvp_#4c	lw61fvp_#4d	lw61fvp_#4e	lw61fvp_#4f	lw61fvp_#4g	lw61fvp_#4h	lw61fvp_#4i
38.00	37.10	37.00	38.04	38.19	38.04	37.38	37.25	38.19	38.14	37.43
40.23	35.91	36.21	40.70	40.71	40.68	37.82	36.80	40.60	40.55	37.28
21.53	26.44	26.46	20.80	20.96	20.81	23.76	25.24	20.89	20.96	24.87
0.15	0.23	0.25	0.14	0.15	0.12	0.17	0.21	0.18	0.14	0.18
0.27	0.39	0.43	0.33	0.25	0.31	0.31	0.43	0.29	0.26	0.36
0.22	0.09	0.06	0.22	0.19	0.25	0.18	0.08	0.23	0.20	0.24
100.40	100.16	100.40	100.23	100.44	100.20	99.62	100.00	100.36	100.24	100.35
0.98	0.99	0.98	0.98	0.99	0.98	0.99	0.99	0.99	0.99	0.99
1.55	1.42	1.43	1.57	1.57	1.57	1.49	1.45	1.56	1.56	1.46
0.47	0.59	0.59	0.45	0.45	0.45	0.52	0.56	0.45	0.45	0.55
0.00	0.01	0.01	0.00	0.00	0.00	0.01	0.01	0.01	0.00	0.01
0.01	0.01	0.01	0.01	0.01	0.01	0.01	0.01	0.01	0.01	0.01
0.01	0.00	0.00	0.00	0.00	0.01	0.00	0.00	0.01	0.00	0.01
76.84	70.69	70.83	77.58	77.53	77.57	73.86	72.08	77.55	77.45	72.66
23.07	29.20	29.04	22.25	22.40	22.26	26.03	27.74	22.39	22.46	27.20

Table 10. Composition of olivine phenocrysts from LW61FVP of Ql3

lw61fvp_#4j	lw61fvp_#4k	lw61fvp_#4l	lw61fvp_#4m	lw61fvp_#4n	lw61fvp_#5a	lw61fvp_#5b	lw61fvp_#5c	lw61fvp_#5d	lw61fvp_#5e	lw61fvp_#5f
37.93	36.91	37.90	38.24	37.24	36.71	37.93	38.26	37.52	36.47	36.49
40.13	34.82	39.86	40.46	35.69	34.71	39.79	40.36	37.40	34.95	35.40
21.11	27.21	21.73	20.56	26.22	27.34	21.50	21.17	24.33	27.20	26.86
0.21	0.28	0.15	0.12	0.26	0.32	0.15	0.14	0.19	0.28	0.26
0.21	0.47	0.32	0.24	0.37	0.48	0.29	0.32	0.34	0.46	0.41
0.20	0.07	0.15	0.15	0.09	0.07	0.23	0.19	0.18	0.05	0.01
99.79	99.75	100.12	99.77	99.87	99.63	99.89	100.42	99.97	99.41	99.43
0.99	0.99	0.99	0.99	0.99	0.99	0.99	0.99	0.99	0.98	0.98
1.56	1.39	1.54	1.56	1.42	1.39	1.54	1.55	1.47	1.40	1.42
0.46	0.61	0.47	0.45	0.58	0.61	0.47	0.46	0.54	0.61	0.60
0.01	0.01	0.00	0.00	0.01	0.01	0.00	0.00	0.01	0.01	0.01
0.01	0.01	0.01	0.01	0.01	0.01	0.01	0.01	0.01	0.01	0.01
0.00	0.00	0.00	0.00	0.00	0.00	0.01	0.00	0.00	0.00	0.00
77.27	69.43	76.47	77.75	70.78	69.29	76.64	77.14	73.17	69.52	70.08
22.80	30.44	23.39	22.16	29.18	30.62	23.24	22.70	26.71	30.36	29.83

Table 10. Composition of olivine phenocrysts from LW61FVP of Ql3

lw61fvp_#5g	lw61fvp_#5h	lw61fvp_#5i	lw61fvp_#5j
38.04	38.09	38.16	36.84
41.27	41.03	39.91	36.25
20.11	20.23	21.43	26.26
0.13	0.10	0.16	0.20
0.26	0.23	0.29	0.38
0.20	0.28	0.14	0.11
100.01	99.96	100.08	100.05
0.98	0.98	0.99	0.98
1.59	1.58	1.54	1.44
0.43	0.44	0.47	0.58
0.00	0.00	0.00	0.01
0.01	0.01	0.01	0.01
0.00	0.01	0.00	0.00
78.45	78.25	76.77	71.01
21.45	21.65	23.13	28.86

Table 11. Composition of olivine phenocrysts from LW80FVP of Qs3

Point	lw80fvp_rim_#1a	lw80fvp_core_#1f	lw80fvp_core_#1e	lw80fvp_rim_#1d	lw80fvp_rim_#1c	lw80fvp_rim_#2a	lw80fvp_core_#2e
SiO_2	37.61	38.46	38.26	38.32	38.22	38.58	38.25
MgO	39.72	40.46	40.44	40.22	40.63	40.29	40.08
FeO	21.45	20.92	20.93	20.72	21.09	20.82	21.92
CaO	0.16	0.16	0.15	0.15	0.16	0.16	0.13
MnO	0.30	0.33	0.29	0.27	0.27	0.31	0.33
NiO	0.07	0.22	0.25	0.14	0.21	0.14	0.20
TOTAL	99.31	100.54	100.32	99.82	100.58	100.29	100.91
Cations based on 4 oxygens							
Si	0.98	0.99	0.99	0.99	0.99	1.00	0.99
Mg	1.55	1.55	1.56	1.55	1.56	1.55	1.54
Fe	0.47	0.45	0.45	0.45	0.46	0.45	0.47
Ca	0.00	0.00	0.00	0.00	0.00	0.00	0.00
Mn	0.01	0.01	0.01	0.01	0.01	0.01	0.01
Ni	0.00	0.01	0.01	0.00	0.00	0.00	0.00
Fo	76.66	77.40	77.41	77.51	77.38	77.43	76.39
Fa	23.22	22.45	22.48	22.41	22.54	22.45	23.44

Table 11. Composition of olivine phenocrysts from LW80FVP of Qs3

lw80fvp_core_#2d	lw80fvp_rim_#2b	lw80fvp_rim_#2f	lw80fvp_core_#2h	lw80fvp_core_#2i	lw80fvp_rim_#2g	lw80fvp_rim_#3a	lw80fvp_core_#3g
37.27	37.57	37.89	37.75	37.52	37.91	37.96	38.45
40.16	40.40	40.25	39.68	39.34	39.63	40.66	41.02
21.13	21.10	21.26	22.14	22.24	21.59	21.03	20.11
0.15	0.17	0.14	0.13	0.13	0.14	0.14	0.11
0.26	0.27	0.29	0.35	0.29	0.28	0.30	0.27
0.13	0.18	0.20	0.14	0.15	0.16	0.20	0.23
99.08	99.69	100.02	100.19	99.67	99.70	100.30	100.19
0.98	0.98	0.98	0.98	0.98	0.99	0.98	0.99
1.57	1.57	1.56	1.54	1.54	1.54	1.57	1.57
0.46	0.46	0.46	0.48	0.49	0.47	0.46	0.43
0.00	0.01	0.00	0.00	0.00	0.00	0.00	0.00
0.01	0.01	0.01	0.01	0.01	0.01	0.01	0.01
0.00	0.00	0.00	0.00	0.00	0.00	0.00	0.01
77.15	77.29	77.05	76.01	75.82	76.50	77.40	78.31
22.78	22.65	22.83	23.79	24.04	23.38	22.47	21.54

Table 11. Composition of olivine phenocrysts from LW80FVP of Qs3

lw80fvp_core_#3e	lw80fvp_rim_#3d	lw80fvp_rim_#3c	lw80fvp_rim_#4a	lw80fvp_core_#4d	lw80fvp_core_#4c	lw80fvp_rim_#4b	lw80fvp_rim_#5b
37.89	38.54	37.76	37.45	38.19	38.32	37.81	37.47
40.72	40.62	40.29	40.17	40.91	40.98	40.90	39.85
20.44	20.82	21.03	21.16	20.44	20.45	20.37	21.26
0.14	0.16	0.14	0.17	0.11	0.13	0.12	0.17
0.25	0.29	0.29	0.30	0.23	0.24	0.28	0.29
0.24	0.14	0.13	0.17	0.22	0.22	0.21	0.16
99.68	100.57	99.63	99.42	100.10	100.35	99.69	99.20
0.98	0.99	0.98	0.98	0.99	0.99	0.98	0.98
1.58	1.56	1.56	1.57	1.57	1.57	1.58	1.56
0.44	0.45	0.46	0.46	0.44	0.44	0.44	0.47
0.00	0.00	0.00	0.01	0.00	0.00	0.00	0.01
0.01	0.01	0.01	0.01	0.01	0.01	0.01	0.01
0.01	0.00	0.00	0.00	0.01	0.01	0.00	0.00
77.95	77.59	77.25	77.11	78.03	78.07	78.06	76.90
21.96	22.31	22.62	22.79	21.87	21.85	21.81	23.02

Table 11. Composition of olivine phenocrysts from LW80FVP of Qs3

lw80fvp_core_#5d	lw80fvp_core_#5e	lw80fvp_rim_#5a	lw80fvp_rim_#5c
38.33	38.24	37.64	38.57
41.20	40.79	40.29	40.48
20.00	20.36	21.32	20.89
0.13	0.11	0.14	0.14
0.19	0.28	0.30	0.30
0.24	0.23	0.15	0.15
100.08	100.01	99.84	100.53
0.99	0.99	0.98	0.99
1.58	1.57	1.56	1.55
0.43	0.44	0.46	0.45
0.00	0.00	0.00	0.00
0.00	0.01	0.01	0.01
0.01	0.01	0.00	0.00
78.57	78.00	77.01	77.45
21.40	21.85	22.86	22.42

Table 12. Composition of olivine phenocrysts from LW78FVP of Qs4b

TAG	lw78fvp_rim_#1b	lw78fvp_core_#1c	lw78fvp_core_#1d	lw78fvp_rim_#1a	lw78fvp_rim_#2a	lw78fvp_rim_#2c	lw78fvp_core_#2d
SiO_2	37.86	38.10	37.98	38.03	37.96	37.96	37.92
MgO	39.78	40.45	40.86	40.37	40.26	39.89	40.30
FeO	20.81	20.24	20.44	20.26	20.28	20.99	20.33
CaO	0.14	0.15	0.13	0.15	0.15	0.16	0.15
MnO	0.28	0.29	0.22	0.24	0.22	0.27	0.23
NiO	0.15	0.26	0.24	0.14	0.16	0.15	0.16
TOTAL	99.03	99.49	99.86	99.19	99.03	99.42	99.08
Cations based on 4 oxygens							
Si	0.99	0.99	0.98	0.99	0.99	0.99	0.99
Mg	1.55	1.57	1.58	1.57	1.57	1.55	1.57
Fe	0.46	0.44	0.44	0.44	0.44	0.46	0.44
Ca	0.00	0.00	0.00	0.00	0.00	0.01	0.00
Mn	0.01	0.01	0.01	0.01	0.01	0.01	0.01
Ni	0.00	0.01	0.01	0.00	0.00	0.00	0.00
Fo	77.22	78.00	78.04	77.99	77.95	77.15	77.91
Fa	22.67	21.89	21.90	21.95	22.03	22.78	22.05

Table 12. Composition of olivine phenocrysts from LW78FVP of Qs4b

lw78fvp_core_#2f	lw78fvp_core_#2e	lw78fvp_rim_#2b	lw78fvp_rim_#3f	lw78fvp_#3g	lw78fvp_#3h	lw78fvp_#3i	lw78fvp_rim_#3j	lw78fvp_rim_#3k
37.79	39.07	37.58	37.04	37.01	38.34	37.60	37.33	37.39
40.90	41.80	39.49	39.42	39.74	40.80	40.27	39.50	39.68
20.60	21.03	21.34	21.48	21.38	20.57	20.66	21.26	21.29
0.14	0.14	0.21	0.19	0.18	0.13	0.13	0.18	0.17
0.24	0.24	0.25	0.22	0.27	0.25	0.27	0.27	0.27
0.23	0.32	0.14	0.11	0.06	0.18	0.26	0.11	0.28
99.90	102.61	99.00	98.46	98.64	100.26	99.19	98.65	99.09
0.98	0.99	0.99	0.98	0.98	0.99	0.98	0.98	0.98
1.58	1.57	1.55	1.55	1.56	1.57	1.57	1.55	1.55
0.45	0.44	0.47	0.48	0.47	0.44	0.45	0.47	0.47
0.00	0.00	0.01	0.01	0.01	0.00	0.00	0.01	0.01
0.01	0.01	0.01	0.01	0.01	0.01	0.01	0.01	0.01
0.01	0.01	0.00	0.00	0.00	0.00	0.01	0.00	0.01
77.91	77.94	76.76	76.60	76.79	77.88	77.56	76.78	76.81
22.01	22.00	23.27	23.42	23.18	22.03	22.33	23.18	23.13

Table 12. Composition of olivine phenocrysts from LW78FVP of Qs4b

lw78fvp_rim_#31	lw78fvp_rim_#4a	lw78fvp_rim_#4b	lw78fvp_core_#4f	lw78fvp_core_#4d	lw78fvp_core_#4h	lw78fvp_rim_#4c	lw78fvp_rim_#5a
37.27	36.82	38.04	38.94	38.04	37.71	37.69	37.59
39.39	39.96	40.29	41.60	40.62	40.74	40.18	39.89
21.82	20.83	20.58	20.80	20.11	20.25	20.93	21.22
0.18	0.16	0.14	0.15	0.15	0.13	0.16	0.16
0.27	0.26	0.30	0.22	0.27	0.26	0.22	0.29
0.09	0.20	0.21	0.30	0.28	0.20	0.12	0.11
99.01	98.22	99.56	102.01	99.46	99.30	99.29	99.25
0.98	0.97	0.99	0.99	0.99	0.98	0.98	0.98
1.55	1.58	1.56	1.57	1.57	1.58	1.56	1.56
0.48	0.46	0.45	0.44	0.44	0.44	0.46	0.46
0.01	0.00	0.00	0.00	0.00	0.00	0.00	0.00
0.01	0.01	0.01	0.01	0.01	0.01	0.01	0.01
0.00	0.00	0.00	0.01	0.01	0.00	0.00	0.00
76.25	77.32	77.62	78.07	78.19	78.12	77.37	76.94
23.70	22.61	22.24	21.90	21.72	21.78	22.61	22.96

Table 12. Composition of olivine phenocrysts from LW78FVP of Qs4b

lw78fvp_rim_#5c	lw78fvp_core_#5e	lw78fvp_core_#5d	lw78fvp_core_#5f	lw78fvp_rim_#5b
38.20	38.22	38.26	38.18	37.93
40.18	40.76	40.52	40.88	40.36
21.08	20.33	20.71	20.45	21.11
0.16	0.09	0.14	0.10	0.15
0.33	0.27	0.28	0.33	0.22
0.20	0.26	0.25	0.29	0.21
100.14	99.92	100.16	100.24	99.96
0.99	0.99	0.99	0.99	0.98
1.55	1.57	1.56	1.57	1.56
0.46	0.44	0.45	0.44	0.46
0.00	0.00	0.00	0.00	0.00
0.01	0.01	0.01	0.01	0.01
0.00	0.01	0.01	0.01	0.00
77.15	78.00	77.63	77.92	77.28
22.71	21.83	22.26	21.87	22.68

Table 13. Compositions of olivine phenocrysts from LW151FVP of Qs4a

Point	lw151fvp#1b	lw151fvp#1	lw151fvp#1	lw151fvp#1	lw151fvp#1	lw151fvp#1	lw151fvp#1e	lw151fvp#2b	lw151fvp#2	lw151fvp#2
SiO_2	38.14	37.94	37.87	37.69	38.06	37.83	38.42	38.05	38.60	38.22
MgO	40.52	40.37	39.89	39.62	40.02	40.70	40.59	39.54	40.50	40.79
FeO	20.41	20.27	20.78	21.22	21.25	20.42	20.38	21.88	20.99	20.42
CaO	0.13	0.14	0.15	0.12	0.14	0.13	0.13	0.18	0.18	0.12
MnO	0.16	0.35	0.22	0.24	0.27	0.23	0.18	0.34	0.24	0.26
NiO	0.24	0.22	0.09	0.24	0.15	0.25	0.27	0.09	0.21	0.20
TOTAL	99.60	99.27	99.00	99.14	99.88	99.57	99.98	100.07	100.71	100.01
Cations based on 4 oxygens										
Si	0.99	0.99	0.99	0.99	0.99	0.98	0.99	0.99	0.99	0.99
Mg	1.57	1.57	1.55	1.55	1.55	1.58	1.56	1.53	1.55	1.57
Fe	0.44	0.44	0.45	0.47	0.46	0.44	0.44	0.48	0.45	0.44
Ca	0.00	0.00	0.00	0.00	0.00	0.00	0.00	0.01	0.01	0.00
Mn	0.00	0.01	0.01	0.01	0.01	0.01	0.00	0.01	0.01	0.01
Ni	0.01	0.00	0.00	0.01	0.00	0.01	0.01	0.00	0.00	0.00
Fo	77.96	77.86	77.36	76.82	76.97	77.97	78.01	76.22	77.46	77.98
Fa	22.03	21.94	22.61	23.08	22.93	21.95	21.98	23.67	22.52	21.91

Table 13. Compositions of olivine phenocrysts from LW151FVP of Qs4a

lw151fvp#2	lw151fvp#2	lw151fvp#2	lw151fvp#2e	lw151fvp#3b	lw151fvp#3	lw151fvp#3	lw151fvp#3	lw151fvp#3	lw151fvp#3	lw151fvp#3e
38.17	38.65	38.06	38.26	38.32	38.13	38.32	38.14	38.46	39.04	38.34
40.74	40.59	40.83	39.87	39.44	39.66	40.20	39.43	38.50	38.54	39.62
20.40	20.62	20.54	21.12	21.47	21.04	21.09	21.56	21.63	21.41	20.49
0.12	0.15	0.15	0.18	0.15	0.19	0.15	0.13	0.15	0.14	0.14
0.21	0.20	0.29	0.37	0.23	0.32	0.30	0.32	0.30	0.34	0.29
0.24	0.30	0.23	0.18	0.14	0.15	0.13	0.19	0.18	0.13	0.22
99.87	100.51	100.09	99.98	99.75	99.48	100.19	99.77	99.22	99.60	99.10
0.99	0.99	0.98	0.99	1.00	0.99	0.99	0.99	1.01	1.01	1.00
1.57	1.56	1.57	1.54	1.53	1.54	1.55	1.53	1.50	1.49	1.54
0.44	0.44	0.44	0.46	0.47	0.46	0.46	0.47	0.47	0.47	0.45
0.00	0.00	0.00	0.01	0.00	0.01	0.00	0.00	0.00	0.00	0.00
0.01	0.00	0.01	0.01	0.01	0.01	0.01	0.01	0.01	0.01	0.01
0.01	0.01	0.01	0.00	0.00	0.00	0.00	0.00	0.00	0.00	0.01
78.02	77.82	77.91	76.97	76.57	77.01	77.16	76.40	75.95	76.09	77.41
21.92	22.17	21.99	22.88	23.39	22.92	22.72	23.43	23.93	23.72	22.47

Table 13. Compositions of olivine phenocrysts from LW151FVP of Qs4a

lw151fvp#4b	lw151fvp#4	lw151fvp#4	lw151fvp#4e	lw151fvp#5b	lw151fvp#5	lw151fvp#5	lw151fvp#5e
37.84	37.92	37.94	37.95	38.86	38.66	38.94	38.77
40.59	40.80	40.77	40.67	40.50	40.83	40.80	41.23
19.93	20.27	20.43	20.48	20.54	20.33	20.37	20.19
0.12	0.12	0.15	0.14	0.17	0.16	0.14	0.13
0.21	0.24	0.20	0.27	0.29	0.22	0.30	0.21
0.29	0.24	0.29	0.23	0.28	0.22	0.30	0.32
98.96	99.60	99.78	99.74	100.65	100.41	100.83	100.86
0.99	0.98	0.98	0.98	1.00	0.99	1.00	0.99
1.58	1.58	1.58	1.57	1.55	1.56	1.56	1.57
0.44	0.44	0.44	0.44	0.44	0.44	0.44	0.43
0.00	0.00	0.00	0.00	0.01	0.00	0.00	0.00
0.01	0.01	0.00	0.01.	0.01	0.01	0.01	0.01
0.01	0.01	0.01	0.01	0.01	0.01	0.01	0.01
78.35	78.13	78.05	77.90	77.78	78.14	78.02	78.41
21.58	21.78	21.94	22.01	22.14	21.83	21.85	21.54

Table 14. Composition of plagioclase phenocrysts and groundmass (gm) from LW21FVP of Ql1d

Point	lw21_#3b	lw21_#3	lw21_#3	lw21_#3e	lw21_#7b	lw21_#7	lw21_#7	lw21_#7e	lw21_#10b	lw21_#10	lw21_#10	lw21_#10	lw21_#10e
SiO_2	51.06	49.45	49.88	50.60	51.98	51.07	48.69	50.37	49.49	49.05	49.50	50.11	50.55
Al_2O_3	29.09	30.61	30.49	29.59	29.79	30.65	29.36	29.67	30.07	30.20	30.06	30.28	30.01
FeO	0.82	0.69	0.83	0.79	0.76	0.73	0.73	0.81	0.82	0.67	0.68	0.74	0.87
CaO	12.63	14.04	14.10	12.99	12.67	13.52	14.57	13.13	13.72	13.83	13.66	13.86	13.36
Na_2O	4.21	3.40	3.56	4.04	4.38	3.79	3.63	3.79	3.57	3.55	3.58	3.52	3.76
K_2O	0.32	0.21	0.22	0.31	0.36	0.23	0.26	0.29	0.25	0.24	0.23	0.23	0.27
SrO	0.33	0.32	0.39	0.31	0.29	0.33	0.32	0.35	0.42	0.34	0.27	0.30	0.39
BaO	0.11	0.01	0.11	0.11	0.08	0.06	0.08	0.07	0.06	0.06	0.03	0.07	0.13
TOTAL	98.55	98.72	99.57	98.73	100.30	100.39	97.64	98.48	98.40	97.95	98.01	99.11	99.33
Cations based on 8 oxygens													
Si	2.37	2.30	2.30	2.35	2.37	2.33	2.30	2.34	2.31	2.30	2.31	2.32	2.33
Al	1.59	1.68	1.66	1.62	1.60	1.65	1.63	1.63	1.65	1.67	1.66	1.65	1.63
Fe	0.03	0.03	0.03	0.03	0.03	0.03	0.03	0.03	0.03	0.03	0.03	0.03	0.03
Ca	0.63	0.70	0.70	0.65	0.62	0.66	0.74	0.65	0.69	0.70	0.68	0.69	0.66
Na	0.38	0.31	0.32	0.36	0.39	0.34	0.33	0.34	0.32	0.32	0.32	0.32	0.34
K	0.02	0.01	0.01	0.02	0.02	0.01	0.02	0.02	0.02	0.02	0.01	0.01	0.02
Sr	0.01	0.01	0.01	0.01	0.01	0.01	0.01	0.01	0.01	0.01	0.01	0.01	0.01
Ba	0.00	0.00	0.00	0.00	0.00	0.00	0.00	0.00	0.00	0.00	0.00	0.00	0.00
Or	1.87	1.24	1.26	1.78	2.03	1.35	1.42	1.68	1.44	1.41	1.36	1.32	1.55
Ab	36.86	30.07	30.89	35.33	37.63	33.17	30.58	33.65	31.55	31.23	31.70	31.04	33.14
An	61.08	68.67	67.66	62.71	60.19	65.37	67.86	64.53	66.90	67.25	66.90	67.51	65.08

Table 14. Composition of plagioclase phenocrysts and groundmass (gm) from LW21FVP of Ql1d

lw21_#11ab	lw21_#11a	lw21_#11ae	lw21_#11bb	lw21_#11b	lw21_#11b	lw21_#11b	lw21_#11be	lw21_#12ab	lw21_#12a	lw21_#12a	lw21_#12a
57.42	50.44	49.76	49.33	49.84	50.35	50.33	50.55	48.34	48.24	48.70	48.29
23.69	29.92	29.44	29.21	30.06	29.96	29.74	29.55	29.21	30.33	30.40	30.30
0.62	0.73	0.80	0.74	0.66	0.58	0.66	0.76	0.93	0.71	0.70	0.78
6.65	13.57	13.01	13.77	13.77	13.49	13.60	12.79	13.69	13.63	13.68	13.92
5.87	3.64	4.02	3.80	3.62	3.64	3.64	4.11	3.79	3.57	3.52	3.52
3.24	0.26	0.32	0.29	0.23	0.23	0.25	0.32	0.32	0.24	0.22	0.26
0.11	0.37	0.29	0.31	0.27	0.37	0.29	0.31	0.31	0.34	0.24	0.31
0.28	0.12	0.10	0.07	0.04	0.07	0.07	0.00	0.04	0.08	0.02	0.08
97.89	99.04	97.73	97.52	98.49	98.68	98.56	98.39	96.63	97.14	97.47	97.46
2.67	2.33	2.34	2.33	2.32	2.34	2.34	2.35	2.30	2.28	2.29	2.28
1.30	1.63	1.63	1.62	1.65	1.64	1.63	1.62	1.64	1.69	1.69	1.69
0.02	0.03	0.03	0.03	0.03	0.02	0.03	0.03	0.04	0.03	0.03	0.03
0.33	0.67	0.65	0.70	0.69	0.67	0.68	0.64	0.70	0.69	0.69	0.70
0.53	0.33	0.37	0.35	0.33	0.33	0.33	0.37	0.35	0.33	0.32	0.32
0.19	0.02	0.02	0.02	0.01	0.01	0.02	0.02	0.02	0.02	0.01	0.02
0.00	0.01	0.01	0.01	0.01	0.01	0.01	0.01	0.01	0.01	0.01	0.01
0.01	0.00	0.00	0.00	0.00	0.00	0.00	0.00	0.00	0.00	0.00	0.00
18.15	1.50	1.82	1.63	1.35	1.35	1.43	1.82	1.80	1.43	1.30	1.49
50.04	32.09	35.15	32.74	31.78	32.31	32.11	36.08	32.72	31.66	31.32	30.87
31.33	66.20	62.85	65.51	66.82	66.23	66.33	62.09	65.40	66.77	67.35	67.49

Table 14. Composition of plagioclase phenocrysts and groundmass (gm) from LW21FVP of Ql1d

lw21_#12ae	lw21_#12bb	lw21_#12b	lw21_#12b	lw21_#12be	lw21_#13b	lw21_#13	lw21_#13	lw21_#13e	lw21_#14ab	lw21_#14a	lw21_#14a
					gm	gm	gm	gm	gm	gm	gm
50.84	50.36	48.67	49.07	50.23	48.57	48.40	48.86	56.04	52.30	48.22	47.90
29.77	30.22	30.07	30.37	29.12	29.65	29.97	29.63	25.34	28.86	29.94	29.94
0.81	0.77	0.65	0.68	0.81	0.77	0.70	0.74	0.71	0.86	0.78	0.73
12.96	13.69	14.32	13.93	12.42	13.29	13.51	13.41	7.76	11.89	13.71	13.85
3.89	3.59	3.47	3.59	4.25	3.64	3.69	3.65	6.42	4.64	3.66	3.62
0.30	0.25	0.24	0.24	0.38	0.27	0.24	0.32	1.01	0.39	0.24	0.23
0.33	0.36	0.31	0.38	0.34	0:46	0.33	0.33	0.24	0.35	0.36	0.33
0.08	0.07	0.05	0.07	0.11	0.08	0.05	0.10	0.41	0.12	0.04	0.02
98.99	99.31	97.77	98.31	97.67	96.72	96.88	97.03	97.93	99.40	96.95	96.62
2.35	2.32	2.29	2.29	2.36	2.31	2.29	2.31	2.59	2.40	2.29	2.28
1.62	1.64	1.67	1.67	1.61	1.66	1.67	1.65	1.38	1.56	1.67	1.68
0.03	0.03	0.03	0.03	0.03	0.03	0.03	0.03	0.03	0.03	0.03	0.03
0.64	0.68	0.72	0.70	0.62	0.68	0.69	0.68	0.39	0.59	0.70	0.71
0.35	0.32	0.32	0.33	0.39	0.34	0.34	0.34	0.58	0.41	0.34	0.33
0.02	0.02	0.01	0.01	0.02	0.02	0.02	0.02	0.06	0.02	0.02	0.01
0.01	0.01	0.01	0.01	0.01	0.01	0.01	0.01	0.01	0.01	0.01	0.01
0.00	0.00	0.00	0.00	0.00	0.00	0.00	0.00	0.01	0.00	0.00	0.00
1.75	1.45	1.36	1.36	2.22	1.57	1.42	1.85	5.80	2.23	1.39	1.32
34.54	31.70	30.04	31.34	37.32	32.57	32.56	32.36	56.03	40.40	32.10	31.68
63.57	66.72	68.52	67.18	60.26	65.71	65.93	65.61	37.44	57.17	66.44	66.96

Table 14. Composition of plagioclase phenocrysts and groundmass (gm) from LW21FVP of Ql1d

lw21_#14ab	lw21_#14bb	lw21_#14b	lw21_#14be
gm	gm	gm	gm
48.51	55.29	49.17	49.41
30.20	21.49	29.45	29.14
0.67	3.45	0.90	0.88
13.79	9.08	13.19	12.53
3.58	4.85	3.94	4.08
0.24	2.07	0.33	0.37
0.34	0.08	0.34	0.36
0.10	0.17	0.06	0.11
97.42	96.49	97.37	96.89
2.29	2.64	2.32	2.34
1.68	1.21	1.64	1.63
0.03	0.14	0.04	0.04
0.70	0.47	0.67	0.64
0.33	0.45	0.36	0.38
0.01	0.13	0.02	0.02
0.01	0.00	0.01	0.01
0.00	0.00	0.00	0.00
1.37	12.10	1.90	2.18
31.44	43.06	34.41	36.19
67.02	44.53	63.60	61.44

Table 15. Composition of plagioclase phenocrysts and groundmass (gm) from LW73FVP of Ql1b

Point	LW73ph1b	LW73ph1	LW73ph1	LW73ph1	LW73ph1	LW73ph1	LW73ph1e	LW73ph2b	LW73ph2	LW73ph2	LW73ph2	LW73ph2e
SiO_2	50.65	50.53	51.10	50.42	50.50	50.30	51.28	51.06	51.15	51.24	51.49	52.13
Al_2O_3	30.55	30.68	30.39	30.98	30.48	30.07	29.90	30.43	30.91	30.35	30.70	29.70
FeO	0.69	0.61	0.71	0.62	0.64	0.59	0.81	0.76	0.68	0.67	0.69	0.87
CaO	13.64	13.70	13.55	13.71	13.80	13.32	13.13	13.76	13.72	13.51	13.55	12.80
Na_2O	3.43	3.50	3.59	3.38	3.43	3.55	3.77	3.51	3.52	3.50	3.58	3.86
K_2O	0.30	0.25	0.32	0.23	0.23	0.28	0.35	0.26	0.21	0.22	0.24	0.35
SrO	0.34	0.21	0.22	0.35	0.33	0.35	0.42	0.24	0.29	0.33	0.34	0.28
BaO	0.07	0.09	0.08	0.05	0.08	0.12	0.13	0.12	0.07	0.07	0.06	0.10
TOTAL	99.67	99.57	99.97	99.75	99.48	98.57	99.78	100.13	100.54	99.89	100.64	100.09
Cations based on 8 oxygens												
Si	2.33	2.32	2.34	2.31	2.32	2.33	2.35	2.33	2.33	2.34	2.34	2.38
Al	1.65	1.66	1.64	1.67	1.65	1.65	1.62	1.64	1.66	1.64	1.64	1.60
Fe	0.03	0.02	0.03	0.02	0.03	0.02	0.03	0.03	0.03	0.03	0.03	0.03
Ca	0.67	0.67	0.66	0.67	0.68	0.66	0.65	0.67	0.67	0.66	0.66	0.63
Na	0.31	0.31	0.32	0.30	0.31	0.32	0.34	0.31	0.31	0.31	0.32	0.34
K	0.02	0.02	0.02	0.01	0.01	0.02	0.02	0.02	0.01	0.01	0.01	0.02
Sr	0.01	0.01	0.01	0.01	0.01	0.01	0.01	0.01	0.01	0.01	0.01	0.01
Ba	0.00	0.00	0.00	0.00	0.00	0.00	0.00	0.00	0.00	0.00	0.00	0.00
Or	1.76	1.48	1.87	1.36	1.34	1.63	2.05	1.50	1.25	1.30	1.41	2.07
Ab	30.71	31.07	31.76	30.40	30.55	31.91	33.42	31.04	31.29	31.45	31.85	34.49
An	67.40	67.28	66.22	68.15	67.97	66.24	64.31	67.24	67.34	67.13	66.63	63.25

Table 15. Composition of plagioclase phenocrysts and groundmass (gm) from LW73FVP of Ql1b

LW73ph4b	LW73ph4	LW73ph4	LW73ph4	LW73ph4	LW73ph4	LW73ph4e	LW73ph1_gm1 gm	LW73ph1_gm1 gm	LW73ph1_gm2 gm	LW73ph1_gm2 gm
49.46	50.34	49.27	48.85	49.51	49.92	49.83	53.54	52.47	54.47	51.33
31.00	30.99	31.06	30.68	30.88	30.80	30.50	28.70	29.73	27.60	29.89
0.72	0.68	0.70	0.69	0.67	0.71	0.66	0.90	1.00	0.86	0.85
13.57	13.88	14.04	13.69	13.74	13.57	13.54	11.64	12.38	10.18	12.87
3.43	3.46	3.34	3.29	3.46	3.53	3.47	4.53	4.06	4.97	3.84
0.27	0.26	0.19	0.20	0.21	0.26	0.27	0.49	0.45	1.05	0.36
0.26	0.27	0.30	0.28	0.32	0.26	0.32	0.22	0.28	0.22	0.36
0.06	0.00	0.03	0.00	0.05	0.05	0.06	0.08	0.10	0.31	0.07
98.77	99.87	98.93	97.67	98.83	99.09	98.64	100.10	100.47	99.67	99.56
2.29	2.31	2.28	2.29	2.30	2.31	2.31	2.44	2.39	2.49	2.36
1.69	1.67	1.70	1.70	1.69	1.68	1.67	1.54	1.59	1.49	1.62
0.03	0.03	0.03	0.03	0.03	0.03	0.03	0.03	0.04	0.03	0.03
0.67	0.68	0.70	0.69	0.68	0.67	0.67	0.57	0.60	0.50	0.63
0.31	0.31	0.30	0.30	0.31	0.32	0.31	0.40	0.36	0.44	0.34
0.02	0.02	0.01	0.01	0.01	0.02	0.02	0.03	0.03	0.06	0.02
0.01	0.01	0.01	0.01	0.01	0.01	0.01	0.01	0.01	0.01	0.01
0.00	0.00	0.00	0.00	0.00	0.00	0.00	0.00	0.00	0.01	0.00
1.58	1.48	1.12	1.22	1.22	1.50	1.61	2.84	2.66	6.10	2.13
30.86	30.63	29.72	29.91	30.87	31.50	31.15	40.07	36.16	43.79	34.25
67.45	67.89	69.12	68.86	67.82	66.91	67.14	56.95	61.00	49.55	63.50

Table 15. Composition of plagioclase phenocrysts and groundmass (gm) from LW73FVP of Ql1b

LW73ph1_gm3	LW73ph1_gm3	LW73ph1_gm3	LW73ph2_gm1	LW73ph2_gm1	LW73ph2_gm1	LW73ph2_gm2	LW73ph2_gm2	LW73ph2_gm2
gm	gm	gm	gm	gm	gm	gm	gm	gm
52.91	56.59	59.98	51.37	51.07	51.74	51.80	51.49	51.87
28.99	25.52	22.48	29.57	30.61	30.02	30.18	30.05	29.50
0.91	0.65	0.63	0.90	0.81	0.99	0.82	0.79	0.93
12.06	8.07	4.62	12.72	13.24	12.75	13.24	13.13	12.19
4.28	6.10	6.52	3.89	3.60	3.97	3.60	3.73	4.19
0.44	0.98	2.80	0.38	0.34	0.37	0.35	0.36	0.44
0.19	0.26	0.16	0.33	0.34	0.24	0.30	0.43	0.32
0.08	0.28	1.01	0.09	0.02	0.13	0.04	0.13	0.09
99.87	98.44	98.20	99.26	100.04	100.21	100.33	100.11	99.52
2.41	2.60	2.76	2.37	2.33	2.36	2.36	2.35	2.38
1.56	1.38	1.22	1.61	1.65	1.61	1.62	1.62	1.60
0.04	0.03	0.02	0.04	0.03	0.04	0.03	0.03	0.04
0.59	0.40	0.23	0.63	0.65	0.62	0.65	0.64	0.60
0.38	0.54	0.58	0.35	0.32	0.35	0.32	0.33	0.37
0.03	0.06	0.17	0.02	0.02	0.02	0.02	0.02	0.03
0.01	0.01	0.00	0.01	0.01	0.01	0.01	0.01	0.01
0.00	0.01	0.02	0.00	0.00	0.00	0.00	0.00	0.00
2.60	5.72	16.59	2.26	2.01	2.17	2.04	2.09	2.57
38.06	54.15	58.63	34.76	32.31	35.15	32.30	33.14	37.33
59.20	39.62	22.94	62.82	65.65	62.44	65.58	64.53	59.94

Table 15. Composition of plagioclase phenocrysts and groundmass (gm) from LW73FVP of Ql1b

LW73ph4_gm1	LW73ph4_gm1	LW73ph4_gm1	LW73ph4_gm2	LW73ph4_gm2	LW73ph4_gm3	LW73ph4_gm3
gm	gm	gm	gm	gm	gm	gm
51.83	52.32	53.32	52.03	51.08	51.89	50.56
30.01	29.45	29.01	29.21	29.94	29.14	29.60
0.95	0.81	0.88	0.93	1.00	0.91	0.90
12.76	12.44	11.88	11.96	12.71	12.06	12.67
3.97	4.19	4.57	4.38	3.97	4.24	3.88
0.38	0.43	0.48	0.47	0.41	0.46	0.40
0.40	0.32	0.25	0.21	0.29	0.22	0.35
0.10	0.07	0.04	0.11	0.05	0.06	0.14
100.39	100.01	100.43	99.29	99.46	98.98	98.50
2.36	2.39	2.42	2.39	2.35	2.39	2.35
1.61	1.58	1.55	1.58	1.62	1.58	1.62
0.04	0.03	0.03	0.04	0.04	0.04	0.04
0.62	0.61	0.58	0.59	0.63	0.60	0.63
0.35	0.37	0.40	0.39	0.35	0.38	0.35
0.02	0.03	0.03	0.03	0.02	0.03	0.02
0.01	0.01	0.01	0.01	0.01	0.01	0.01
0.00	0.00	0.00	0.00	0.00	0.00	0.00
2.21	2.47	2.72	2.74	2.40	2.70	2.35
35.15	36.87	39.91	38.66	35.21	37.78	34.71
62.46	60.54	57.30	58.39	62.30	59.41	62.68

Table 16. Composition of groundmass plagioclase from LW40FVP of Ql2a

Point	lw40#6_1_1	lw40#6_2_1	lw40#6_2_2	lw40#6_2_3	lw40#3_1_1	lw40#3_1_2	lw40#3_2_1
SiO_2	53.89	51.87	50.65	51.24	51.36	52.40	51.76
Al_2O_3	28.06	29.97	30.71	30.27	30.20	29.22	29.92
FeO	0.95	0.92	0.82	1.00	1.05	1.01	0.96
CaO	10.88	12.60	13.76	13.21	13.18	11.92	12.50
Na_2O	4.91	4.00	3.52	3.67	3.78	4.40	4.21
K_2O	0.60	0.39	0.29	0.32	0.34	0.51	0.43
SrO	0.25	0.38	0.31	0.31	0.32	0.27	0.27
TOTAL	99.64	100.27	100.08	100.08	100.30	99.88	100.14
Cations based on 8 oxygens							
Si	2.46	2.37	2.32	2.34	2.35	2.40	2.36
Al	1.51	1.61	1.66	1.63	1.63	1.58	1.61
Fe	0.04	0.04	0.03	0.04	0.04	0.04	0.04
Ca	0.53	0.62	0.68	0.65	0.65	0.58	0.61
Na	0.44	0.35	0.31	0.33	0.33	0.39	0.37
K	0.04	0.02	0.02	0.02	0.02	0.03	0.03
Sr	0.01	0.01	0.01	0.01	0.01	0.01	0.01
Or	3.51	2.27	1.71	1.85	1.97	2.97	2.50
Ab	43.27	35.55	31.10	32.77	33.42	38.76	36.84
An	53.03	61.92	67.13	65.24	64.46	57.99	60.49

Table 17. Composition of groundmass plagioclase from LW61FVP of Q13

Point	lw61fvp_#1_f1	lw61fvp_#1_f2	lw61fvp_#1_f3	lw61fvp_#1_f4
SiO_2	50.74	50.82	49.82	49.77
Al_2O_3	30.43	29.59	30.83	30.88
FeO	1.02	0.95	0.84	0.81
CaO	13.05	12.43	13.62	13.36
Na_2O	3.67	3.97	3.34	3.55
K_2O	0.37	0.40	0.27	0.30
SrO	0.30	0.29	0.25	0.28
TOTAL	99.57	98.45	98.97	98.94
Cations based on 8 oxygens				
Si	2.33	2.36	2.30	2.30
Al	1.65	1.62	1.68	1.68
Fe	0.04	0.04	0.03	0.03
Ca	0.64	0.62	0.68	0.66
Na	0.33	0.36	0.30	0.32
K	0.02	0.02	0.02	0.02
Sr	0.01	0.01	0.01	0.01
Or	2.18	2.38	1.60	1.79
Ab	33.00	35.75	30.21	31.88
An	64.82	61.87	68.19	66.33

Table 18. Composition of groundmass pyroxene from LW21FVP of Ql1d

Point	lw21_#13_b	lw21_#13_c	lw21_#14_c
SiO_2	48.24	48.90	50.10
TiO_2	2.29	2.05	1.56
Al_2O_3	4.22	3.56	2.61
Fe_2O_3	7.32	8.09	8.16
FeO	3.16	2.86	1.94
MnO	0.22	0.27	0.31
Cr_2O_3	0.02	0.03	0.00
Na_2O	0.41	0.44	0.34
MgO	13.27	13.64	14.26
CaO	20.79	20.00	20.19
TOTAL	99.92	99.83	99.47
Cations based on 6 oxygens			
Si	1.81	1.84	1.88
Ti	0.07	0.06	0.04
Al	0.19	0.16	0.12
Fe^{3+}	0.09	0.08	0.06
Fe^{2+}	0.23	0.25	0.26
Mn	0.01	0.01	0.01
Cr	0.00	0.00	0.00
Na	0.03	0.03	0.03
Mg	0.74	0.76	0.80
Ca	0.84	0.81	0.81
Wo	46.06	43.95	43.28
En	40.91	41.71	42.54
Fs	13.03	14.35	14.18

Table 19. Composition of groundmass pyroxene from LW40FVP of Ql2a

Point	lw40_#3_a1	lw40_#3_a2	lw40_#3_b1	lw40_#3_b2	lw40_#3_c1	lw40_#3_c2
SiO_2	47.73	46.45	46.88	46.68	46.15	46.88
TiO_2	3.03	3.30	3.54	3.50	3.62	3.43
Al_2O_3	4.16	4.03	4.42	4.13	4.19	4.76
Fe_2O_3	11.83	8.69	10.15	9.30	9.89	10.46
FeO	0.00	3.13	1.72	2.77	2.71	1.55
MnO	0.31	0.23	0.26	0.28	0.22	0.21
Cr_2O_3	0.02	0.01	0.00	0.02	0.01	0.01
Na_2O	0.62	0.52	0.48	0.51	0.55	0.64
MgO	10.92	11.95	11.69	11.72	11.40	11.27
CaO	19.18	20.20	20.12	20.41	19.88	19.84
TOTAL	97.80	98.51	99.26	99.31	98.62	99.05
Cations based on 6 oxygens						
Si	1.85	1.79	1.79	1.79	1.78	1.80
Ti	0.09	0.10	0.10	0.10	0.11	0.10
Al	0.19	0.18	0.20	0.19	0.19	0.22
Fe^{3+}	0.00	0.09	0.05	0.08	0.08	0.05
Fe^{2+}	0.38	0.28	0.33	0.30	0.32	0.34
Mn	0.01	0.01	0.01	0.01	0.01	0.01
Cr	0.00	0.00	0.00	0.00	0.00	0.00
Na	0.05	0.04	0.04	0.04	0.04	0.05
Mg	0.63	0.69	0.67	0.67	0.66	0.64
Ca	0.80	0.83	0.82	0.84	0.82	0.81
Wo	43.75	46.13	45.20	46.18	45.57	45.24
En	34.63	37.97	36.53	36.89	36.34	35.76
Fs	21.62	15.89	18.27	16.93	18.10	19.00

Table 20. Composition of magnetite inclusions in olivine and groundmass (gm) magnetite from LW21FVP of Ql1d

Point	lw21fvp_2m	lw21fvp_2m	lw21fvp_2ma	lw21fvp_2ma	lw21fvp_4m	lw21fvp_4m	lw21fvp_4m	lw21fvp_4ma	lw21fvp_4ma	lw21fvp_5m
SiO_2	0.11	0.10	0.15	0.09	0.11	0.10	0.08	0.08	0.07	0.10
TiO_2	10.14	8.81	13.38	11.00	14.46	16.79	18.21	16.75	16.07	7.70
Al_2O_3	8.49	9.10	5.56	8.15	4.20	3.39	2.67	3.52	4.19	13.15
Cr_2O_3	4.16	7.21	3.94	4.60	4.44	2.20	2.88	3.42	3.41	8.68
FeO	32.93	31.22	37.19	35.02	39.36	41.42	42.78	41.31	41.05	30.60
Fe_2O_3	35.66	35.18	32.36	34.16	31.80	30.58	28.58	29.78	30.28	32.37
MnO	0.23	0.31	0.38	0.34	0.42	0.55	0.59	0.49	0.42	0.28
MgO	5.08	5.59	3.83	4.32	3.13	3.03	3.07	3.26	3.14	6.12
ZnO	0.16	0.11	0.04	0.17	0.02	0.09	0.11	0.05	0.09	0.08
TOTAL	96.96	97.62	96.81	97.86	97.94	98.15	98.97	98.66	98.73	99.06
Cations based on 32 oxygens										
Si	0.03	0.03	0.04	0.03	0.03	0.03	0.02	0.02	0.02	0.03
Ti	2.20	1.88	2.97	2.38	3.21	3.73	4.03	3.70	3.54	1.59
Al	2.88	3.05	1.93	2.76	1.46	1.18	0.93	1.22	1.44	4.24
Cr	0.95	1.62	0.92	1.05	1.04	0.51	0.67	0.79	0.79	1.88
Fe^{2+}	7.73	7.53	7.18	7.39	7.06	6.80	6.32	6.57	6.67	6.67
Fe^{3+}	7.93	7.42	9.17	8.42	9.71	10.24	10.52	10.13	10.04	7.01
Mn	0.06	0.08	0.09	0.08	0.11	0.14	0.15	0.12	0.11	0.06
Mg	2.18	2.37	1.68	1.85	1.38	1.34	1.35	1.43	1.37	2.50
Zn	0.03	0.02	0.01	0.04	0.01	0.02	0.03	0.01	0.02	0.02

Table 20. Composition of magnetite inclusions in olivine and groundmass (gm) magnetite from LW21FVP of Ql1d

lw21fvp_5m	lw21fvp_5m	lw21fvp_5ma	lw21fvp_5ma	lw21fvp_5mb	lw21fvp_5mb	lw21fvp_5mc gm	lw21fvp_5mc gm	lw21fvp_5mc gm	lw21fvp_5mc gm	lw21fvp_13m gm
0.08	0.08	0.12	0.10	0.09	0.11	0.14	0.07	0.10	0.10	0.12
7.53	7.51	10.78	10.67	12.75	14.02	14.51	12.52	12.20	12.60	21.61
12.96	12.33	7.66	7.60	6.20	5.45	5.40	6.26	6.20	6.11	1.95
9.21	8.43	1.95	2.41	3.48	2.89	0.38	0.37	0.37	0.33	0.07
30.32	30.09	34.06	34.00	36.88	38.57	39.83	38.11	37.55	38.18	46.09
32.59	33.27	39.01	39.33	34.58	34.08	35.01	38.52	39.22	38.43	22.84
0.21	0.26	0.27	0.28	0.38	0.46	0.40	0.32	0.39	0.32	0.43
6.26	6.06	5.01	5.11	4.07	3.77	3.14	3.37	3.48	3.31	2.26
0.10	0.07	0.12	0.17	0.09	0.08	0.08	0.14	0.07	0.00	0.12
99.25	98.10	98.98	99.66	98.51	99.42	98.89	99.66	99.58	99.37	95.49
0.02	0.02	0.03	0.03	0.03	0.03	0.04	0.02	0.03	0.03	0.04
1.55	1.57	2.31	2.27	2.77	3.04	3.17	2.71	2.64	2.74	4.98
4.18	4.03	2.56	2.53	2.11	1.85	1.85	2.12	2.10	2.08	0.71
1.99	1.85	0.44	0.54	0.80	0.66	0.09	0.08	0.08	0.08	0.02
6.71	6.95	8.34	8.36	7.52	7.38	7.66	8.34	8.49	8.35	5.27
6.93	6.98	8.10	8.03	8.91	9.29	9.69	9.17	9.04	9.22	11.81
0.05	0.06	0.06	0.07	0.09	0.11	0.10	0.08	0.09	0.08	0.11
2.55	2.51	2.12	2.15	1.75	1.62	1.36	1.44	1.49	1.42	1.03
0.02	0.02	0.03	0.03	0.02	0.02	0.02	0.03	0.02	0.00	0.03

Table 20. Composition of magnetite inclusions in olivine and groundmass (gm) magnetite from LW21FVP of Ql1d

lw21fvp_13m gm	lw21_#13_a gm	lw21_#13_a gm	lw21_#13_a gm	lw21fvp_14m gm	lw21_#14_a gm	lw21_#14_a gm	lw21_#14_b gm	lw21_#14_b gm	lw21_#14_b gm	lw21_#14_b gm
0.13	0.11	0.12	0.12	0.11	0.13	0.15	0.15	0.15	0.12	0.11
21.72	20.43	19.87	20.70	18.39	18.05	20.64	20.12	20.16	19.45	19.34
1.61	1.79	1.71	1.93	2.65	1.43	1.69	1.54	1.62	1.76	1.68
0.09	0.02	0.05	0.09	0.04	0.05	0.02	0.12	0.12	0.14	0.24
45.97	44.91	44.44	45.10	42.29	44.00	44.73	44.51	44.82	43.72	43.65
23.00	27.25	27.74	26.10	30.28	31.38	26.07	27.43	27.88	28.96	29.37
0.62	0.60	0.54	0.62	0.54	0.49	0.55	0.63	0.59	0.67	0.57
2.24	2.67	2.49	2.61	3.22	1.74	2.67	2.54	2.57	2.76	2.84
0.08	0.04	0.13	0.04	0.12	0.16	0.17	0.09	0.15	0.19	0.11
95.45	97.82	97.09	97.31	97.63	97.43	96.69	97.14	98.07	97.77	97.90
0.04	0.03	0.04	0.04	0.03	0.04	0.05	0.05	0.04	0.04	0.03
5.02	4.60	4.51	4.68	4.12	4.12	4.70	4.57	4.53	4.38	4.35
0.58	0.63	0.61	0.68	0.93	0.51	0.60	0.55	0.57	0.62	0.59
0.02	0.01	0.01	0.02	0.01	0.01	0.01	0.03	0.03	0.03	0.06
5.32	6.13	6.30	5.90	6.78	7.17	5.94	6.23	6.27	6.53	6.61
11.81	11.23	11.23	11.33	10.53	11.18	11.32	11.24	11.21	10.95	10.92
0.16	0.15	0.14	0.16	0.14	0.13	0.14	0.16	0.15	0.17	0.14
1.02	1.19	1.12	1.17	1.43	0.79	1.21	1.14	1.15	1.23	1.27
0.02	0.01	0.03	0.01	0.03	0.04	0.04	0.02	0.03	0.04	0.02

Table 21. Composition of magnetite inclusions in olivine and groundmass (gm) magnetite from LW40FVP of Ql2a

Point	lw40#1_a	lw40#1_a	lw40#1_a	lw40#1_b	lw40#1_b	lw40#1_b	lw40#1_c gm	lw40#1_c gm	lw40#1_c gm	lw40#6_a gm	lw40#6_a gm
SiO_2	0.10	0.09	0.11	0.10	0.71	0.12	0.13	0.10	0.14	0.11	0.10
TiO_2	15.58	15.08	13.85	7.28	7.34	7.21	18.23	18.10	17.89	17.12	16.18
Al_2O_3	3.03	3.24	3.74	13.21	12.87	12.73	1.97	1.87	1.72	2.06	2.49
Cr_2O_3	1.67	2.00	3.84	9.37	9.35	8.85	0.32	0.21	0.17	0.41	0.68
FeO	40.62	40.02	38.60	29.09	28.61	28.83	44.24	44.11	43.66	42.56	41.57
Fe_2O_3	34.76	35.17	35.26	32.01	32.19	32.71	30.34	30.39	31.05	33.07	34.48
MnO	0.43	0.39	0.49	0.29	0.23	0.24	0.51	0.51	0.51	0.53	0.51
MgO	3.11	3.24	3.44	6.66	6.92	6.60	1.81	1.70	1.83	2.37	2.58
ZnO	0.10	0.02	0.05	0.12	0.15	0.16	0.00	0.12	0.08	0.20	0.10
TOTAL	99.39	99.23	99.37	98.12	98.37	97.44	97.56	97.10	97.04	98.42	98.68
Cations based on 32 oxygens											
Si	0.03	0.03	0.03	0.03	0.19	0.03	0.04	0.03	0.04	0.03	0.03
Ti	3.43	3.32	3.03	1.51	1.51	1.51	4.14	4.14	4.09	3.85	3.61
Al	1.05	1.12	1.28	4.28	4.14	4.17	0.70	0.67	0.62	0.72	0.87
Cr	0.39	0.46	0.88	2.04	2.02	1.94	0.08	0.05	0.04	0.10	0.16
Fe^{2+}	7.66	7.75	7.73	6.63	6.61	6.83	6.90	6.96	7.11	7.43	7.70
Fe^{3+}	9.95	9.80	9.40	6.69	6.53	6.69	11.18	11.22	11.11	10.63	10.32
Mn	0.11	0.10	0.12	0.07	0.05	0.06	0.13	0.13	0.13	0.13	0.13
Mg	1.36	1.41	1.49	2.73	2.82	2.73	0.81	0.77	0.83	1.05	1.14
Zn	0.02	0.00	0.01	0.02	0.03	0.03	0.00	0.03	0.02	0.04	0.02

Table 21. Composition of magnetite inclusions in olivine and groundmass (gm) magnetite from LW40FVP of Ql2a

lw40#6_a gm	lw40#6_b gm	lw40#6_b gm	lw40#6_b gm	lw40#6_c	lw40#6_c	lw40#6_c	lw40fvp#3_m1 gm	lw40fvp#3_m2 gm	lw40fvp#3_m3 gm
0.13	0.11	0.12	0.11	0.10	0.13	0.11	0.11	0.11	0.11
16.49	17.13	16.70	16.79	14.32	15.45	16.81	17.27	21.66	20.53
2.18	1.94	2.35	2.08	3.46	2.80	1.89	2.45	1.50	1.62
0.58	0.47	0.59	0.46	3.10	1.91	1.38	0.41	0.21	0.32
41.91	42.67	42.44	42.26	39.06	40.05	41.58	42.79	47.87	46.94
34.51	34.11	34.88	34.50	35.09	34.55	33.27	32.59	22.73	25.31
0.51	0.47	0.42	0.52	0.42	0.45	0.50	0.46	0.46	0.48
2.57	2.58	2.69	2.60	3.34	3.19	2.86	2.45	1.13	1.22
0.05	0.10	0.27	0.20	0.09	0.17	0.05	0.19	0.11	0.05
98.91	99.58	100.45	99.51	98.98	98.70	98.43	98.71	95.78	96.58
0.04	0.03	0.03	0.03	0.03	0.04	0.03	0.03	0.04	0.03
3.68	3.80	3.67	3.73	3.16	3.43	3.76	3.86	5.03	4.73
0.76	0.68	0.81	0.72	1.20	0.97	0.66	0.86	0.55	0.59
0.14	0.11	0.14	0.11	0.72	0.44	0.32	0.10	0.05	0.08
7.70	7.57	7.66	7.66	7.74	7.67	7.45	7.28	5.29	5.84
10.40	10.53	10.36	10.43	9.57	9.88	10.35	10.63	12.37	12.03
0.13	0.12	0.11	0.13	0.10	0.11	0.13	0.12	0.12	0.12
1.13	1.13	1.17	1.14	1.46	1.40	1.27	1.09	0.52	0.56
0.01	0.02	0.06	0.04	0.02	0.04	0.01	0.04	0.03	0.01

Table 22. Composition of magnetite inclusions in olivine from LW135FVP of Qs2fs

Point	lw135_1_mt1	lw135_1_mt2	lw135_3_mt1	lw135_3_mt2	lw135_3_mt3	lw135_3_mt4	lw135_3_mt5	lw135_4_mt1	lw135_4_mt2
SiO_2	0.09	0.10	0.10	0.09	0.09	0.08	0.12	0.09	0.09
TiO_2	9.44	9.11	9.96	9.58	9.45	9.22	10.03	8.79	8.45
Al_2O_3	6.64	7.45	7.47	7.70	7.57	8.07	7.31	8.40	8.91
Cr_2O_3	3.96	4.46	3.66	4.25	4.03	5.42	4.69	6.06	6.93
FeO	41.24	40.65	39.28	39.45	39.69	38.62	38.18	38.15	37.76
Fe_2O_3	33.05	32.58	33.67	33.31	32.03	32.29	33.66	31.43	31.07
MnO	0.25	0.22	0.28	0.28	0.17	0.23	0.31	0.29	0.27
MgO	4.92	5.18	4.84	4.95	5.54	5.43	4.83	5.63	5.84
TOTAL	99.59	99.75	99.25	99.62	98.56	99.35	99.12	98.85	99.32
Cations based on 32 oxygens									
Si	0.03	0.03	0.03	0.03	0.03	0.02	0.03	0.03	0.02
Ti	2.02	1.93	2.13	2.04	2.02	1.95	2.15	1.87	1.78
Al	2.23	2.48	2.50	2.56	2.54	2.68	2.45	2.79	2.94
Cr	0.89	1.00	0.82	0.95	0.91	1.21	1.06	1.35	1.53
Fe^{2+}	8.82	8.63	8.40	8.39	8.49	8.19	8.17	8.10	7.95
Fe^{3+}	7.86	7.69	8.00	7.87	7.62	7.61	8.01	7.42	7.27
Mn	0.06	0.05	0.07	0.07	0.04	0.06	0.07	0.07	0.06
Mg	2.08	2.18	2.05	2.09	2.35	2.28	2.05	2.37	2.43